CLIMATE AND MANAGEMENT CONTROLS ON FOREST GROWTH AND FOREST CARBON BALANCE IN THE WESTERN UNITED STATES

by

Katharine Cashman Kelsey

B.S. University of Puget Sound, 2007

M.S. University of Colorado Boulder, 2011

A thesis submitted to the

Faculty of the Graduate School of the

University of Colorado in partial fulfillment

of the requirement for the degree of

Doctor of Philosophy

Environmental Studies Program

2015

This thesis entitled:
Climate and Management Controls on
Forest Growth and Forest Carbon Balance in the Western United States
written by Katharine Cashman Kelsey
has been approved for the Environmental Studies Program

_____
(Jason C. Neff)

_____
(Waleed Abdalati)

_____
(Nichole N. Barger)

_____
(Jana B. Milford)

_____
(Michael G. Ryan)

Date_____

The final copy of this thesis has been examined by the signatories, and we find that both the content and the form meet acceptable presentation standards of scholarly work in the above mentioned discipline.

Kelsey, Katharine Cashman (Ph.D., Environmental Studies)

Climate and Management Controls on Forest Growth and Forest Carbon Balance in the Western United States

Thesis directed by Associate Professor Jason C. Neff

ABSTRACT

Climate change is resulting in a number of rapid changes in forests worldwide. Forests comprise a critical component of the global carbon cycle, and therefore climate-induced changes in forest carbon balance have the potential to create a feedback within the global carbon cycle and affect future trajectories of climate change. In order to further understanding of climate-driven changes in forest carbon balance, I (1) develop a method to improve spatial estimates forest carbon stocks, (2) investigate the effect of climate change and forest management actions on forest recovery and carbon balance following disturbance, and (3) explore the relationship between climate and forest growth, and identify climate-driven trends in forest growth through time, within San Juan National Forest in southwest Colorado, USA. I find that forest carbon estimates based on texture analysis from LandsatTM imagery improve regional forest carbon maps, and this method is particularly useful for estimating carbon stocks in forested regions affected by disturbance. Forest recovery from disturbance is also a critical component of future forest carbon stocks, and my results indicate that both climate and forest management actions have important implications for forest recovery and carbon dynamics following disturbance. Specifically, forest treatments that use woody biomass removed from the forest for electricity production can reduce carbon emissions to the atmosphere, but climate driven changes in fire severity and forest recovery can have the opposite effect on forest carbon stocks. In addition to the effects of disturbance and recovery on forest condition, I also find that climate change is

decreasing rates of forest growth in some species, likely in response to warming summer temperatures. These growth declines could result in changes of vegetation composition, or in extreme cases, a shift in vegetation type that would alter forest carbon storage. This work provides insight into both current and future changes in forest carbon balance as a consequence of climate change and forest management in the western US.

ACKNOWLEDGEMENTS

This work was completed with the help of many individuals. I would first like to thank my committee, Waleed Abdalati, Nichole Barger, Jana Milford and Mike Ryan, who helped me produce high-quality science and offered many words of encouragement along the way, and especially to my advisor Jason Neff, who is a role model both as a scientist and as a human being. I am also grateful to numerous people at San Juan National Forest, particularly Gretchen Fitzgerald, who assisted with many stages of this work. I would like to thank my field assistants Tyler Conquest, Tyler Kane, Michelle Pitcher, Hannah Smith and Natalie Volin who maintained cheerful attitudes and collected high quality data under both fun and trying field conditions. Dan Fernandez provided assistance and guidance with nearly every step of this research. Jock Blackard and Don Vandendriesche provided technical assistance working with Forest Service forestry data and modeling. Mahsa Mousavvi and Miranda Redmond patiently helped me learn new analysis techniques. The Barger-Collinge lab group provided support and feedback on all stages of this research. Financial support for this research was provided by USDA NIFA Award COLW-2011-00831. Finally, I am grateful to my family for their extensive emotional and moral support over the past four years, which is undoubtedly what truly made this dissertation possible.

CONTENTS

CHAPTER 1.
INTRODUCTION

1.1 Background....1
1.2 Frequency and Severity of Disturbance....5
1.3 Forest Recovery Following Disturbance and Management....8
1.3 Trends of Forest Decline....10

CHAPTER 2.
ESTIMATES OF ABOVEGROUND BIOMASS FROM TEXTURE ANALYSIS OF LANDSAT IMAGERY

2.1 Introduction....13
2.2 Materials and Methods....15
2.2.1Field and Satellite Data....17
2.2.2 Landsat TM Image Analysis....18
2.2.3 Biomass Prediction....19
2.2.4 Statistical Analysis....20
2.3 Results....21
2.4 Discussion....27
2.4.1 Biomass Prediction from Image Texture....27
2.4.2 Texture Analysis for Local Biomass Maps....28
2.5 Conclusions....29

CHAPTER 3.
SHORT AND LONG-TERM CARBON BALANCE OF BIOENERGY ELECTRICITY PRODUCTION FUELED BY FOREST TREATMENTS

3.1 Introduction....31
3.2 Materials and Methods....35
3.2.1Study Site....35
3.2.2 Forest Biomass....36
3.2.3 Bioenergy and Coal Reference Systems....36
3.2.4 Bioenergy and Forest Harvest Emissions....37
3.2.5 Forest Growth and Disturbance Modeling....38
3.3 Results....40
3.3.1 Relative Carbon Intensity of Biomass and Coal Electricity Production....40
3.3.2 Short-term Carbon Balance of Bioenergy Production....41
3.3.3 Long-term Carbon Balance of Bioenergy Production....42
3.3.4 Carbon Balance of Bioenergy Treatments and Future Wildfire....44
3.4 Discussion....48
3.4.1 Short-term Carbon Balance of Bioenergy Production....48
3.4.2 Long-term Carbon Balance of Bioenergy Production....50
3.4.4 Carbon Balance of Bioenergy Treatments and Future Wildfire....51

3.4.4 a) Forest Growth..... 52
3.4.4 b) Treatment Effectiveness..... 53
3.4.4 c) Wildfire Probability..... 54
3.5 Conclusions.....56

CHAPTER 4.

CLIMATE AND LANDSCAPE PHYSIOGRAPHY DRIVE TRENDS OF GROWTH AND DECLINE IN SUBALPINE FORESTS

4.1 Introduction.....57
4.2 Methods.....60
4.2.1Study Site.....60
4.2.2 Sampling Design and Tree Growth Data.....61
4.2.3 Physiographic Variables.....63
4.2.4 Climate Data and Variable Selection.....64
4.2.5 Modeling the Effects of Climate and Physiography on Tree Growth..... 67
4.2.6 Analysis of Long Term Growth Trends..... 69
4.3 Results.....70
4.3.1 Climate Growth Relations.....70
4.3.2 Interactions of Climate and Physiography.....72
4.3.3 Trends in Growth.....73
4.4 Discussion.....75
4.4.1 Climate Growth Relations.....76
4.4.2 Interactions of Climate and Physiography.....78
4.4.3 Trends in Growth.....79
4.5 Conclusions.....80

CHAPTER 5.

CONCLUSIONS..... 81

REFERENCES..... 86

LIST OF TABLES

Table 2.1 Correlation between predicted and observed biomass (r), Akaike's Information Criteria (AIC), Root Mean Square Error (RMSE) and Coefficient of Variation Root Mean Square Error (CV-RMSE) for the five best performing neural network models constructed with texture metrics (top 5 rows), and the five best performing neural network models constructed without texture metrics (lower 5 rows).....22

Table 3.1 Total carbon emissions, total carbon stabilized and net carbon emissions over one year from forest treatment considering three fates of harvested biomass: no biomass stabilized (business-as-usual scenario), merchantable timber stabilized in durable goods, and use of woody biomass in bioenergy production.....41

Table 3.2 Effects of treatment on fire behavior and forest carbon balance.....46

Table 3.3 Effects of bioenergy production on forest carbon balance.....47

Table 3.4 Effects of regeneration production on forest carbon balance.....47

Table 4.1 Site characteristics of tree ring sampling sites.....62

Table 4.2 Statistical parameters (± 1 standard error) of the top three performing linear mixed effects models evaluate by BIC for growth of Subalpine Fir and Engelmann Spruce. Growth is equal to basal area increment standardized by tree size. All parameters were centered and scaled such that the mean is equal to zero and the standard deviation is equal to 1.....72

Table 4.3 Statistical parameters of the top five performing linear mixed effects models for basal area increment trend for Subalpine Fir (top) and Engelmann Spruce (bottom). Site temperature refers to the average monthly minimum temperature for the growing season from 1975 through 2012.....75

LIST OF FIGURES

Figure 1.1. Conceptual diagram of the temporal and spatial scales on which common forest processes controlling forest carbon balance occur.....2

Figure 1.2 Conceptual diagram of forest carbon storage in live biomass through time for the following forest processes: a) annual growth and respiration, b) forest management, and c) forest disturbance over seasonal, decadal and centennial timescales.....3

Figure 1.3 Conceptual diagram showing changes in forest biomass through time in response to a) seasonal growth and respiration, b) forest disturbance, c) forest disturbance with shortened return interval, d) forest disturbance with shortened return interval and seasonal exchange, e) decadal trend of forest carbon in response to shortened return interval of disturbance.....6

Figure 2.1 Location of San Juan National Forest within southwest Colorado, and distribution of Forest Inventory and Analysis plots within San Juan National Forest. Scale bar applies to regional San Juan National Forest map.....16

Figure 2.2 Observed *versus* predicted biomass values for Landsat TM image texture based biomass map.....23

Figure 2.3 Landsat TM image texture-based map of aboveground biomass within forested regions of San Juan National Forest. The boxes labeled 4 and 5 indicate the location of Figure 2.4 and Figure 2.5, respectively.....24

Figure 2.4 a) True color image from National Agricultural Imagery Program acquired by a Leica ADS80 Airborne Digital Sensor; b) image texture-based biomass map; and (c) physical-spectral (slope, aspect, elevation, Normalized Difference Vegetation Index) based biomass map for a region of San Juan National Forest containing forested stands clear-cut in the 1970's. Color bar and scale bar apply to a), b) and c). d) Observed and modeled stand-average aboveground biomass from adjacent untreated and treated (clear-cut) forest stands. Observed values are calculated from nearby stands of the same vegetation type. Modeled stand-average biomass of treated stands was compared to the stand-average biomass of the untreated stand located directly to the west. Letters indicate locations of biomass comparisons, shown on a).....25

Figure 2.5 a) True color image from National Agricultural Imagery Program, acquired by a Leica ADS80 Airborne Digital Sensor; b) image texture-based biomass map; and (c) physical-spectral (slope, aspect, elevation, Normalized Difference Vegetation Index) based biomass map for a region of San Juan National Forest burned by a wildfire in 2002. Color bar and scale bar apply to a), b) and c). d) Modeled stand-average biomass of the burned region was compared to the unburned region to the East of the fire.....26

Figure 3.1 Sources of carbon emissions and types of carbon stabilization for different fates of harvested biomass following a forest fuel reduction treatment.....33

Figure 3.2 Arial image of the study area within San Juan National Forest, and location of San Juan National Forest in Southwest Colorado, USA.....35

Figure 3.3 Carbon emissions for 8000 hours of 5 MW electricity produced from bioenergy and a coal reference system.....40

Figure 3.4 a) Total stand carbon b) net stand carbon c) cumulative carbon offset through bioenergy production and avoided coal emissions and d) net stand carbon including carbon offset in a stand with repeated treatments. e) Forest wide carbon balance with forest treatments to fuel bioenergy production every year through 2100.....43

Figure 3.5 a) Total stand carbon in a forest stand treated mechanically in 2011 and with prescribed fire in 2013, followed by multiple simulations of varying intensity wildfire and regeneration in 2030; b) total stand carbon in an untreated forest stand with simulations of varying intensity wildfire and regeneration in 2030. Dark lines (numbered 1, 2, 3, 4, 5) represent the selected comparisons presented in Tables 3.2, 3.3 and 3.4.....45

Figure 3.6 Conceptual model of the effect of a) regrowth time, b) treatment effectiveness, and c) fire probability on carbon benefit of forest treatment. The timeframe is assumed to be smaller than the disturbance cycle in the specified forest.....52

Figure 4.1 a) Distribution of Spruce-fir type subalpine forest through North America and location of Colorado; b) Location of San Juan National Forest in Colorado; c) Location of study plots within San Juan Nation Forest.....61

Figure 4.2 a) Average annual temperature and b) summer average monthly minimum temperature from NOAA Divisional Data for western Colorado during the period 1895 through 2012. The dashed line shows the temperature trend from 1895 through 2012 and the solid line shows the temperature trend from 1975 through 2012.....65

Figure 4.3 Median Pearson product moment correlation of ring width index and seasonal climate variables calculated from National Ocean and Atmospheric Administration Divisional climate data for a) subalpine fir and b) Engelmann spruce.....71

Figure 4.4 Interaction effect of summer average monthly minimum temperature by elevation on tree growth (expressed as basal area increment standardized by basal area; BAI/BA) for Subalpine Fir. Growth versus elevation is shown for five progressive temperature intervals: a) lowest 0-19%, b) 20-39%, c) 40-59%, d) 60-79% and e) 80-100%. This interaction was identified in the top-performing model (evaluated by BIC) generated in a generalized linear-mixed modeling framework. Dashed lines denote the 95% confidence intervals.....73

Figure 4.5 Top: Mean basal area increment (BAI) through time for trees located on different aspects, north (N), south (S), east (E), west (W), for a) Subalpine Fir and b)

Engelmann Spruce. Bottom: Box plot of BAI trend (correlation of BAI and year) from 1975-2012 by aspect for c) subalpine fir and d) Engelmann spruce; bars represent median trend, boxes represent 25-75 quartiles, whiskers represent range and open circles are outliers.....74

CHAPTER I

INTRODUCTION

1.1 Background

Global climate change and increasing pressures from a growing human population are resulting in rapid changes to forests around the world. Drought and insect outbreaks are causing widespread forest mortality, rates of forest growth are changing and wildfire activity is increasing in many regions [*Westerling et al*., 2006; *Soja et al*., 2007; *Beck et al*., 2011; *Carnicer et al*., 2011]. These forest changes have been observed on every forested continent, and are largely attributed to increasing temperatures and the resultant drought and heat stress [*Allen et al*., 2010; *Choat et al*., 2012]. With global temperatures expected to increase further in the future, these trends may be an indication of the future trajectory of many forests worldwide.

Forests make up a critical component of the carbon cycle, and broad-scale changes in forest condition in response to climate change could have large effects on forest carbon storage and terrestrial carbon balance [*Reichstein et al*., 2013]. Altered forest dynamics that result in greater forest growth may increase carbon storage in forest biomass and therefore remove carbon dioxide from the atmosphere. Conversely, forest modifications that decrease forest biomass and increase carbon emissions may increase the rate that CO_2 accumulates in the atmosphere. Globally forests store nearly half of the carbon contained within terrestrial ecosystems [*Sabine et al*., 2004], and therefore changes in forest carbon dynamics due to climate change have the potential to create a feedback within the global carbon-climate system. Thus understanding the

nature of forest response to regional climate change, and quantifying increases or decreases in forest carbon storage in response to climate trends, are critical to informing current and future changes within the global climate system.

The rate and magnitude of carbon exchange between forests and the atmosphere varies through space and time, and the relevance of different forest processes to carbon exchange depends on the time and spatial scale in question (Figure 1.1).

Figure 1.1 Conceptual diagram of the temporal and spatial scales on which common forest processes controlling forest carbon balance occur.

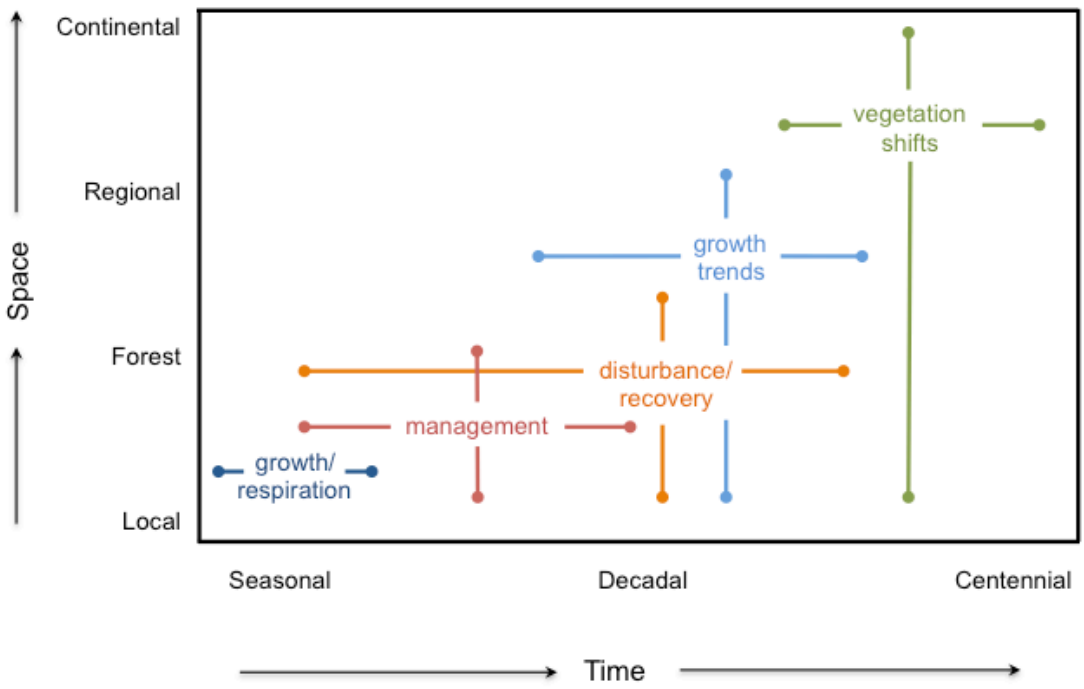

Processes that drive forest carbon exchange occur on timescales ranging from seasonal to decadal to centennial. At the seasonal scale, carbon exchange is dominated by annual growth and respiration, at the decadal scale disturbance processes and trends in growth, mortality and regeneration affect carbon exchange, and over the centennial timescales forest carbon can change as a result of shifts in vegetation type or composition. The dominant processes driving forest carbon exchange also vary across spatial scales ranging from the scale of a tree, forest scale, to

region and continent. At the scale of an individual tree, respiration and growth control carbon exchange. At the spatial scale of a forest, forest management, disturbance and trends in growth, mortality and regeneration control carbon exchange. On regional to continental scales, carbon exchange is controlled by vegetation composition and large disturbances. In addition to variable processes acting on forests at different time and spatial scales, a given forest process may have a different effect on forest exchange depending on the time or spatial scale in question (Figure 1.2).

Figure 1.2 Conceptual diagram of forest carbon storage in live biomass through time for the following forest processes: a) annual growth and respiration, b) forest management, and c) forest disturbance over seasonal, decadal and centennial timescales.

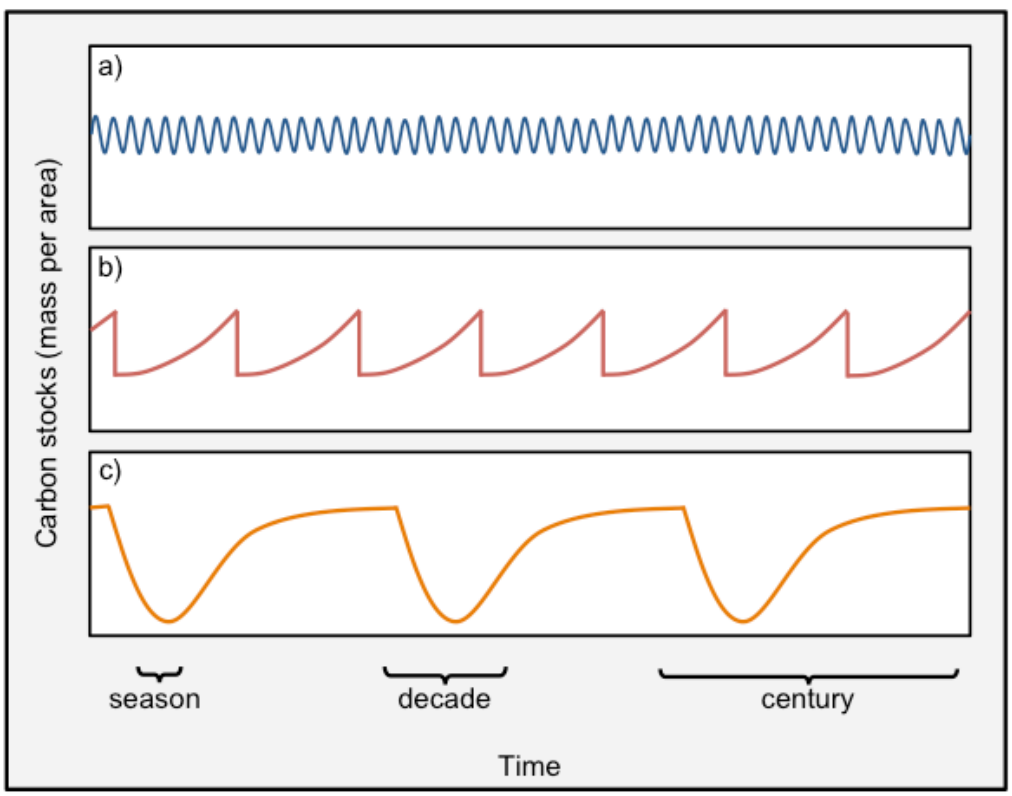

For example, a disturbance such as wildfire may result in a net flux of carbon to the atmosphere over the timescale of a decade, but could result in a net carbon balance of zero over the time scale of a century following forest recovery. Therefore, the timescale and spatial scale of forest

dynamics are critical when considering the carbon balance of forest ecosystems, particularly in the context of forest carbon policy.

Forests can impact the global carbon-climate system by acting as either a source or sink of carbon on the timescales that are important for human response to global climate change. Forest policy planning horizons are generally no longer than decadal timescales. Global assessments, such as reports produced by the International Panel on Climate Change, focus most heavily on the time period before 2100 [*Pachauri et al*., 2014], and forest policies, such as National Forest plans, are frequently on the order of 10 years [*Forest and Rangeland Renewable Resources Planning Act of 1974*, 2001]. Considering the decadal timeframe meaningful for policy response to anthropogenic climate change, there are three processes that can affect forest carbon exchange on this timescale: (1) an increase the frequency or severity of forest disturbance events, (2) an increase in the time necessary for a forest to recover from disturbance, or (3) trends in forest processes of growth, mortality and regeneration in response to climate change.

There are extensive and well-documented cases of forest changes in response to climate change already underway in the western United States (US). The frequency and duration of wildfires in the western US has increased [*Westerling et al*., 2006], insect outbreaks are occurring at higher elevations and latitudes [*Hicke et al*., 2006; *Raffa et al*., 2008], rates of background tree mortality are accelerating [*van Mantgem et al*., 2009] and human population is growing in fire-prone areas [*Radeloff et al*., 2005; *Theobald and Romme*, 2007] leading to an increased need for forest management in order to protect private property from wildfire. In the southwestern region of the US, wildfire and insect outbreaks have resulted in some degree of forest mortality, ranging from local mortality to widespread events, on nearly 20% of forested regions between 1997 and 2008 [*Williams et al*., 2010]. These changes have taken place during a time when the climate of the western US is becoming warmer [*Diaz and Eischeid*, 2007], and

projections of future climate change indicate that this region will become increasingly warm and dry in the coming decades [*Seager et al*., 2007; *Rangwala et al*., 2012]. Warming temperatures in the future have the potential to produce changes in carbon storage over the next several decades by influencing disturbance regimes, forest recovery, and trends in forest growth, mortality and regeneration.

1.2 Frequency and Severity of Disturbance

Forest disturbances lead to a release of carbon over several seasons or a decade, followed by forest re-accumulation of carbon over the next decades to centuries. This longer-term carbon exchange is superimposed on seasonal variations in carbon exchange from forest growth and respiration. Over the time period of several centuries, periodic disturbances followed by forest recovery, combined with seasonal carbon exchange, will result in no net carbon exchange between the forest and the atmosphere. However, if the frequency or severity of disturbance increases, the forest will establish a new equilibrium with the atmosphere. Forest atmosphere carbon exchange during the time it takes for the system to re-equilibrate can result in a decrease in carbon stocks, and net efflux of carbon from the forest to the atmosphere (Figure 1.3). Therefore, increased severity or frequency of disturbances in forests of the western US (hereafter Western forests) could reduce forest-level carbon storage over the coming decades.

Figure 1.3 Conceptual diagram showing changes in forest biomass through time in response to a) seasonal growth and respiration, b) forest disturbance, c) forest disturbance with shortened return interval, d) forest disturbance with shortened return interval and seasonal exchange, e) decadal trend of forest carbon in response to shortened return interval of disturbance.

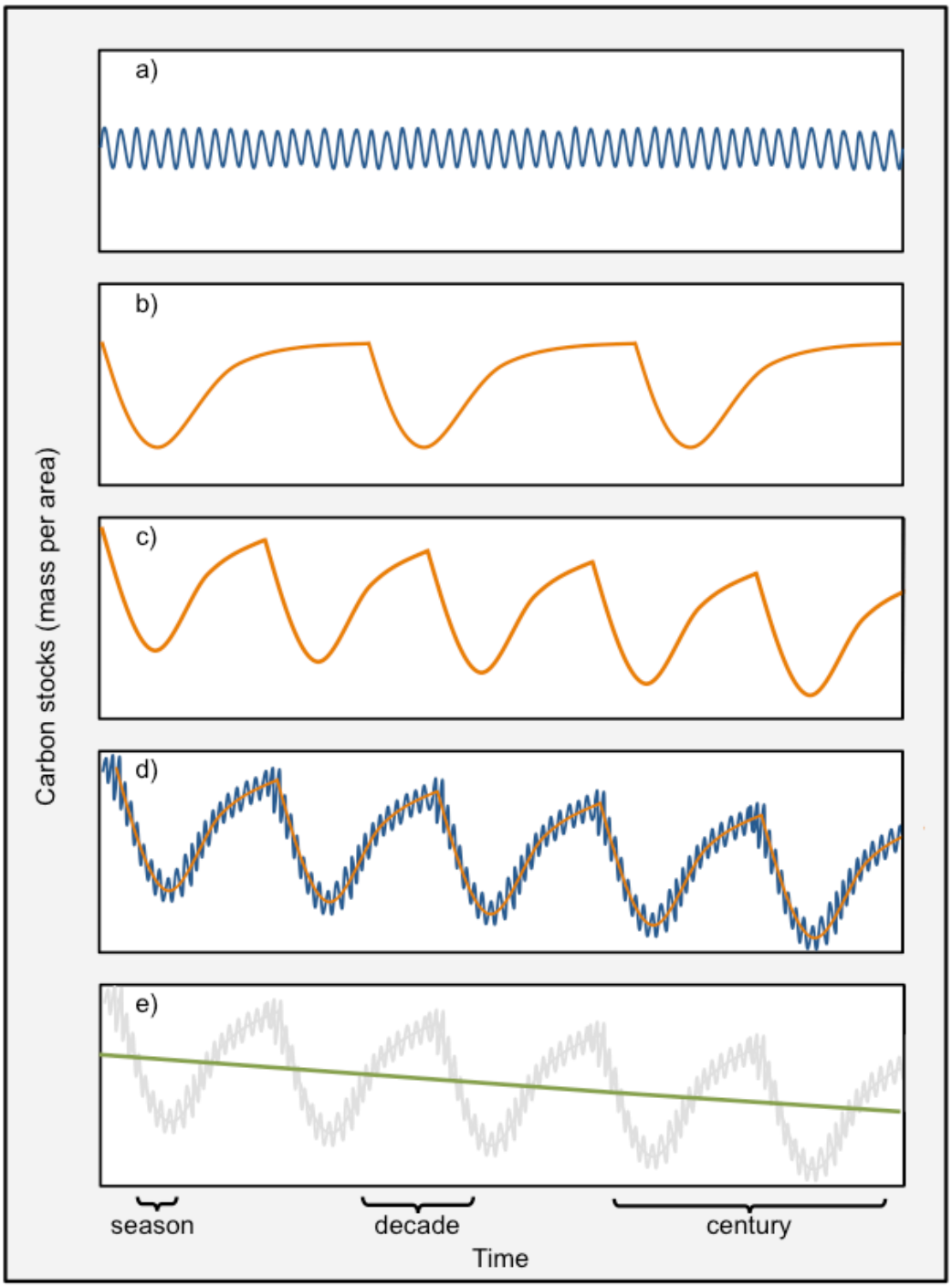

Wildfires are a regular disturbance in Western forests and have substantial impacts on forest carbon dynamics. Wildfires change forest carbon balance both by releasing pyrogenic carbon to the atmosphere as a direct result of combustion, and also through the decomposition of trees killed during the fires [*Meigs et al*., 2009; *Dore et al*., 2010]. In the western US, warmer spring temperatures and longer fire seasons in the last several decades have led to an increase in the number of large fires in Western states [*Westerling et al*., 2006]. In the future, annual wildfire area burned is expected to further increase [*Littell et al*., 2009], and potentially double relative to current levels by the end of the century [*McKenzie et al*., 2004]. An increase in wildfire area burned means a decrease in fire return interval at the forest scale, and could result in a net efflux of carbon from the forest to the atmosphere as the forest carbon dynamics in that region reach a new equilibrium. Fires can also lead to vegetation change. A recent example highlights the potential for increased wildfire frequency to produce a substantial vegetation change in an ecosystem within the Rocky Mountains. In the Greater Yellowstone region of the northern Rocky Mountains, shorter fire return intervals are projected to change the dominant vegetation type from lodgepole pine to ponderosa pine by the end of the century [*Westerling et al*., 2011], which could result in a decrease of forest carbon storage as a consequence of the change in vegetation type. Future potential vegetation shifts in this forest and other forests have large implications for carbon storage, and specifically could result in lower carbon storage in biomass of forests of the western US over the coming decades, particularly timescales relevant to forest policy.

Periodic outbreaks of tree-killing insects are another natural part of forest ecosystem function within Rocky Mountain forests, but current trends in insect outbreaks in response to climate trends could change decade-scale forest carbon balance in some Western forests. Recent years have seen a number of large insect outbreaks within Rocky Mountain forests [*Raffa et al*., 2008]. The location and timing of these outbreaks is closely linked to climatic factors because many of the life-history strategies of the beetles are dependent on temperature [*Bentz et al*.,

1991; *Logan et al*., 2003], and also because climate conditions such as drought can influence host trees and therefore leave a stand more vulnerable to a beetle outbreak [*Raffa et al*., 2008; *McDowell et al*., 2011]. Mortality as a result of insect outbreaks can result in large changes to forest carbon balance. For example, in British Columbia the cumulative impact of a current Mountain pine beetle outbreak is projected to release 270 Mt (270,000,000 Mg) of carbon between 2000 and 2020 [*Kurz et al*., 2008]. In some regions of the western US the extent and severity of outbreaks may be increasing as a result of climate trends [*Breshears et al*., 2005; *Hicke et al*., 2006]. If warming climate conditions reduce the vigor of host trees, beetle infestations could occur at greater frequency and severity in the future [*Bentz et al*., 2010]. Such a change could increase the area of forest affected by insects, and therefore increase the area of forest acting as a carbon source in the next few decades, and reduce the potential for forest recovery between disturbance events.

1.3 Forest Recovery Following Disturbance and Management

Modified or reduced rates of forest recovery following disturbance is the second process that can change forest carbon storage over decadal timescales. Forest recovery is important in determining both the carbon balance in the decades following natural disturbances such as wildfire or insect outbreaks, and also in determining decadal carbon balance of forest management actions. Many forests of the western US are routinely managed for purposes such as timber production or wildfire risk reduction. While controlling carbon stocks is not the objective of most forest management actions [*Hurteau et al*., 2008], management does alter forest carbon dynamics for a period of years to decades [*North et al*., 2009; *Stephens et al*., 2009], and therefore forest recovery is important in determining the decadal scale carbon balance

of management actions. Forest recovery following natural disturbances and management is primarily dependent on the processes of regeneration and growth.

Rates of regeneration are controlled by several factors but in particular are altered where severe disturbance, such as a high severity wildfire, removes the seed source necessary for regeneration [*Donato et al*., 2009; *Greene and Johnson*, 2011]. Instances of reduced regeneration following severe wildfire have been observed in some regions of the American Southwest. A recent study found that conifer regeneration was completely lacking on 57% of sites investigated up to two decades following wildfire [*Roccaforte et al*., 2012]. In some cases, low or no regeneration following wildfire can lead to previously forested regions transitioning to meadow and shrubland ecosystems post-fire [*Savage and Mast*, 2005]. In the last several decades, warmer conditions in the western US have resulted in larger fire sizes and increased wildfire area burned, and these larger fires have in turn produced an increase in area burned at high severity [*Cansler and Mckenzie*, 2014]. High severity wildfire is more likely to remove an overstory seed-source, or increase the distance seeds must travel to re-establish within a burned area [*Greene and Johnson*, 2011]. Therefore, increasing area burned by high severity wildfire will likely reduce regeneration after fire, and where no regeneration occurs, the forest may transition to meadow or shrubland. Forest transition to a non-forest vegetation type, or delayed regeneration in regions of severe wildfire, could reduce forest-scale carbon stocks over the next several decades.

Changes in the rates of forest recovery are also important when evaluating the carbon consequences of forest management actions on decadal timescales. Direct management actions are frequently used in many forests of the western US to reduce the risk of high severity wildfire. These fuel reduction treatments are designed to 'thin' the forest and reduce the risk of fires

spreading within a forest canopy [*Agee and Skinner*, 2005]. Although forests are not currently managed for carbon management goals, these management practices can alter decadal scale forest carbon balance in several ways. First, fuel reduction treatments are designed to reduce overstory tree mortality and therefore they will limit pyrogenic emissions in the case of a wildfire [*Finkral and Evans*, 2008; *Mitchell et al*., 2009; *Stephens et al*., 2009; *North and Hurteau*, 2011]. Secondly, forest treatments require removing woody biomass from the forest and thereby reduce forest carbon storage [*North et al*., 2009; *Stephens et al*., 2009]. As a result, the decadal-scale carbon balance of forest treatments is highly dependent on forest re-growth following treatment. Future climate change may alter the re-sequestration of carbon in a forest following treatment or disturbance by changing rates of forest recovery, and in some cases the forest may not recover to pre-treatment carbon levels [*Azpeleta et al*., 2014]. If this is the case, then the fuel-reduction treatment produced flux of carbon to the atmosphere that is not re-sequestered via forest growth over decadal timescales. Therefore, forest recovery rates are an important part of determining the decadal-scale carbon balance of forest management actions.

1.4 Trends of Forest Decline

Trends in forest processes such as rates of mortality, regeneration and growth compose the final forest change that can alter forest-scale carbon storage over decadal timescales. Changes of this nature, such as an increase in background forest mortality without commensurate increases regeneration, have the potential to slowly reduce forest-scale carbon stocks over several decades. Furthermore, trends in changing rates of growth, mortality or regeneration do not replace disturbance processes, so the effects of trends could be compounded by subsequent

disturbance. Therefore, trends persisting over a period of decades can change forest-scale carbon balance.

Over the past several decades, forests of the western US have been undergoing a trend of increasing rates of background mortality. This increasing rate of background forest mortality is observed in old (>200 year) undisturbed forest stands across all elevations, tree sizes, genera, and in ecosystems with varying fire return intervals [*van Mantgem et al*., 2009]. This trend is attributed to regional warming taking place across the western US [*van Mantgem et al*., 2009]. Rates of recruitment have not increased commensurately with mortality, so this trend has the possibility to decrease carbon storage in forest biomass over decadal time scales through persistent changes in forest age and structure.

Regional warming in the western US could also affect carbon storage in forest biomass through changes in rates of forest growth. Particularly in low elevation regions of the American Southwestern US, many conifer species grow less in years with especially warm temperatures [*Williams et al*., 2010] and continued warming in this region could reduce tree growth and potentially leave these forests vulnerable to other types of disturbance [*Williams et al*., 2012]. Warming temperatures have resulted in sustained growth declines in forests in other parts of the world [*Jump et al*., 2006; *Beck et al*., 2011], and similar trends in the western US could affect forest carbon storage and make forested ecosystems of the western US more vulnerable to other types of forest disturbance.

Many of the changes taking place in forests of the western US in response to climate change and increasing human populations could affect decadal-scale forest carbon storage by altering the frequency and severity of disturbance, prolonging forest recovery times, or

producing trends of forest decline. In this dissertation I address these three mechanisms of carbon balance change in Western forests through the following objectives:

(1) Develop a method to improve regional-scale maps of forest carbon storage and identify changes in forest carbon stocks in response to disturbance;

(2) Evaluate climate controls on forest recovery and short and long-term carbon balance following forest management;

(3) Investigate patterns of forest growth and decline as a result of current climate change.

This dissertation provides insight to the nature and magnitude of changes in forest condition and carbon balance as a result of climate and management in forests of the western US.

CHAPTER II

ESTIMATES OF ABOVEGROUND BIOMASS FROM TEXTURE ANALYSIS OF LANDSAT IMAGERY

2.1 Introduction

Accurate spatial maps of forest biomass are necessary for managing forest resources, informing climate change modeling studies, and meeting national and international reporting requirements for greenhouse gas inventories [*Ryan et al*., 2010; *EPA*, 2011]. Forest biomass maps are also necessary at the sub-national level for purposes such as completing the US Forest Service Climate Change Scorecard that necessitates annual estimates of carbon stocks and fluxes for each National Forest [*USDA*, 2011], and for quantifying changes in forest biomass on regional scales in response to disturbance. However, there are few spatially explicit regional and local biomass maps available, and as a consequence, relatively few resources available to determine how local biomass changes with disturbance. In this study I evaluate an alternative to traditional spectral analysis approaches to create local biomass maps.

There are two primary methods of mapping aboveground forest biomass. The first is an approach that assigns a biomass value, or a range of biomass values, to areas of land distinguished by characteristics such as vegetation type or land use. This approach, frequently referred to as 'stratify and multiply,' uses ground-based measurements to determine biomass values, and spatial datasets to delineate mapping units. Although the stratify and multiply approach is relatively simple to implement, there are some limitations to this technique, namely the ambiguities present in land area classification, and the wide range of variability in aboveground biomass within a given land cover type [*Goetz et al*., 2009].

The second common approach to mapping aboveground biomass employs a set of spatially continuous variables to predict biomass values at unobserved locations. In this direct

mapping approach, a relationship is established between aboveground biomass and one or several spatially continuous variables, and these relationships are used to predict biomass across the population. The direct mapping approach takes advantage of a variety of geospatial variables such as climate and topography, and information from remote sensing platforms. Many types of remotely sensed information can be used to aid in mapping biomass such as spectral information from remotely sensed imagery [*Richards*, 2013], backscattered energy from Synthetic Aperture Radar (SAR) [*Le Toan et al*., 1992; *Kasischke et al*., 1997], and Light Detection and Ranging (LiDAR) [*Dubayah and Drake*, 2000]. The two primary advantages to using a direct mapping approach are 1) the resulting map will more accurately depict variations in biomass across the landscape, and 2) changes to mapped forest biomass are easier to update [*Goetz et al*., 2009].

There are also some limitations to the direct mapping techniques, particularly related to the use of remotely sensed information. One limitation is the mismatch of spatial scale between the area encompassed by a measurement plot and the area of a remotely sensed pixel. In the case of Landsat imagery, the area of a measurement plot only accounts for a small part of the area represented by a pixel and the plot measurement value may not accurately represent the aggregate value of biomass within that pixel. This disparity in spatial scale can introduce error into the resulting map. Secondly, direct mapping techniques that employ spectral band ratios, such as the Normalized Difference Vegetation Index (NDVI) and the Enhanced Vegetation Index (EVI) tend to under-predict forest biomass in regions of high biomass and multi-storied forest canopies where NDVI in particular can saturate [*Huete and van Leeuwen*, 1997]. SAR is a promising technique for biomass estimation, particularly when used in conjunction with methods that model forest biomass by empirically relating backscatter to ground-based biomass measurements, and interferometric SAR (InSAR) techniques that can estimate forest height [*Ouchi*, 2013]. However, SAR biomass estimation techniques also saturate in regions of dense forest canopy [*Kasischke et al*., 1997; *Ouchi*, 2013], and SAR data is only available on a limited bases. Finally, LiDAR provides a direct measure of forest canopy height [*Dubayah and Drake*, 2000; *Lim et al*., 2003], but its wide scale use is currently limited by the expense of acquiring

LiDAR data at fine spatial scales. Until these data access limitations are resolved, other publically available remote sensing products will be required to create regional biomass maps.

Texture analysis is an image processing technique that may address some of the existing problems with vegetation index saturation and the data acquisition constrains related to mapping forest biomass at regional scales. Texture is a measure of variability in pixel values among neighboring pixels for a defined analysis window. A primary advantage of texture is that it can be calculated from optical data, among other types of raster data. The use of optical imagery in calculating texture is advantageous because there are several sources of publically available optical imagery, including Landsat, and therefore mapping biomass with image texture analysis is not subject to the constraints in obtaining data that are present for SAR or LiDAR. Furthermore, image texture has been used to aid in mapping forest biomass in dense tropical forests [*Cutler et al*., 2012], and in some regions texture is a better predictor of biomass than spectral vegetation indices [*Lu*, 2005; *Eckert*, 2012]. Because texture has been shown to be an effective method of mapping biomass in dense canopies, and can be calculated on widely available optical imagery, texture may be a useful technique for improving biomass maps at local and regional scales.

In this work I use a case study of San Juan National Forest in southwest Colorado to evaluate whether inclusion of image texture features can be used to improve the prediction quality of local scale biomass maps for use in land management and research. I evaluate the prediction quality of local scale biomass maps constructed with physical variables, spectral variables, and image texture metrics. These methods include only publically available data. The wide range of vegetation types and the complex topography of this region make San Juan National Forest an ideal location to evaluate remote sensing based biomass mapping methods.

2.2 Materials and Methods

The San Juan National Forest in southwest Colorado, USA is centered at 37°N and 108°W (Figure 2.1).

Figure 2.1 Location of San Juan National Forest within southwest Colorado, and distribution of Forest Inventory and Analysis plots within San Juan National Forest. Scale bar applies to regional San Juan National Forest map. Base map for San Juan National Forest extent: ESRI shaded relief imagery [*ArcGIS Services Directory*, 2013]. Projection: Albers NAD83.

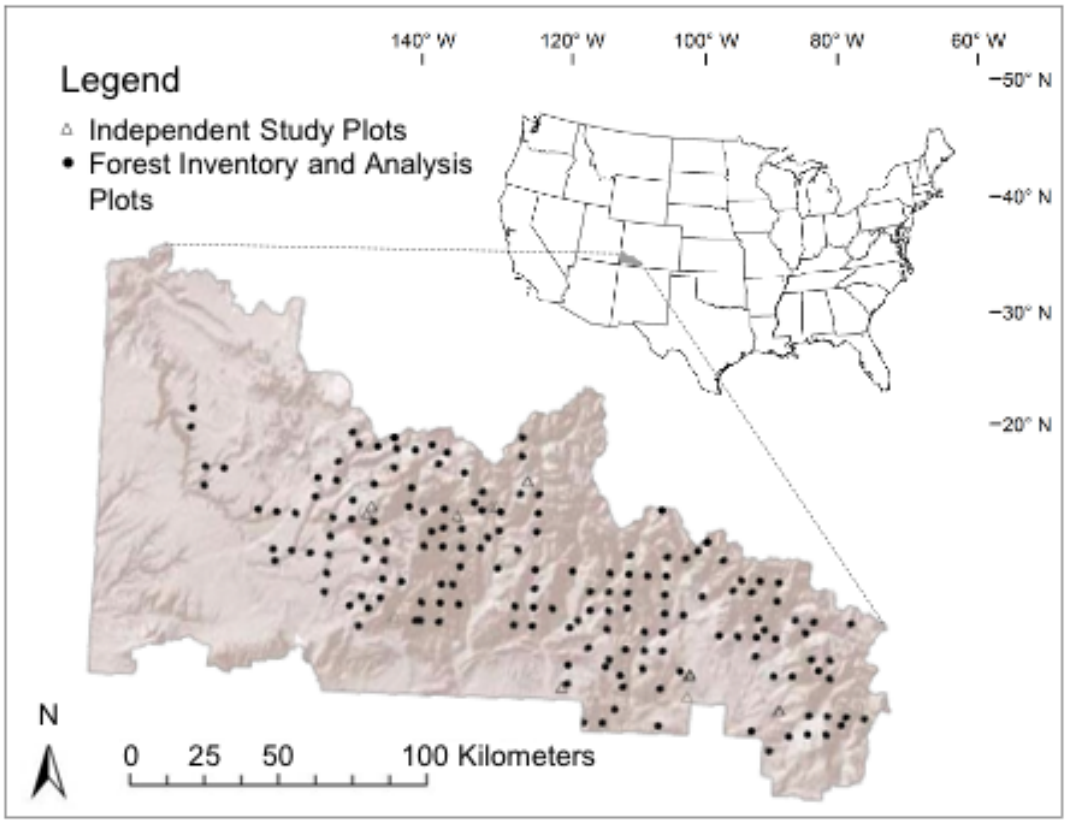

This forest is roughly 7000 km^2 in area and ranges in elevation from 1500m to 3800m. Total annual average precipitation ranges from 400mm in the lower elevations to over a meter (1150mm) in the higher elevation forests [*PRISM*, 2013]. Forests of this region contain Ponderosa Pine woodlands, Warm-Dry Mixed Conifer forests, Cool-Moist Mixed Conifer forests, and Spruce-Fir forests. San Juan National Forest is managed for recreation, timber production and wildfire fuel reduction, and is divided into stands that vary in stand age, treatment, and disturbance history. Landcover type for this region was determined from the Field Sampled Vegetation (FSVeg) database, an online inventory of information on trees, fuels,

down woody material, surface cover and understory vegetation, sampled and maintained by San Juan National Forest [*SJNF*, 2013]. Only regions defined as forest were included in this study.

2.2.1 Field and Satellite Data. A total of 164 Forest Inventory and Analysis (FIA) Program plots from forested regions within San Juan National Forest (SJNF) were used for this study. The FIA Program consists of a system of ground-based forest inventory plots that are situated approximately one every 2400 ha throughout the coterminous United States, and are measured every 5 to 10 years [*Blackard et al.*, 2008]. FIA ground-based plot biomass data was obtained from the FIA online DataMart: [*FIA*, 2013]. FIA plots consist of four 1/24 acre (168.7 m^2) subplots in which live tree biomass is determined from measurements of tree dimensions. This biomass value is hereafter referred to as observed biomass. The observed biomass values for FIA plots within SJNF range from 2.1 to 490.2 Mg ha^{-1}, with a mean biomass of 134.8 Mg ha^{-1}. Although the exact location of FIA plots are not provided to the public, exact locations of the FIA plots within SJNF were obtained from the FIA program for the purposes of this study. All FIA plots used in this study were measured between 2002 and 2009. All plot locations were measured by FIA using the Global Positioning System (GPS), and have a horizontal accuracy of around 5 meters [*Hoppus and Lister*, 2005].

Observed biomass values from eight independently sampled plots within or near forest stands clear-cut in the 1970's were used to validate biomass predictions for clear-cut stands and adjacent untreated forest. Of these eight plots, five plots were located in untreated forest and three plots were located in stands clear-cut in the 1970's. Aboveground biomass measurements consisted of 50 m diameter circular plots (1963.49 m^2) surveyed in 2012. Within each plot the diameter of every tree over 1.37 m tall was measured at 1.37 m to obtain a measure of diameter at breast height (DBH) for all trees within the plot. Aboveground live tree biomass was calculated from tree DBH using allometric equations [*Jenkins et al.*, 2004; *Kaye et al.*, 2005]. Total observed aboveground live tree biomass was determined as the sum of all trees present within plot.

2.2.2 Landsat TM Image Analysis. For each FIA plot, spectral information was obtained for the corresponding geographic location from Landsat 5 TM imagery. Images from two adjacent Landsat TM paths were necessary to cover the entire spatial extent of the study area; the two images were acquired in June and July of 2011 (June 18; July 21). The two scenes used in this study were selected because they are high-quality, cloud-free scenes acquired at similar dates and processed with Level 1T Standard Terrain Correction. All Landsat TM scenes were converted to top of atmosphere (TOA) reflectance using post-launch calibration coefficients [*Chander et al*., 2009], and an atmospheric correction was applied using Dark Subtraction Method [*Chavez*, 1988]. A C-correction [*Teillet et al*., 1982] was applied to correct for illumination differences due to sun-earth-sensor geometry across the variable topography of these two Landsat scenes using a 30-meter resolution digital elevation model [*NED*, 2014].

In this study, I evaluate the prediction quality of regional biomass maps constructed from physical variables, spectral variables, and image texture variables. The physical variables used included slope, aspect, and elevation calculated from regional digital elevation models [*NED*, 2014], vegetation type determined from the SJNF FSVeg database, and precipitation obtained from the PRISM Climate Group [*PRISM*, 2013]. The spectral information used included both the Normalized Difference Vegetation Index (NDVI) and the Enhanced Vegetation Index (EVI) calculated from Landsat TM imagery. Finally, image texture metrics were generated statistically using a Gray Level Co-occurrence Matrix (GLCM) computed from a relative displacement vector (d, θ) that describes the spatial distribution of grey level pairs separated by distance d in direction θ. Many textural metrics can be derived from the GLCM; I use the eight metrics of mean, variance, homogeneity, contrast, dissimilarity, entropy, second moment and correlation [*Haralick et al*., 1973] as these eight have previously been used to good effect in mapping forest biomass in dense tropical forests [*Lu and Batistella*, 2005; *Cutler et al*., 2012; *Eckert*, 2012]. In addition to d and θ, texture metrics are also dependent on the window size, or the number of pixels, used to calculate the GLCM. A small window size will identify fine-scale variations in

pixel brightness while a large window will be sensitive to larger-scale variations. Therefore, a window that is too small may identify variations in pixel brightness that are irrelevant for the task at hand, whereas a window that is too large may overlook important variations in pixel brightness. For purposes of mapping forest biomass, the optimal window size was determined by the window size that had the strongest correlation between texture-predicted biomass and observed biomass. In order to determine the optimal window size for this study, all texture metrics were calculated on four Landsat TM bands (Bands 2-5) using four window sizes: 3 × 3, 5 × 5, 7 × 7, and 9 × 9 pixels. For each window size, texture was also calculated at four offsets, (θ), represented in Cartesian coordinates as [0,1], [1,1], [1,0], and [1,–1]. All GLCMs were constructed using a 64 gray level quantization; this value was chosen to reduce computational effort during GLCM construction, and to avoid creating sparse GLCMs [*Clausi*, 2002].

2.2.3 Biomass Prediction. Physical variables, spectral vegetation indices, and texture metrics were used to predict aboveground forest biomass using feedforward neural networks built in Statistica12 (StatSoft, Inc., Tulsa, OK). Neural networks are advantageous for this sort of modeling because they do not require any assumptions about the distribution and independence of input data. This neural network model was constructed using FIA biomass values, and the corresponding physical, spectral and image texture information for that plot location. The observed biomass values from FIA plots were randomly divided into three groups: training, testing and validation data. Seventy percent of the plots were used as training data (116 plots), 15% as testing data (24 plots), and the remaining 15% as validation data (24 plots). Training data were used to build the network, testing data were used to refine the network as it was being built, and validation data were withheld from the training process and used to evaluate the map. The correlation between observed and predicted values for the training and testing groups was carefully monitored as the networks were being built in order to avoid over fitting; the correlation between the testing data and observed data was maintained below 0.7. The relative importance of each variable used in the neural network was evaluated using a global

sensitivity analysis in Statistica. The sensitivity analysis is designed to test how the neural network predictions respond to changes in the input variable. The dataset is repeatedly submitted to the network, but each time one variable is replaced with its mean as calculated from the training data. The error in the resulting network is recorded, and the most important variables are identified as those that, when modified, result in the greatest increase in network error.

Forest biomass was predicted on a pixel-by-pixel basis for all forested regions of SJNF by using physical variables, spectral information and Landsat TM texture calculations as input to the neural network model. The model feature selection process is as follows: initial models were constructed using all combinations of physical, spectral, and texture variables. The model complexity was systematically reduced using the global sensitivity analysis to identify the most important variables in the model. I continued reducing the model complexity by removing the least important predictors as long as reductions continued to improve the model. Model quality was repeatedly evaluated using the four measures of error described below, and these measures were used to choose the final model.

2.2.4 Statistical Analysis. I used four statistical measures to evaluate model performance: Pearson's Correlation (r),

$$r = \frac{\sum(x_i - \bar{x})(y_i - \bar{y})}{\sqrt{\sum(x_i - \bar{x})^2}\sqrt{\sum(y_i - \bar{y})^2}}$$

where x is the observed value, $\bar{x}$ is the average of the observed values, y is the predicted value and $\bar{y}$ is the average of the predicted values; the Root Mean Square Error (RMSE):

$$\text{RMSE} = \sqrt{\frac{\sum(x_i - y_i)^2}{n}}$$

where n is the number of observed values; the Coefficient of Variation of the Root Mean Square Error (CV-RMSE),

$$\text{CV-RMSE} = \frac{RMSE}{\bar{y}}$$

where RMSE is the root mean square error; and Akaike's Information Criteria (AIC),

$$\text{AIC} = \text{n} \cdot \ln\left(\frac{\text{SSE}}{\text{n}}\right) + 2\text{k}$$

where SSE is the summed square error of the model and k is the number of model parameters. AIC is a relative measure of model quality for a given dataset and it provides a means for model selection based on both model fit and model parsimony. In other words, AIC values aid in identifying the model that provides the best description of the data using the smallest number of parameters. Higher quality models are identified by lower AIC values; generally AIC values that differ by >2 indicate that the model with the lower AIC is superior, whereas models with AIC values differing by <2 are similarly effective in describing the data [*Spendelow et al*., 1995].

Biomass prediction quality was also evaluated at fine spatial scales within two regions of the forest with a history of forest disturbance. Forest biomass predicted by the best performing texture-based map was compared to the biomass predicted by the best performing physical-spectral based map for two regions: a region with five forest stands clear-cut in the 1970's, and a region of forest burned by a wildfire in 2002. In each case the average predicted biomass within the disturbed stand was compared to the average predicted biomass in an adjacent undisturbed stand. Stand delineations were obtained from the SJNF FSVeg database.

2.3 Results

The final biomass map was constructed using the best performing neural network model constructed from the texture metrics of entropy, mean and correlation calculated from Landsat Band 2 on a 3x3 window and an offset of [0,1], and the physical variable slope (Table 3.1).

Table 2.1 Correlation between predicted and observed biomass (r), Akaike's Information Criteria (AIC), Root Mean Square Error (RMSE) and Coefficient of Variation Root Mean Square Error (CV-RMSE) for the five best performing neural network models constructed with texture metrics (top 5 rows), and the five best performing neural network models constructed without texture metrics (lower 5 rows). The architecture of each neural network is indicated in the form of input-hidden-output units. The GLCM texture metrics used in the highest preforming models were calculated on Band 2, on a 3x3 window at an (0,1) offset; they are: 1-mean, 2-variance, 3-homogeneity, 4-contrast, 5-dissimilarity, 6-entropy, 7-second moment and 8-correlation.

Parameters	Network Architecture	r	AIC	RMSE	CV-RMSE
6, 1, 8, Slope	4-10-1	0.86	199.0	45.6	0.31
1, 6, 7, Slope, 8, 5	6-9-1	0.81	204.2	52.7	0.36
1, 8, Slope, 6, 5	5-6-1	0.84	207.4	51.9	0.36
1, Slope, 6	3-4-1	0.78	209.1	58.1	0.40
1, Slope, Aspect, 6, NDVI	5-9-1	0.79	211.7	56.4	0.39
Elevation, NDVI, Aspect, Slope	4-8-1	0.57	224.9	76.5	0.53
Elevation, Slope, Aspect	3-3-1	0.44	224.9	79.7	0.55
Elevation, Aspect, Slope, EVI, Precipitation	5-9-1	0.51	226.7	76.3	0.53
Elevation, Aspect, Slope, EVI	4-5-1	0.43	227.6	80.8	0.56
Vegetation Type, Aspect, Slope, Elevation	9-3-1	0.34	229.5	83.9	0.58

The best performing network was determined as the model with the lowest RMSE and CV-RMSE, 45.6 Mg ha^{-1} and 0.31 respectively, the highest correlation between predicted and observed biomass values, 0.86, and the lowest AIC, 199.0 (Table 2.1; Figure 2.2).

Figure 2.2 Observed *versus* predicted biomass values for Landsat TM image texture based biomass map.

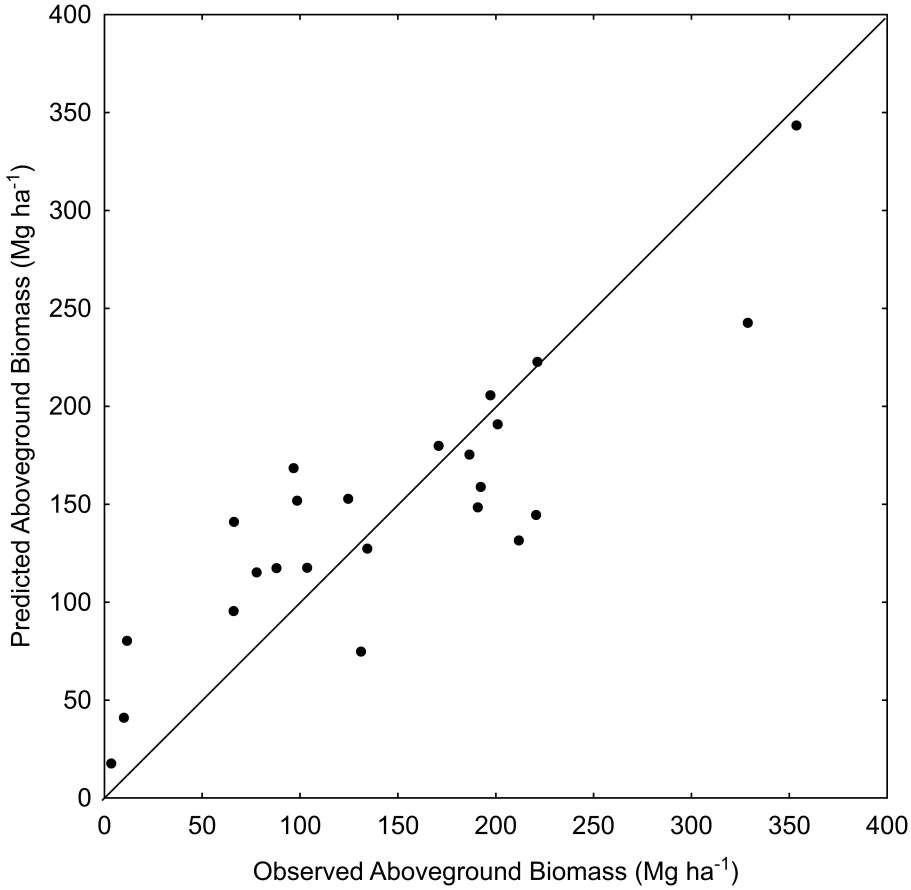

The AIC value of the best performing model differs from the next smallest AIC value of 204.2 by > 5 indicating this model is preferable to the other models investigated (Table 2.1). The texture-based biomass model predicts a wide range of aboveground biomass values across SJNF, with a maximum biomass value of 394 Mg ha^{-1}. Generally the greatest biomass values were predicted in the high elevation regions and smaller biomass values in the lower elevations (Figure 2.3).

Figure 2.3 Landsat TM image texture-based map of aboveground biomass within forested regions of San Juan National Forest. The boxes labeled 4 and 5 indicate the location of Figure 2.4 and Figure 2.5, respectively.

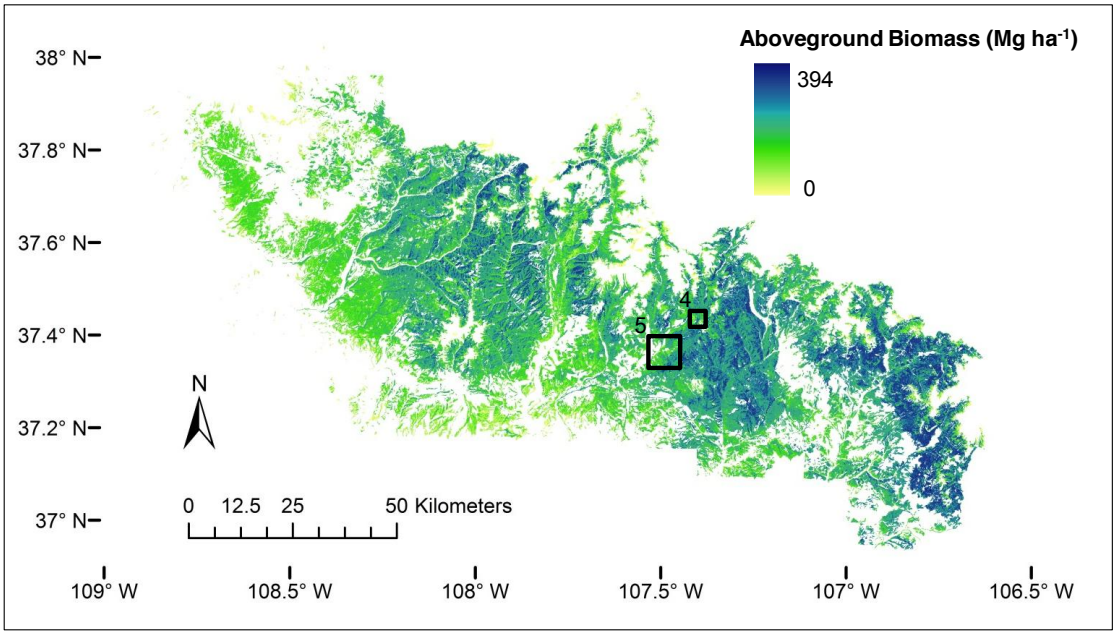

A global sensitivity analysis was used to determine the importance of each variable in the context of this neural network. The texture variable mean contributed the most to this model, followed by correlation, the physical variable slope and the texture variable entropy. The relative importance of each variable is represented by the ratio of model error when the model is constructed excluding and including the variable in question. The relative sensitivities of mean, correlation, slope and entropy are 3.7, 1.8, 1.5, and 1.3 respectively.

Models including texture metrics performed better than those constructed with only physical variables (slope, aspect, elevation, precipitation and vegetation type) and spectral variables (NDVI and EVI; Table 2.1). The best-performing model constructed without any texture information was produced by a network including slope, aspect, elevation and NDVI (Table 2.1), and had a lower correlation, higher error and higher AIC than models including texture.

The texture-based biomass map also appears better able to capture the magnitude and direction of biomass change due to forest disturbance compared to spectral approaches. The texture-based map predicted a larger difference in biomass between untreated stands and adjacent clear-cut stands than the physical-spectral map (Figure 2.4).

Figure 2.4 a) True color image from National Agricultural Imagery Program acquired by a Leica ADS80 Airborne Digital Sensor; b) image texture-based biomass map; and c) physical-spectral (slope, aspect, elevation, Normalized Difference Vegetation Index) based biomass map for a region of San Juan National Forest containing forested stands clear-cut in the 1970's. Color bar and scale bar apply to a), b) and c). d) Observed and modeled stand-average aboveground biomass from adjacent untreated and treated (clear-cut) forest stands. Observed values are calculated from nearby stands of the same vegetation type. Modeled stand-average biomass of treated stands was compared to the stand-average biomass of the untreated stand located directly to the west. Letters indicate locations of biomass comparisons, shown on a).

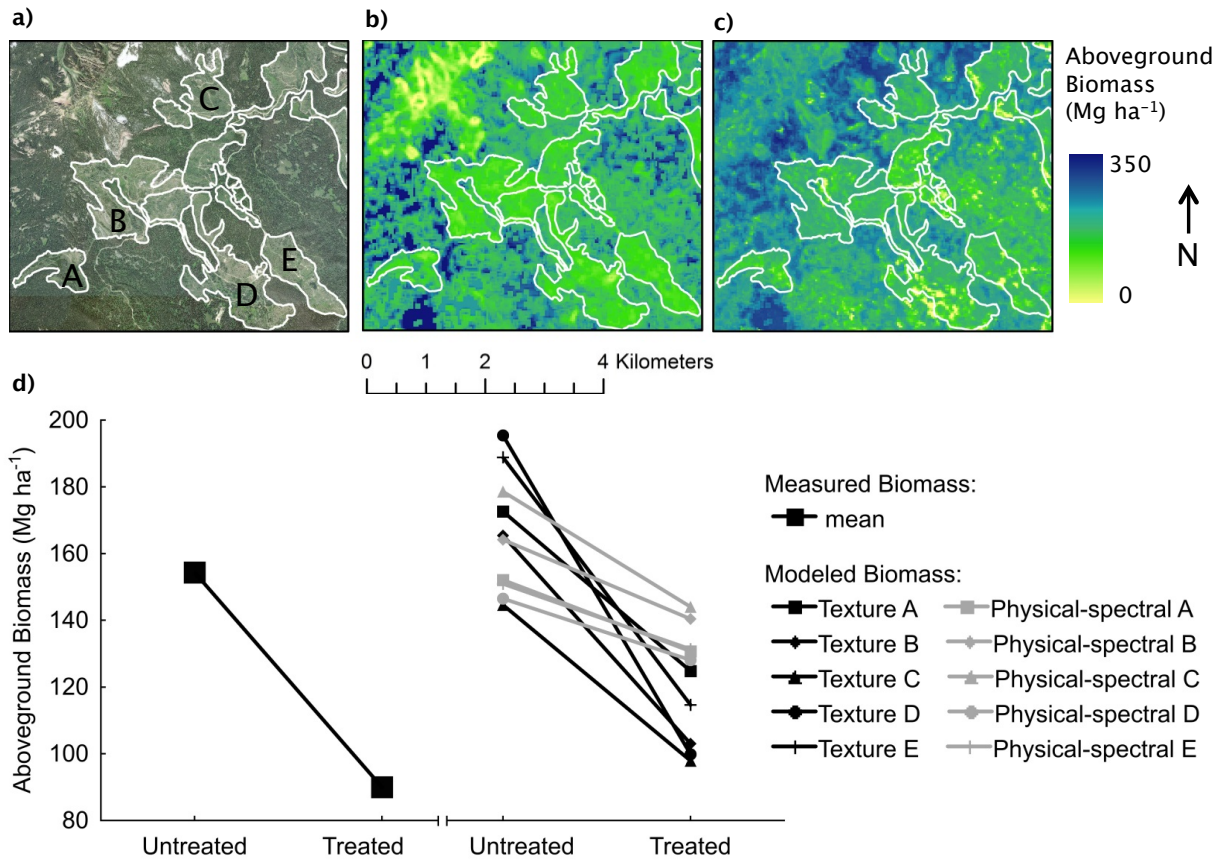

The observed biomass values suggest an average difference of 64.5 Mg ha^{-1} between untreated and clear-cut stands. The texture-based biomass predicted an average difference of 65.3 Mg ha^{-1}

between the clear-cut and untreated stands, whereas the physical-spectral map predicted an average difference of 23.53 Mg ha^{-1} between the clear-cut and untreated stands (Figure 2.4).

The texture-based biomass map also improved prediction quality over the physical-spectral map in a region of San Juan National Forest burned in a wildfire in 2002 (Figure 2.5).

Figure 2.5 a) True color image from National Agricultural Imagery Program, acquired by a Leica ADS80 Airborne Digital Sensor; b) image texture-based biomass map; and c) physical-spectral (slope, aspect, elevation, Normalized Difference Vegetation Index) based biomass map for a region of San Juan National Forest burned by a wildfire in 2002. Color bar and scale bar apply to a), b) and c). d) Modeled stand-average biomass of the burned region was compared to the unburned region to the East of the fire.

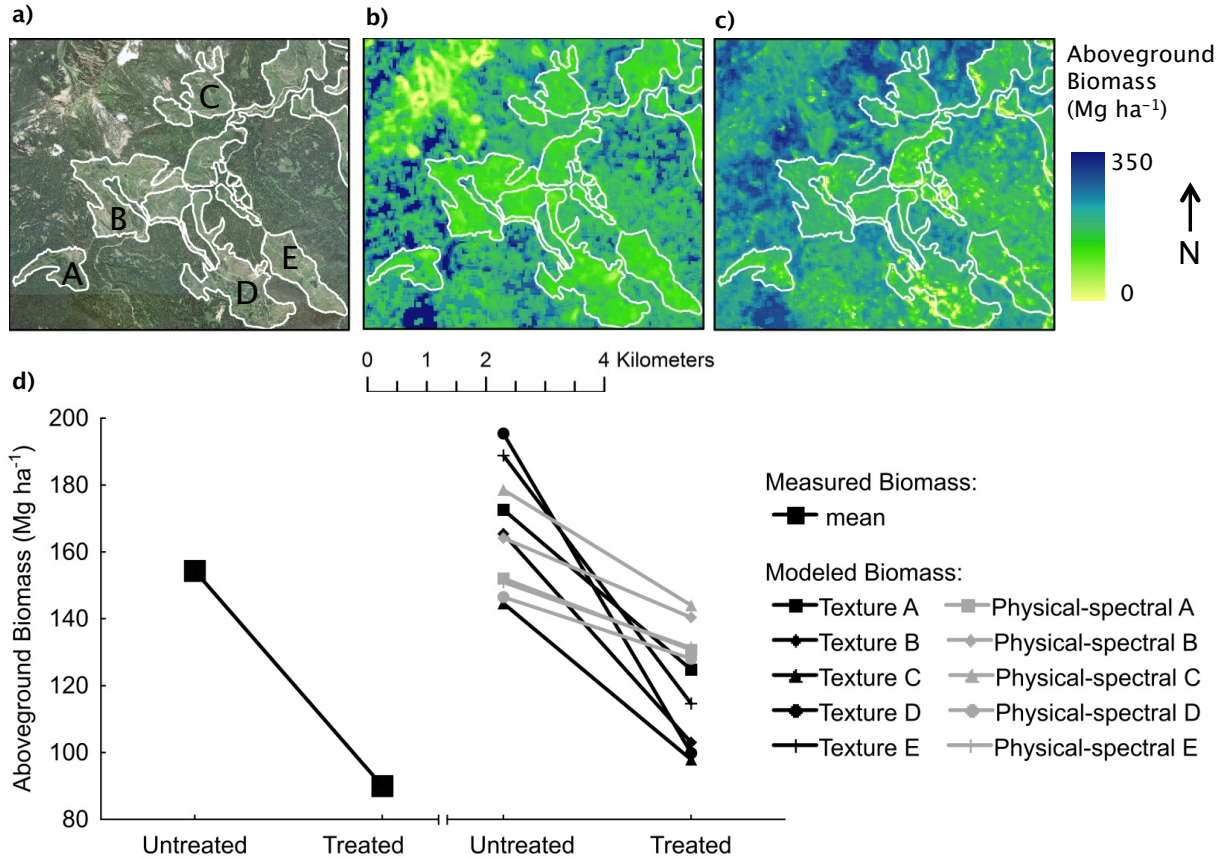

In the eastern portion of the Missionary Ridge Fire burn area, the texture-based map predicted a 52.64 Mg ha^{-1} decrease in biomass between the burned area and the adjacent unburned forest, where as the physical-spectral based biomass map predicted a 14.0 Mg ha^{-1} increase in the amount of biomass present in the burned forest relative to the adjacent unburned forest (Figure 2.5).

2.4 Discussion

In this study I demonstrate the utility of image texture analysis on Landsat TM imagery as a method of improving local biomass estimates. Biomass maps including image texture variables perform better than biomass maps created from physical and spectral variables only. Furthermore, the texture-based biomass map is better able to capture biomass change in response to disturbance than maps created excluding image texture. This analysis provides an alternative avenue for advancing the development of more accurate local biomass maps through a novel application of a widely established remote sensing tool.

2.4.1 Biomass Prediction from Image Texture. Aboveground biomass predicted by the texture-based model was greatest in high elevation regions, and smallest in the low elevation regions (Figure 2.3). This pattern is generally spatially consistent with national scale biomass maps for this region [*Kellndorfer et al*., 2000; *Blackard et al*., 2008], however, the greatest biomass value predicted by the texture-based map, 394 Mg ha^{-1}, is lower than the highest observed biomass for this region (490 Mg ha^{-1}). The correlation between the texture-based model biomass predictions and observed biomass values was r = 0.86 (Table 2.1; Figure 2.2).

My successful use of texture to map biomass in SJNF is encouraging for several reasons. First, the texture-based model was constructed using only publically available data and Landsat TM imagery, whereas most existing biomass maps are constructed from a large suite of geospatial predictors. Although I recognize that many spatial predictors are needed for national scale maps, I suggest that alternate approaches, such as use of texture analysis, may be more appropriate for local maps. Secondly, I believe that texture analysis may be able to improve biomass estimation in regions of forest where spectral indices such as NDVI can saturate. Unlike NDVI, which is calculated on a pixel-by-pixel basis, texture is calculated from a small neighborhood of pixels and the size of this neighborhood can be adjusted to maximize the potential for texture to predict biomass. I find that texture is particularly useful in regions of

disturbed forest (Figures 2.4 and 2.5), where the texture-based map is more sensitive to changes in forest biomass than a map produced from physical and spectral variables. Furthermore, texture analysis also has the potential to be sensitive to changes in forest biomass even in regions of dense canopy; studies from tropical forests indicate that texture correlates with biomass more strongly than spectral indices [*Eckert*, 2012], and texture is correlated with biomass in some regions where spectral signatures are not [*Lu*, 2005]. Finally, I also acknowledge the possibility that the success of texture in predicting forest biomass is partially due to the aggregation process of the window used in texture analysis accounting for errors between image geo-rectification and GPS field locations. If the Landsat image is offset by even just one pixel, the plot locations will be 30 meters removed from the corresponding pixel in the Landsat image. In this case texture analysis may help account for this geographic error by aggregating pixel values over the window used in texture analysis (*i.e.*, 3×3).

There are several opportunities for introduction of error into the texture-based biomass model. First, the ground-based FIA plots used in the model were sampled between 2002 and 2009, whereas the Landsat scenes used for the texture calculation were acquired in 2011. While the Landsat scenes I used in the analysis are temporally consistent with the recently sampled FIA plots, there is almost a 10-year lag between the sampling date of the earliest plots, and the time of Landsat image acquisition. During this time the amount of biomass on the landscape could have changed due to growth or disturbance, thereby introducing error into the resulting map. However, the direction of the map errors (the map under predicts biomass) is not consistent with errors introduced due to forest disturbances that remove biomass such as forest treatment or wildfire. In the case of disturbances including treatment and wildfire, forest biomass on the landscape would decrease, and therefore the biomass map would over predict forest biomass for disturbed areas. In contrast, my map under predicts forest biomass in some regions.

2.4.2 Texture Analysis for Local Biomass Maps. The texture-based biomass map I present here is an effective method for developing local forest biomass maps, and could have

substantial implications for carbon accounting and land management purposes. Local biomass maps are important for tracking biomass stocks and carbon fluxes in regions such as National Forests, which are sites of frequent land management and disturbance. My texture-based biomass map is particularly sensitive to changes in biomass following disturbance, and actually improves biomass predictions within disturbed regions relative to maps made from exclusively physical and spectral variables. Specifically, the texture-based map produced biomass predictions that closely match observed biomass values from nearby forest stands of the same vegetation type and treatment history (Figure 2.4). Furthermore, the physical-spectral map predicted an increase in forest biomass in a region of recently burned forest relative to the adjacent unburned forest, whereas the texture-based map predicted a decline in forest biomass in the burned region (Figure 2.5). I believe this result is due to high prevalence of understory vegetation growing in the burned region, resulting in high NDVI but low biomass. Because texture appears to be sensitive to changes in forest biomass following disturbance in SJNF, I suggest that texture may be an important tool not only for creating biomass maps in regions such as national forests, but also for updating these maps following disturbance or management. The Landsat data used to construct this map are available on sub-annual timescales so map updates are not subject to constraints in data acquisition. Potential future climate change mitigation policies enacted through forest management, or trading schemes introduced under cap-and-trade type policy, will rely on biomass maps to inform decisions, and image texture analysis provides a potential avenue to make necessary improvements to local biomass estimates.

2.5 Conclusions

Local forest biomass maps are necessary for understanding and anticipating the effects of disturbance and management on forest area, habitat, and local carbon stocks and fluxes. In this study I use a combination of physical variables, spectral information and image texture metrics calculated from Landsat TM imagery to create a local forest biomass map within San Juan National Forest in southwest Colorado, USA. Aboveground biomass maps were created using

neural networks constructed from Forest Inventory and Analysis Program ground-based biomass observations and the corresponding physical, spectral and image texture information for each plot location. I draw the following conclusions:

- Biomass models constructed including image texture variables are more strongly correlated with observed biomass than those constructed using physical and spectral information alone.
- This texture-based biomass model is sensitive to changes in forest biomass following disturbance such as logging and wildfire; the texture-based model I present in this paper is better able to predict the direction and magnitude of biomass change following disturbance than biomass models constructed without the use of image texture.
- Because the Landsat data used to construct this map are available on sub-annual timescales, texture may be an important tool for creating and updating biomass maps following local forest disturbance or land management actions.
- The methods I present here are widely applicable across the US because I use entirely publically available data processed with relatively simple analytical routines.

The next steps of this research will include evaluating the transferability of this local texture-based biomass model to other geographic regions with varying vegetation and disturbance regimes.

CHAPTER III

SHORT AND LONG-TERM CARBON BALANCE OF BIOENERGY ELECTRICITY PRODUCTION FUELED BY FOREST TREATMENTS

3.1 Introduction

Forests are an important component of the global carbon cycle because of their role as a terrestrial carbon sink and their potential for long-term carbon storage. Many types of natural and human induced disturbances affect forest carbon storage including wildfire, insect outbreaks and drought. In the Intermountain West, forests are also commonly modified by fuel reduction treatments performed to reduce the risk of high severity wildfire, restore forests modified by fire suppression, and to protect homes in the wildland urban interface. Fuel reduction treatments also influence forest carbon balance both through their potential to modify fire behavior in recently treated forest stands, and because the treatments themselves remove woody biomass from the forest [*Finkral and Evans*, 2008; *North et al*., 2009; *Stephens et al*., 2009; *Dore et al*., 2010].

Forest fuel reduction treatments are designed to reduce fire severity by modifying surface fire behavior, reducing the risk of fire spreading from the ground surface to the forest canopy, and limiting fire spread within the forest canopy by decreasing canopy bulk density [*Agee and Skinner*, 2005]. A number of studies indicate that fuel reduction treatments do reduce wildfire severity [*Weatherspoon and Skinner*, 1995; *Pollet and Omi*, 2002; *Cram et al*., 2006; *Ritchie et al*., 2007; *Fulé et al*., 2012], and in some cases fuel treatments have been credited with altering the course of a wildfire when it encounters a previously treated area [*Finney et al*., 2005].

Forest fuel reduction treatments have also been proposed as a potential technique to limit carbon emissions from wildfire in some ecosystems [*Hurteau et al*., 2008; *Hurteau and North*, 2009]. Forest treatments are designed to reduce mortality that would result from a high severity fire, and therefore they may ultimately limit wildfire carbon emissions to the atmosphere because carbon is maintained in the biomass of live trees [*Finkral and Evans*, 2008; *Mitchell et al*., 2009; *Stephens et al*., 2009; *Hurteau et al*., 2011]. However, because forest treatments also remove woody biomass from the forest [*North et al*., 2009; *Stephens et al*., 2009], there is debate regarding whether the reduction in pyrogenic emissions is greater than the reduction in biomass during treatment [*Campbell et al*., 2012]. Most pyrogenic emissions result from the combustion of surface fuels that burn comparably in both high and low intensity fires [*Meigs et al*., 2009]. High intensity fires produce only 30% more direct emissions than low intensity fires, and fuel reduction treatments can remove as much or more biomass from the forest as is lost in a high intensity wildfire [*Campbell et al*., 2012]. In some cases the total carbon emissions from treatment and subsequent wildfire may be greater in a treated forest stand than an untreated stand [*North and Hurteau*, 2011]. Furthermore, not all treated forest stands are likely to experience a wildfire because of the low probability of fire occurring in one location during a given time period [*Campbell et al*., 2012], so some treated stands will have reduced carbon stores without any benefit from avoided pyrogenic emissions. Ultimately the carbon balance of a forest treatment will depend both on the fate of biomass harvested during treatment and the timeline of investigation.

There are two potential fates of carbon in harvested biomass, emission to the atmosphere or stabilization, and the balance between emission and stability may shift depending on the timeline of interest (1, 10, 100 years). Immediately following a forest treatment, woody debris

may be burned or left in the forest to decompose where it will result in emission of carbon to the atmosphere, or the carbon contained within harvested biomass may be may be stabilized if it used for timber and ultimately converted to durable goods [*Finkral and Evans*, 2008]. An increasingly common fate for woody biomass is as a fuel for bioenergy-based electricity generation (Figure 3.1).

Figure 3.1 Sources of carbon emissions and types of carbon stabilization for different fates of harvested biomass following a forest fuel reduction treatment.

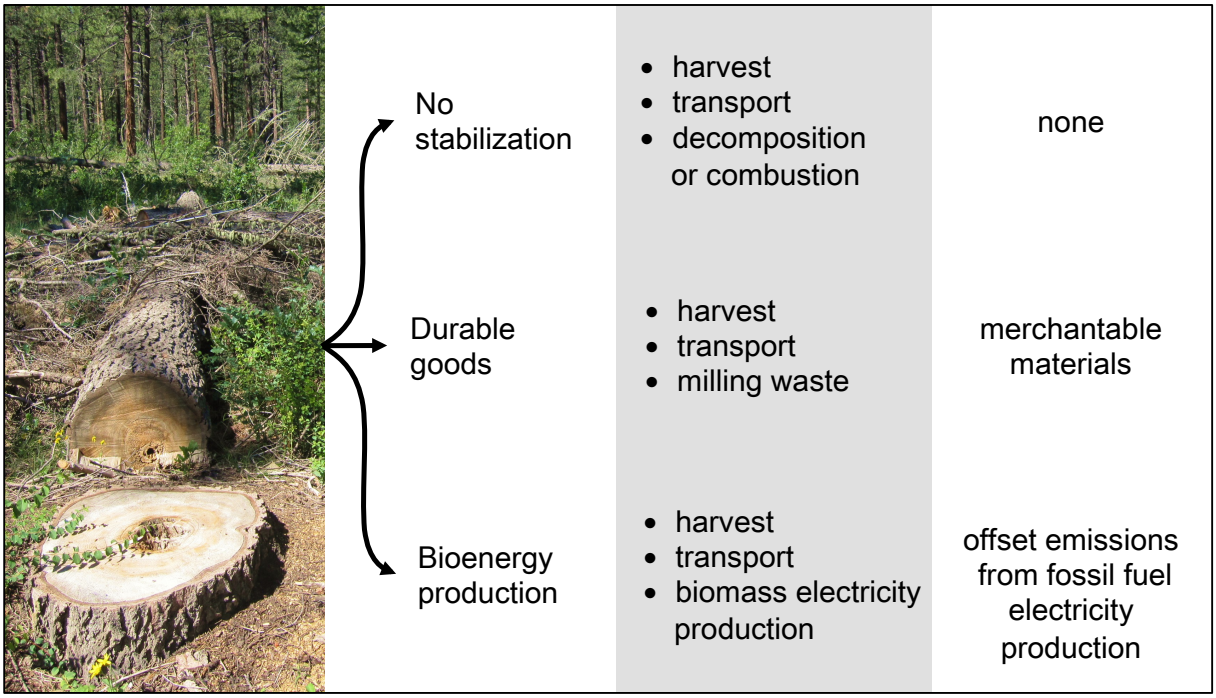

The small diameter trees and understory biomass removed from forests during treatment can be directly combusted or converted to a synthetic natural gas, with both used for electricity production. Such use of biomass can stabilize carbon by offsetting carbon emissions from fossil fuels, and via sequestration of carbon during forest regrowth. However, bioenergy use also results in emissions of carbon during harvest, transport and electricity generation, with potential implications for overall carbon sequestration. Further, these processes can be of variable

efficiency. For example, synthetic natural gas, or syngas, is produced from biomass by a thermochemical process called gasification (only partially efficient) that converts the biomass into fuel through partial oxidation at elevated temperatures [*Pereira et al.*, 2012]. High moisture content of the woody biomass can reduce the efficiency of the gasification process [*Ruiz et al.*, 2013], producing further emissions. During electricity production, the syngas is combusted and the carbon within the syngas is emitted to the atmosphere.

To investigate the carbon implications of fuel reduction treatments and the use of woody biomass for bioenergy electricity generation, I evaluate the carbon emissions and the short-term and long-term carbon balance of a 5MW demonstration biomass gasification power plant in San Juan National Forest in southwest Colorado (Figure 3.2) under varying scenarios of forest treatment, disturbance and regeneration. I ask these questions:

(1) What are the relative carbon emissions of electricity generation from biomass and electricity generation from coal?

(2) How does the use of woody biomass for electricity generation change the carbon balance of forest fuel reduction treatments on a short-term (1 year) and long-term (100 years) time frame?

(3) How do treatment and bioenergy production affect forest carbon balance after a fire? How does post-fire carbon balance vary over differing scenarios of future fire intensity and regeneration?

Figure 3.2 Arial image of the study area within San Juan National Forest, and location of San Juan National Forest in Southwest Colorado, USA.

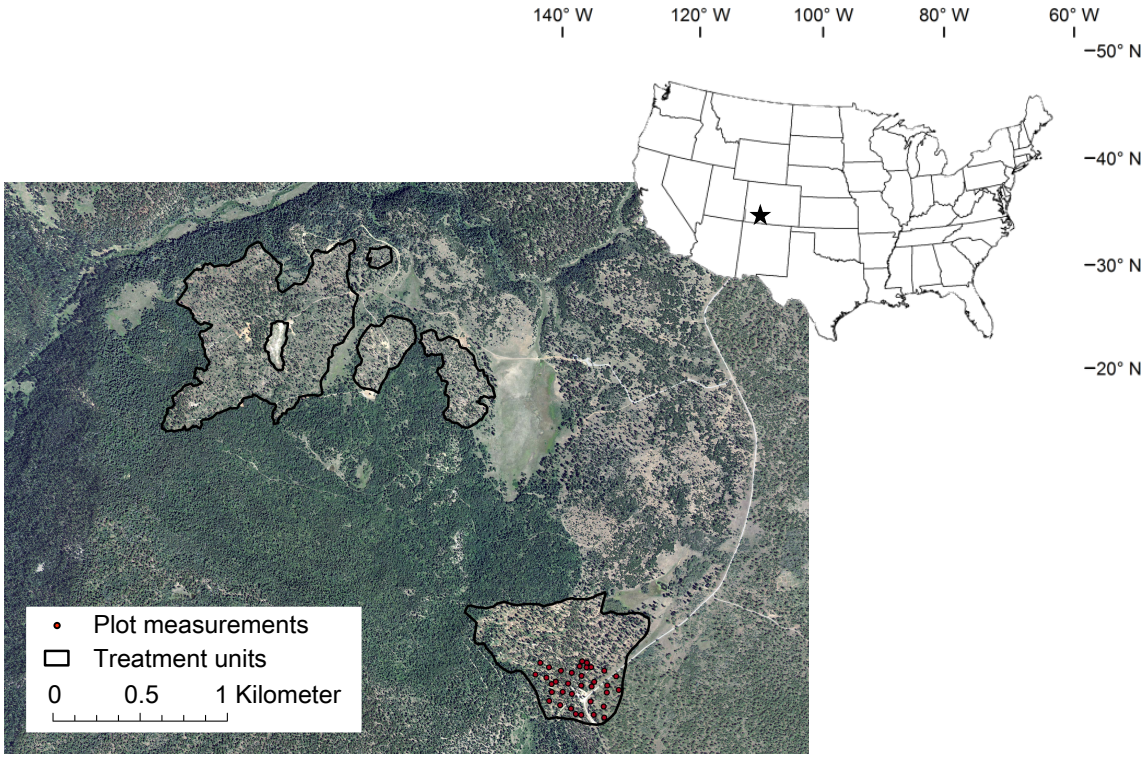

3.2 Materials and Methods

3.2.1 Study Site. The site of this study was the Turkey Springs Demonstration Area in the eastern portion of San Juan National Forest (SJNF). The site is located at 37° 15' N and 107° 10' W, and at 2500 meters elevation (Figure 3.2). Average maximum and minimum temperatures are 14.2°C and -2.16°C respectively, and average annual precipitation is 618.4 mm (http://prismmap.nacse.org/nn/). The total area of the Turkey Springs demonstration site is 116 hectares. The site is broken into five units, Units 1-5. All biomass measurements were made on Unit 5, which is 39 hectares in size. Biomass values from Unit 5 were used for the area of all units, which are covered by the same vegetation type. Units 1 through 4 have a similar management history as Unit 5; records of historical treatment activities maintained by the Forest Service indicate that all units were harvested by individual tree selection in 1967, parts of Units

3, 4 and 5 were commercially thinned in 1968, and the east half of Unit 5 was logged again in 1983. Vegetation present at the site is dominantly ponderosa pine (*Pinus ponderosa* Dougl. Ex Laws) with scattered pockets quaking aspen (*Populus tremuloides* (Michx.)), douglas fir *(Pseudotsuga menziesii* Mirb.), white fir *(Abies concolor* (Gord. & Glend.)) and gambel oak (*Quercus gambelii* Nutt.).

3.2.2 Forest Biomass. Forest biomass present before treatment was measured in 2011 using 34 circular inventory plots, each 80 m^2 in area (diameter = 10.24 m). Within each plot the diameter of every tree over 1.37 m tall was measured at 1.37 m to obtain a measure of diameter at breast height (DBH) for all trees within the plot. Aboveground live tree biomass was calculated from tree DBH using allometric equations from Jenkins et al. (2004) and Kaye et al. (2005). Aboveground live tree biomass for the plot was determined as the sum of all trees present on that plot, and carbon was calculated as 50% of dry biomass [*Penman et al*., 2003]. Biomass inventory plots were re-measured in 2012 following the fuel reduction treatment using the same inventory methodology. The amount of forest biomass removed during the demonstration fuel reduction treatment was determined by weighing all woody material as it was removed from site. Dry biomass was determined by assuming 45% moisture content of material removed.

3.2.3 Bioenergy and Coal Reference Systems. The reference bioenergy system I investigate is assumed to produce 5.0 Megawatts of electrical power (MW) and operate 8000 hours per year (91% operating time). 58,400 Mt of wet biomass (45% moisture) will be necessary to fuel 5 MWe production. Once the raw wood is harvested and transported, it is dried

to 20% moisture. The wood is then converted to syngas, which is used to fuel the internal combustion engines of the plant.

Total carbon emissions from a hypothetical 5 MW coal reference system were calculated to compare the carbon intensity, or the carbon emissions per unit energy, of the coal to that of the bioenergy electricity generation system. Coal was chosen as a reference system because coal is the primary energy source for Southwest Colorado [*CGEO*, 2010]. Total emissions from the coal reference system included three components: mining, transportation, and combustion. Mining, transportation and combustion emissions were calculated based on values from Kerr, Mann and Spath [1999]. The coal reference system was assumed to operate at 32% efficiency and use coal with 70% carbon content [*Spath et al.*, 1999]. I also calculated ash production during coal combustion, and subtracted ash carbon content from total carbon emissions from the system. No assumption was made regarding the eventual fate of the ash; for this work here I do not consider further emissions from ash decomposition.

3.2.4 Bioenergy and Forest Harvest Emissions Expected carbon emissions from the bioenergy power plant are derived from three primary sources: emissions associated with biomass removal and transport, emissions from syngas production, and emissions from syngas combustion. The first source of emissions from bioenergy production was emissions associated with biomass harvest and transport. Operational hours for each piece of equipment used in all 5 Units (116 hectares) of the fuel treatment area were tracked by the biomass harvesting team and used to calculate total emissions [*EPA*, 2010]. Emissions from transportation of biomass from the treatment site to the bioenergy facility were also calculated based on the total hours of operation, and the average fuel consumption per hour for both gasoline and diesel [*EPA*, 2010].

I calculated carbon emissions for syngas production (gasification) based on projections that 8000 operational hours are necessary to produce 5 MW of electricity, and carbon emissions from biomass gasification obtained from Basu [2010]. Total emissions from combustion within the bioenergy system included both syngas production for electricity generation, and also the combustion of natural gas necessary to maintain the high internal temperature of the gasification operation. Using the projected syngas composition and the volumes of biomass and natural gas necessary for 5 MW of electricity production, gas volumes for each constituent of gas were converted to grams of carbon, and summed to determine total projected emissions for syngas combustion. Carbon emissions from natural gas combustion were determined from projections of net gas consumption and gas composition obtained Liuewen et al. [2010]. All char produced through the gasification process was considered an emission to the atmosphere.

3.2.5 Forest Growth and Disturbance Modeling. Forest growth and the effects of future disturbance were modeled using the Central Rockies variant of the Forest Vegetation Simulator (FVS) and the Fire and Fuels Extension (FEE) [*Dixon*, 2008]. FVS is a widely used forest growth and yield model, and is frequently used to inform ponderosa pine management [*Teck et al.*, 1996]. The FEE can be used to predict tree mortality, fuel consumption and carbon emissions following fire based on inputs of weather, fuel, and stand characteristics [*Reinhardt and Holsinger*, 2010]. I used FVS-FEE to simulate the carbon emissions associated with the fuel reduction treatment in 2011 and the prescribed fire following treatment in 2013. FVS was also used to determine live tree and total stand carbon following repeated treatments recurring every 40 years designed to reduce stand basal area to 7.4 m^2 (80 ft^2).

I also investigated three scenarios concerning the fate of biomass removed during forest treatment: a 'no stabilization' scenario which is considered the 'business-as-usual scenario, a scenario where biomass is used for durable goods, and finally one in which all biomass removed during treatment is used for bioenergy electricity production. FVS was used to simulate the amount of biomass removed from the forest during treatment. Projections from FVS were also used to determine what fraction of the biomass removed was considered merchantable, defined as a bole with a top diameter greater than 10.2 cm. Forty percent of merchantable material was assumed to be lost as milling waste, and the remaining 60% converted to durable goods [*Skog and Nicholson*, 2000; *North et al*., 2009].

FVS was also used to project changes in total stand carbon and live tree carbon associated with a future wildfire at this site in 2030. Wildfires tend to burn in a highly heterogeneous manner, with patches of lightly burned and intensely burned forest depending on variables including weather conditions and landscape patterns [*Turner and Romme*, 1994]. Because it is impossible to know the severity and intensity of a future wildfire at this site, I simulated 96 future wildfires by varying the wildfire controls present within FVS. The wildfire controls present within FVS are: wind speed, fuel moisture, air temperature, percentage of stand burned, and the season of the fire. For my model simulations, I varied wind speed between 16.09, 32.18, 48.28 and 64.37 kilometers per hour, fuel moisture was varied between 'very dry' and 'moist' settings, percentage of stand burned was varied between 40 and 90 percent in increments of 10, and the season of the fire was set as 'early season (compact leaves)' and 'after greenup (before fall)'. Air temperature was maintained at 29.4 degrees Celcius. I also varied the prescription of future forest regeneration to account for uncertainties in regeneration under future climate and wildfire conditions. Regeneration scenarios were based on empirical data from

Savage and Mast [2005], indicating that 50% of ponderosa pine sites investigated following a stand-replacing fire did not regenerate. No regeneration was prescribed in either the treated or untreated stand until after the wildfire. All fire and regeneration scenarios were run on a treated and untreated forest stand for a total of 384 simulations.

3.3 Results

3.3.1 Relative Carbon Intensity of Biomass and Coal Electricity Production. I found that electricity generation through biomass gasification produces almost twice the carbon emissions of a hypothetical coal reference system for the same amount of electricity production (Figure 3.3).

Figure 3.3 Carbon emissions for 8000 hours of 5 MW electricity produced from bioenergy and a coal reference system.

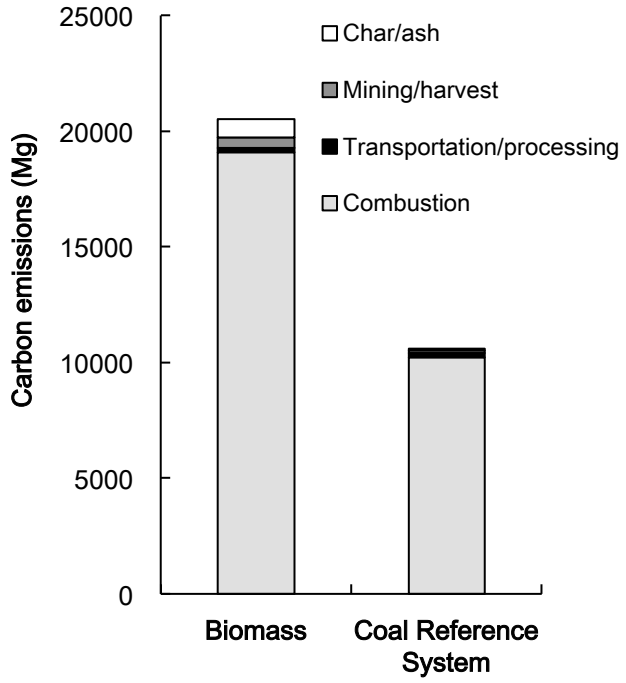

The projected carbon emissions from biomass harvest, transportation, and electricity production for the amount of biomass necessary to fuel 5 MW electricity production for 8000 operational

hours (estimated operation for one year), was 20,510 Mg C. The calculated emissions from the coal reference system for 8000 operational hours was 10,580 Mg carbon (Figure 3.3). These emissions are equivalent to emissions of 20.0 Mg carbon ha^{-1} for biomass electricity production and 10.3 Mg carbon ha^{-1} for coal electricity production according the number of hectares that must be treated annually on SJNF (1024 ha) to harvest the necessary amount of biomass.

3.3.2 Short-term Carbon Balance of Bioenergy Production. The use of woody biomass for electricity generation reduces short-term net carbon emissions relative to other forest treatment scenarios investigated: one in which merchantable biomass is stored in durable goods, and a second 'business-as-usual' scenario in which the forest is treated, but all of the woody biomass removed from the forest is all allowed to decompose (Table 3.1).

Table 3.1 Total carbon (C) emissions, total carbon stabilized and net carbon emissions over one year from forest treatment considering three fates of harvested biomass: no biomass stabilized (business-as-usual scenario), merchantable timber stabilized in durable goods, and use of woody biomass in bioenergy production.

	Total Emissions	C Stabilized in Durable Goods	C Offset through avoided coal emissions	Net Emissions
No Stabilization (Business-as-usual)	-19.23	0.00	0.00	-19.23
C Stabilized in Durable Goods	-13.75	5.48	0.00	-13.75
C Stabilized in Bioenergy production	-20.03	0.00	10.33	-9.70

The bioenergy scenario reduces carbon emissions relative to the other two scenarios largely because the carbon emissions from bioenergy production (20,510 Mg C) were partially offset by the avoided emissions from coal-generated electricity production (10,580 Mg C). To determine emissions from the 'durable goods' scenario, I used simulations from the forest growth model

that indicate that 49.5% of the biomass removed from the forest during treatment is considered merchantable. I assume that 60% of the total amount of carbon contained within the merchantable biomass (5611.6 Mg C) is sequestered in durable goods and therefore the total emissions from the forest treatment are equal to 14,082.4 Mg carbon or 13.8 Mg carbon ha^{-1}. The net short-term emissions from bioenergy production were 9929 Mg carbon or 9.7 Mg carbon ha^{-1}. The projected emissions for the no stabilization scenario are 19,694 Mg carbon, or 19.2 Mg carbon ha^{-1}.

3.3.3 Long-term Carbon Balance of Bioenergy Production. On a long-term time frame (>100 years), the use of woody biomass removed during forest treatments for electricity generation has a large effect on forest carbon balance. Repeated forest treatments reduce total stand C. Stand regrowth following treatment allows for some recovery of stand carbon storage through time (Figure 3.4a), but in many cases the repeated treatments necessary to maintain low risk of wildfire result in total stand carbon remaining below the pre-treatment stock (Figure 3.4b).

Figure 3.4 a) Total stand carbon b) net stand carbon c) cumulative carbon offset through bioenergy production and avoided coal emissions and d) net stand carbon including carbon offset in a stand with repeated treatments. e) Forest wide carbon balance with forest treatments to fuel bioenergy production every year through 2100.

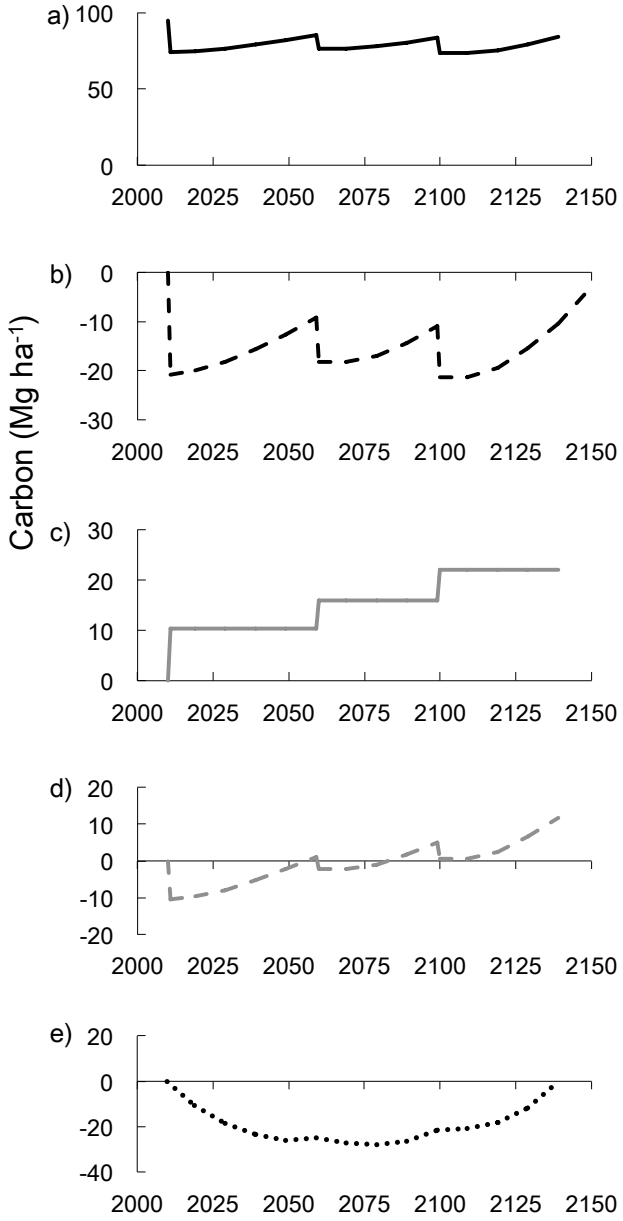

Without any sequestration of the harvested biomass, the repeated treatments will result in a net emission of carbon to the atmosphere, even if there is forest regrowth between treatments. However, the use of woody biomass for bioenergy production sequesters carbon in the form of an offset of coal-generation carbon emissions. Through time as more treatments are completed,

and more coal emissions are offset through bioenergy electricity production, the total amount of carbon sequestered increases (Figure 3.4c). I find that for the forest stand investigated here, the amount of carbon sequestered by bioenergy production via syngas and forest re-growth surpasses the carbon deficit incurred by the reduction in forest biomass before the end of this century (Figure 3.4d). If the treatments are repeated forest wide through 2100, the net carbon balance, including the coal offset, reaches zero around 2140 (Figure 3.4e). Following 2140, the net carbon balance of the forest is going to remain positive, even if the forest treatments are repeated indefinitely. The positive carbon balance is maintained because the amount of carbon offset due to bioenergy production increases with each treatment, even though repeated treatments continue reducing forest biomass below pre-treatment levels. In other words, once the cumulative amount of carbon removed during treatment is surpassed by the cumulative amount of carbon offset through bioenergy production and carbon sequestered during forest regrowth, the forest carbon balance will remain positive.

3.3.4 Carbon Balance of Bioenergy Treatments and Future Wildfire. Simulated post-wildfire stand carbon stocks vary depending on wildfire intensity and stand treatment history. I found that the range of simulated post-wildfire total stand carbon values was greater in an untreated stand than in a treated stand. Potential total stand carbon in 2100 ranged from 87 to 166 Mg carbon ha^{-1} in the untreated forest, and from 75 to 109 Mg carbon ha^{-1} in the treated forest (Figure 3.5).

Figure 3.5 a) Total stand carbon in a forest stand treated mechanically in 2011 and with prescribed fire in 2013, followed by multiple simulations of varying intensity wildfire and regeneration in 2030; b) total stand carbon in an untreated forest stand with simulations of varying intensity wildfire and regeneration in 2030. Dark lines (numbered 1, 2, 3, 4, 5) represent the selected comparisons presented in Tables 3.2, 3.3 and 3.4.

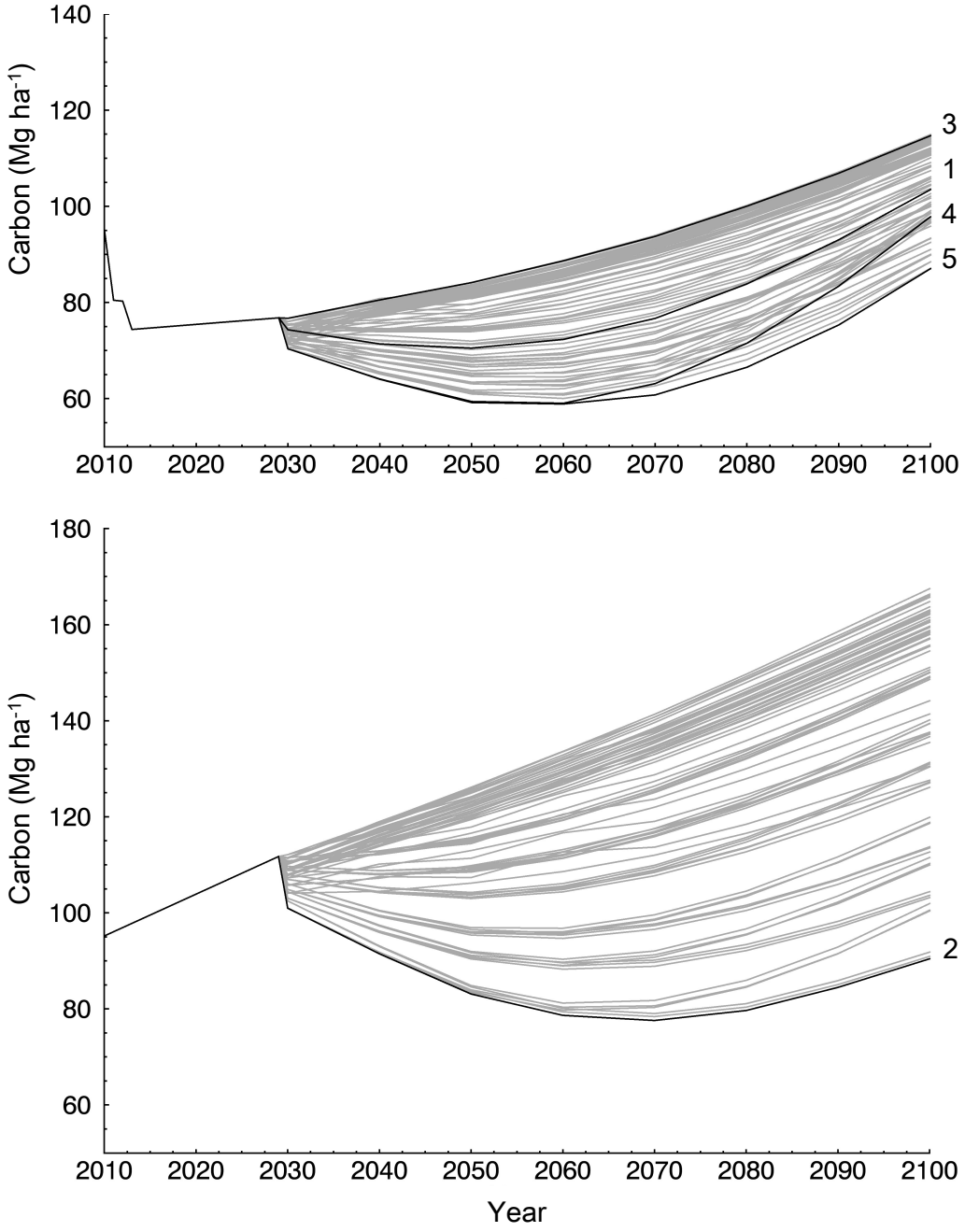

The untreated forest also had a greater minimum and maximum total stand carbon value than the treated forest. However, the introduction of fuel treatments modified fire behavior; I find that in a selected comparison of a treated and untreated forest stand that both burn in a wildfire, the treated stand maintains more live tree carbon and total stand carbon in 2100 than the untreated stand, due to the difference in wildfire fire intensity and severity following forest treatment (Table 3.2).

Table 3.2 Effects of treatment on fire behavior and forest carbon (C) balance.

					2100		
Plot	Treated	Bioenergy	Wildfire Intensity	Regeneration	Δ Live Tree C (Mg ha^{-1})	Δ Total Stand C (Mg ha^{-1})	Net C balance (Mg ha^{-1})
1[a]	Y	Y	moderate	normal	35.98	10.01	20.31
2[b]	N	N	high	reduced	-31.19	-4.75	-4.75

[a] Wildfire parameters in FVS: windspeed, 16.09 km/hr; fuel moisture, very dry; 40% stand burned; season, 'before fall'; regeneration, 300 trees per acre
[b] Wildfire parameters in FVS: windspeed, 64.37 km/hr; fuel moisture, very dry; 90% stand burned; season, 'before fall'; regeneration, 0 trees per acre

A selected comparison of the effects of forest treatment on year 2100 forest carbon balance following wildfire. The effects of the treatment and subsequent changes in wildfire intensity and regeneration are reflected in the 'Δ Live Tree C' and 'Δ Total Stand C' columns, and the effect of treatment and bioenergy production is shown in the 'Net C balance' column. 'Wildfire Intensity' is a qualitative descriptor of the wildfire parameterizations used in the forest growth model. The Plot column indicates the line number depicted in Figure 3.5.

In this example, the treatment results in 14.76 Mg ha^{-1} of avoided pyrogenic carbon emissions, plus 10.3 Mg ha^{-1} of carbon due to the offset of carbon emissions from the replacement of coal energy production with bioenergy production.

Forest treatment and bioenergy production also have the potential to reduce carbon emissions even without avoided pyrogenic emissions due to the offset of coal-generated emissions. In a selected comparison of two treated forest stands with low severity fire, the use of biomass for electricity production increased the net carbon balance from 19.50 Mg ha^{-1} in a

treatment without bioenergy production to 29.80 Mg ha^{-1} in a treatment with bioenergy production (Table 3.3).

Table 3.3 Effects of bioenergy production on forest carbon (C) balance

					2100		
Plot	Treated	Bioenergy	Wildfire Intensity	Regeneration	Δ Live Tree C (Mg ha^{-1})	Δ Total Stand C (Mg ha^{-1})	Net C balance (Mg ha^{-1})
3[a]	Y	Y	low	normal	19.53	19.50	29.80
3[a]	Y	N	low	normal	19.53	19.50	19.50

[a] Wildfire parameters in FVS: windspeed, 16.09 km/hr; fuel moisture, moist; 40% stand burned; season, 'early season'; regeneration, 300 trees per acre

A selected comparison of the effects of bioenergy production from biomass harvested during forest treatment on year 2100 forest carbon balance following wildfire. The effects of bioenergy production on carbon balance are evident in 'Net C balance' column, and would be the same regardless of wildfire intensity or regeneration parameters. 'Wildfire Intensity' is a qualitative descriptor of the wildfire parameterizations used in the forest growth model. The Plot column indicates the line number depicted in Figure 3.5.

Finally, regeneration following wildfire also influences forest net carbon balance in 2100. In a comparison investigated here, a forest stand with normal regeneration following a high severity fire reaches a positive carbon balance by 2100, whereas a stand that burns in the same wildfire but does not regenerate has a negative carbon balance in 2100 (Table 3.4).

Table 3.4 Effects of regeneration on forest carbon (C) balance

					2100		
Plot	Treated	Bioenergy	Wildfire Intensity	Regeneration	Δ Live Tree C (Mg ha^{-1})	Δ Total Stand C (Mg ha^{-1})	Net C balance (Mg ha^{-1})
4[a]	Y	Y	high	normal	-17.68	2.65	12.95
5[b]	Y	N	high	reduced	-27.06	-8.15	-8.15

[a] Wildfire parameters in FVS: windspeed, 64.37 km/hr; fuel moisture, very dry; 90% stand burned; season, 'before fall'; regeneration, 300 trees per acre
[b] Wildfire parameters in FVS: windspeed, 64.37 km/hr; fuel moisture, very dry; 90% stand burned; season, 'before fall'; regeneration, 0 trees per acre

A selected comparison of the effects of varying regeneration and bioenergy production on year 2100 forest carbon balance following wildfire. The effect of regeneration on carbon balance is shown in the difference in 'Δ Total Stand C' and the effects of bioenergy production plus regeneration is shown in the 'Net C balance' column. 'Wildfire Intensity' is a qualitative descriptor of the wildfire parameterizations used in the forest growth model. The Plot column indicates the line number depicted in Figure 3.5.

3.4 Discussion

Here I explore the short-term (~1 year) and long-term (~100 year) carbon balance of a demonstration fuel reduction treatment with use of woody biomass for bioenergy electricity production. I find that although bioenergy is a more carbon intensive energy source than coal, the use of bioenergy production in this forest reduces overall treatment emissions relative to other treatment scenarios investigated. I also find that while repeated forest treatments can lower forest carbon storage, when the harvested biomass is used for electricity generation, the carbon sequestered by offsetting coal-generated carbon emissions results in a net carbon sink by 2140. In addition to the carbon benefit obtained through bioenergy production, the forest treatment may also reduce carbon emissions through avoided pyrogenic emissions in a subsequent wildfire. However, the carbon benefit incurred through the bioenergy production is comparable, or in some cases smaller, than the changes in stand carbon due to variable wildfire intensity or regeneration. Future changes in disturbance or regeneration regimes also have the potential to affect forest carbon balance in addition to the use of bioenergy for electricity generation.

3.4.1 Short-term Carbon Balance of Bioenergy Production. Bioenergy electricity generation results in lower carbon emissions to the atmosphere than the other treatment scenarios investigated (Table 3.1). There are several factors that explain the relatively low emission from the bioenergy scenario. First, although biomass electricity generation produces carbon emissions through the combustion of biofuel, nearly half of the carbon emissions from bioenergy production are offset by avoided coal emissions. Secondly, there are relatively few carbon emissions from biomass waste in the bioenergy production process because the bioenergy production facility used as a reference for these calculations has few limitations regarding the

size of woody material that can be used in electricity production. Therefore, small biomass scraps that cannot be used in durable goods can be utilized in bioenergy production. Furthermore, the reduction in carbon emissions of the bioenergy scenario relative to the durable goods scenario may be even greater than that represented here. Transportation emissions from the treatment site to a mill were assumed to be the same as the emissions recorded for transporting the biomass from the treatment site to the bioenergy production site, even through there is currently no mill located within that proximity to the forest. Finally, the durable goods scenario does not include any further emissions incurred for transportation of the final product, or during processing. However, emissions incurred during processing, such as from milling waste, can be difficult to estimate because many mills will use waste to generate electricity or another type of non-durable product [*Skog and Nicholson*, 2000].

The relative future emissions of the these three scenarios will vary depending on several factors including the distance between the harvest site and the bioenergy facility, the efficiency of the bioenergy production process, and the size of biomass available for harvest. The distance between the harvest site and the bioenergy production facility can impact the carbon balance of the bioenergy production process because a longer haul distance that requires greater carbon emissions during transportation of biomass may reverse the carbon benefit provided from bioenergy production. I calculated two maximum haul distances for this study: the maximum haul distance at which bioenergy production will provide a carbon benefit over the durable goods scenario, and the maximum haul distance at which the bioenergy scenario will provide a carbon benefit over the no stabilization scenario. In both cases, the maximum haul distance is great enough that biomass could be retrieved from all available regions of San Juan National Forest. In addition to changes in the haul distance of harvested biomass, there also may be future

changes in the efficiency of the bioenergy production process, which would increase the carbon benefit provided by this scenario relative to the other two. Finally, the size of biomass available for harvest will vary with time and in the future there may be fewer trees of merchantable size, which would decrease the amount of biomass that could be stored in durable goods.

3.4.2 Long-term Carbon Balance of Bioenergy Production. Treatments designed to reduce the risk of high intensity wildfire necessarily lower the amount of forest biomass present on the landscape because biomass is removed from the forest [*Finkral and Evans*, 2008; *North et al*., 2009; *Stephens et al*., 2009; *Dore et al*., 2010]. When these treatments are periodically repeated in order to maintain reduced fire risk, they result in lower carbon storage on the landscape (Figure 3.4a). If the treatment reduces emissions from a future wildfire by an amount greater than the amount of carbon removed during treatment, then the treatment will result in a net carbon benefit. However, this is only possible in the case of a future wildfire, and considering only a portion of the landscape is burned in a wildfire each year, many treated areas will not be subsequently burned during the lifespan of treatment effectiveness [*Campbell et al*., 2012].

I find that in the bioenergy scenario I investigate here, repeated treatments with bioenergy electricity production result in a net carbon benefit even without a future wildfire. Because some carbon is 'sequestered' from every treatment through the offset of coal energy production (Figure 3.4c), and carbon is also taken up through forest regrowth, the cumulative carbon emission to the atmosphere is reduced with every treatment. In the case of the forest stand investigated here, repeated treatments result in a net carbon balance of zero by 2080 (Figure 3.4d). A forest level analysis, assuming continued operation of the bioenergy plant every year

through the end of the century indicates that the net carbon balance of the forest reaches 0 by the year 2140, and will remain positive thereafter (Figure 3.4e). The results I report here are contingent on the size of the forest investigated and the use of coal as the energy reference system, however these results are highly applicable to decision makers in Southwest Colorado. Because current forest policy mandates forest treatments to reduce wildfire risk [*USDA-USDI*, 2000], these types of forest treatments are routinely performed on Western forests whether or not there is an opportunity to produce electricity from the harvested biomass. My results indicate that the use of biomass for electricity generation may reduce the overall carbon emissions resulting from these ongoing forest treatment practices.

3.4.4 Carbon Balance of Bioenergy Treatments and Future Wildfire. In addition to the carbon offset from bioenergy production, forest treatments may also provide a carbon benefit by reducing emissions from a future wildfire. I find that in a comparison of two scenarios of future wildfires occurring in treated and untreated stands, the treated stand provides a carbon benefit due to avoided emissions as a result of the treatment. However, over larger temporal and spatial scales, the carbon benefit of forest treatment is contingent on three factors: (1) the rate of forest growth following treatment, (2) the effectiveness of the treatment in modifying fire behavior, and (3) the probability of future wildfire (Figure 3.6).

Figure 3.6 Conceptual model of the effect of a) regrowth time, b) treatment effectiveness, and c) fire probability on carbon benefit of forest treatment. The timeframe is assumed to be smaller than the disturbance cycle in the specified forest.

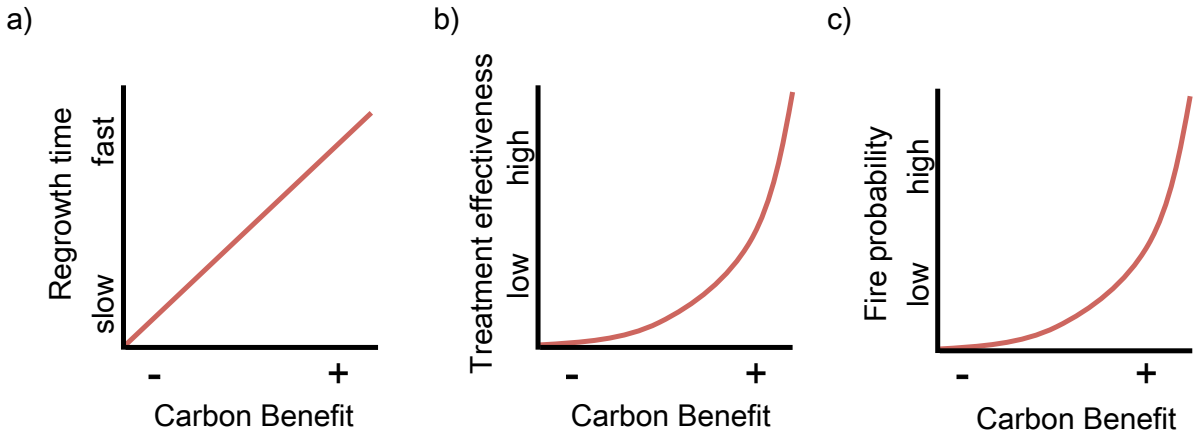

3.4.4 a) Forest Growth. The carbon benefit of forest treatments is dependent on the rate of forest growth following treatment (Figure 3.6a). Indeed the long-term carbon balance of all forest disturbances is dependent on the forest recovery and the frequency of the disturbance. Over a time scale of one hundred to several hundred years, forest disturbances including treatment or wildfire will only result in forest carbon loss if the forests are not allowed to recover in the time period between disturbances [*Hurteau and Brooks*, 2011; *Campbell et al*., 2012]. In other words, net carbon loss to the atmosphere occurs in instances where the disturbance interval is shorter than the time required for the forest to regrow to its pre-disturbance state, or where the forest experiences a permanent conversion to a different vegetation type. I find that in the scenario I investigate here, repeated treatments necessary to maintain the forest at a low risk of high severity wildfire do not allow the forest to recover to its pretreatment carbon stock (Figure 3.4b). However, because bioenergy production offsets some carbon emissions with every treatment, the net carbon balance of these treatments in the demonstration stand eventually does

reach zero around the end of the century (Figure 3.4d), and forest wide net carbon balance equals zero by 2140.

Treatment Effectiveness. The effectiveness of forest treatments is critical in determining the ultimate carbon benefit of a forest treatment; a treatment that does not effectively reduce future emissions will incur a low, or no, carbon benefit, whereas a treatment that is highly effective in decreasing future wildfire emissions will incur a larger carbon benefit. Ultimately this effect will saturate when so much biomass has been removed from the forest that further treatment will not further reduce fire potential (Figure 3.6b).

The effects of forest treatments on wildfire behavior are difficult to characterize, but there are many studies indicating that treatments can effectively reduce fire behavior and post-fire mortality in dry Western forests. A comparison of fire severity indices, fireline intensity, stand characteristics and post-fire recovery in treated and untreated stands in New Mexico and Arizona indicates that fire severity was lower in treated areas, and more aggressive treatments made stands less susceptible to crown fire [*Cram et al*., 2006]. Analyses with satellite data indicate that treatments reduced wildfire severity and also changed the progress of the Rodeo and Chediski fires in Arizona [*Finney et al*., 2005], and Pollet and Omi [2002] found that among four sites in the western US revisited following wildfire, crown fire severity was mitigated (fire severity and crown scorch was lower) in stands that had some type of fuel reduction treatment. Investigations of stand structure, composition and mortality following a wildfire in adjacent treated and untreated stands indicate that treated stands have lower post-wildfire mortality [*Safford et al*., 2012], and greater carbon storage in live tree carbon pools [*North and Hurteau*, 2011; *Carlson et al*., 2012].

Given the current understanding of the effects of forest treatments on wildfire behavior, it is nearly impossible to definitively determine how treatments will affect wildfire carbon emissions. However, projections of avoided pyrogenic emission due to forest treatments are critical in determining future forest carbon balance. In the selected scenario I investigate here, the forest treatment results in 14.76 Mg ha^{-1} of avoided carbon emissions, while the carbon emissions offset through bioenergy electricity production is 10.3 Mg ha^{-1}, indicating that a reduction from high intensity to low intensity fire in this region could potentially have a larger effect on stand carbon balance that the use of bioenergy along. Projections of pyrogenic carbon emissions and the effects of forest treatment on fire behavior can have substantial implications for projecting future forest carbon balance and therefore this is an area of research that deserves careful analysis in the future.

Wildfire Probability. In addition to forest growth and treatment effectiveness, the carbon benefit of a forest treatment is also dependent on the probability of a future wildfire in the treated area (Figure 3.6c). If the area of the treatment does not experience a wildfire during the lifespan of the treatment effectiveness, then the emissions resulting from the treatment are not offset by a subsequent reduction in pyrogenic emissions. Within San Juan National Forest there are 171,400 hectares of ponderosa pine forest, and according to data from LANDFIRE, 56,600 hectares of ponderosa pine on SJNF burned between 1999 and 2010, indicating that an average of 0.3%, or 5150 hectares, of ponderosa pine forest on SJNF burned each year during that time period. Given the relatively small probability of a specific treated stand experiencing a fire during the life span of the treatment, and the fact that 1024 ha must be treated annually to harvest enough

biomass to fuel the plant, the primary carbon benefit of the treatment will likely come from the bioenergy production and the associated carbon offset, not avoided pyrogenic emissions.

In the future, wildfire probability may be influenced by climate-induced changes in wildfire regimes. Recent analyses indicate that annual wildfire area burned is correlated with climate [*McKenzie et al*., 2004; *Littell et al*., 2009]; large wildfire activity and wildfire season duration have increased since the mid-1980's [*Westerling et al*., 2006] and in many western states the annual wildfire area burned may double by the end of the century [*McKenzie et al*., 2004]. An increased probability of wildfire also increases the potential for a stand treatment to incur a carbon benefit through avoided pyrogenic emissions. Under future conditions of more frequent wildfire in this region, the potential for stand treatments to provide a carbon benefit may increase, although this increase will likely remain small, as the probability of wildfire in one particular location is low.

In addition to wildfire size and frequency, potential future changes in wildfire intensity and severity may also have consequences for ecosystem recovery. In a study surveying 10 sites following stand-replacing wildfire in ponderosa pine ecosystems, Savage and Mast [2005] found that only 50% of the sites experienced any regeneration, and the remaining sites appeared to have transitioned to grassland or shrub land with reduced potential to recover C. In my analyses I find that in the absence of regeneration following wildfire, it takes longer for the forest to re-sequester carbon emitted during the wildfire. Indeed, the difference in year 2100 total stand carbon stocks between a burned stand with reduced regeneration and a burned stand with normal regeneration is as large as the carbon offset obtained through bioenergy production (Table 3.3; Table 3.4). While more frequent wildfires in the future may mean that forest treatments have a greater potential to reduce total carbon emissions, reduced forest regeneration or recovery may lessen

the potential carbon benefit of forest treatment for bioenergy. Further investigation of treatment effects on fire behavior and projected trends in forest regeneration and recovery following disturbance are critical in determining the ultimate carbon balance of treatments and bioenergy production.

3.5 Conclusions

Forest treatments influence forest carbon balance by removing woody biomass from the forest, and also by affecting future wildfire behavior. I find that the use of harvested biomass for electricity generation can reduce carbon emissions to the atmosphere by offsetting emissions from fossil fuel electricity generation, and potentially avoiding pyrogenic emissions by reducing the intensity of a future wildfire. However, future variations in fire frequency and intensity, and in forest regeneration following disturbance, may also influence forest carbon stocks and in some cases these changes in forest carbon stocks are larger than the carbon sequestered through offsetting coal emissions.

CHAPTER IV

CLIMATE AND LANDSCAPE PHYSIOGRAPHY DRIVE TRENDS OF GROWTH AND DECLINE IN SUBALPINE FORESTS

4.1 Introduction

The response of forest ecosystems to rising CO_2 concentrations and changing climate is one of the most important and complex feedbacks within the climate system. Rising CO_2 concentrations in the atmosphere may increase productivity of forest ecosystems, and thereby increase the rate at which forests remove CO_2 from the atmosphere via photosynthesis (Korner, 1993). Conversely, climate change, and specifically changing temperature and precipitation regimes may counteract or overwhelm the effects of CO_2 fertilization (Reichstein, 2013). The mechanisms that determine the nature of a future carbon cycle-climate feedback lie in the physiological response of trees to external forcings, and most global biogeochemical dynamic vegetation models include some representation of this feedback. The results of model simulation studies universally highlight the importance forest-climate system feedbacks [*Purves and Pacala*, 2008], but also underscore the uncertainty regarding the direction and magnitude of future forest change [*Friedlingstein et al*., 2006; *Dolman et al*., 2010; *Arora et al*., 2013]. There are a number of factors that are responsible for the varied projections of forest responses, but some of the largest uncertainties come from the physiological links between increasing CO_2 concentrations, climate change, and the forest processes of regeneration, mortality and growth

that collectively determine long-term changes in forest biomass and composition [*Moorcroft*, 2006]. While changes in regeneration and mortality frequently lag changes in climate, tree growth responds to climate conditions over relatively short timescales of one to several years such that current growth rates are generally indicative of current climate conditions. Growth rates are also specific to a given tree meaning that growth can vary between individuals within close proximity to one another depending on their local environmental conditions [*Bunn et al.*, 2005]. The immediacy of growth response to climate, and the individual nature of tree growth according to local conditions, makes climate-induced growth rates an important, but uncertain, component of forest carbon dynamics.

The growth of an individual tree is controlled by climate, specifically a tree's access to sufficient water and energy. In regions where potential evapotranspiration exceeds precipitation, tree growth is usually limited by access to water. Conversely, in ecosystems characterized by higher rates of precipitation, growth is primarily limited by short growing seasons [*Waring and Running*, 2007]. Despite these general patterns, local scale factors including species, stand dynamics, topography and soil type all influence how climate affects forest growth. Within the same ecosystem, different species may respond differently to the same climate conditions due to species-level variation physiology [*Villalba and Veblen*, 1994; *Adams and Kolb*, 2005; *Miyamoto et al.*, 2010]. Suppressed trees growing under the forest canopy typically have a muted response to climate variables relative to dominant trees [*Martín-Benito et al.*, 2007]. Finally, local stands of trees may respond differently to climate than neighboring stands depending on their local physiographic environment including aspect [*Peterson and Peterson*, 1994], elevation [*Littell et al.*, 2008; *Lo et al.*, 2010] and soil properties (Barger & Woodhouse, *in press*).

In order to understand the relationship between tree growth and climate in the face of large variations in local physiography, studies of tree growth generally focus on a collection of trees from the same forest stand (Frits and Shatz, 1975). This approach offers a robust understanding of how localized groups of trees respond to climate, but provides little insight into how relationships between tree growth and climate may vary in a predictable manner between landscape positions. The basic physiology of trees suggests that the variation in growth patterns between neighboring stands is likely a function of the local environment and how that environment mediates climate, but currently we lack a detailed understanding of how tree response to climate varies as a function of local physiographic factors. Because growth at the forest-scale is an aggregate response of many individual stands of trees to both climate and local physiographic conditions, identifying how local physiography interacts with climate to drive growth is necessary in order to understand the response of forests to climate at the landscape-scale.

The interacting effects of climate and local physiography are particularly important in determining growth within subalpine forests of North America. These regions have experienced greater warming than lower elevation regions over the past several decades (Diaz and Eischeid, 2007), and are generally characterized by highly complex topography that likely leads to variable tree growth patterns in response to climate. Subalpine regions usually have cool and wet climates, and therefore tree growth in these regions is primarily related to climate variables associated to the length of the growing season and the depth of seasonal snowpack [*Peterson and Peterson*, 1994; *Splechtna et al*., 2000; *Miyamoto et al*., 2010]. However, some studies show that in locally drier and warmer landscape positions these species respond negatively to warm summer temperatures (Adams & Kolb, 2005, Villalba & Veblen, 1994; Peterson *et al*., 2002),

indicating local water limitation. Continuing warming in these regions could mean that more subalpine forests are vulnerable to water limitation, but anticipating the future condition of forests requires understanding how forest response to climate varies as a function of landscape physiography.

The purpose of this work is to examine the effect of climate on subalpine forest growth across variable elevation, aspect and soil types. My overarching hypothesis is that the response of subalpine forest growth to climate will vary across physiographic gradients, specifically those that affect local temperature and moisture conditions such as elevation, aspect and soil properties. The three primary objectives of this work are: 1) identify the climate variables that most strongly influence growth in two subalpine forest species of southwest Colorado; 2) investigate how climatic drivers interact with local physiological variables to influence forest growth; and 3) explore long-term growth trends in response to warming across physiographic gradients. My findings have important implications for anticipating the effects of future climate on subalpine forest species in a region already experiencing substantial climatic and ecological change.

4.2 Materials and Methods

4.2.1 Study Area. The study was conducted in San Juan National Forest located in southwest Colorado (~38°N, ~108°W; Figure 4.1).

Figure 4.1 a) Distribution of Spruce-fir type subalpine forest through North America and location of Colorado; b) Location of San Juan National Forest in Colorado; c) Location of study plots within San Juan Nation Forest.

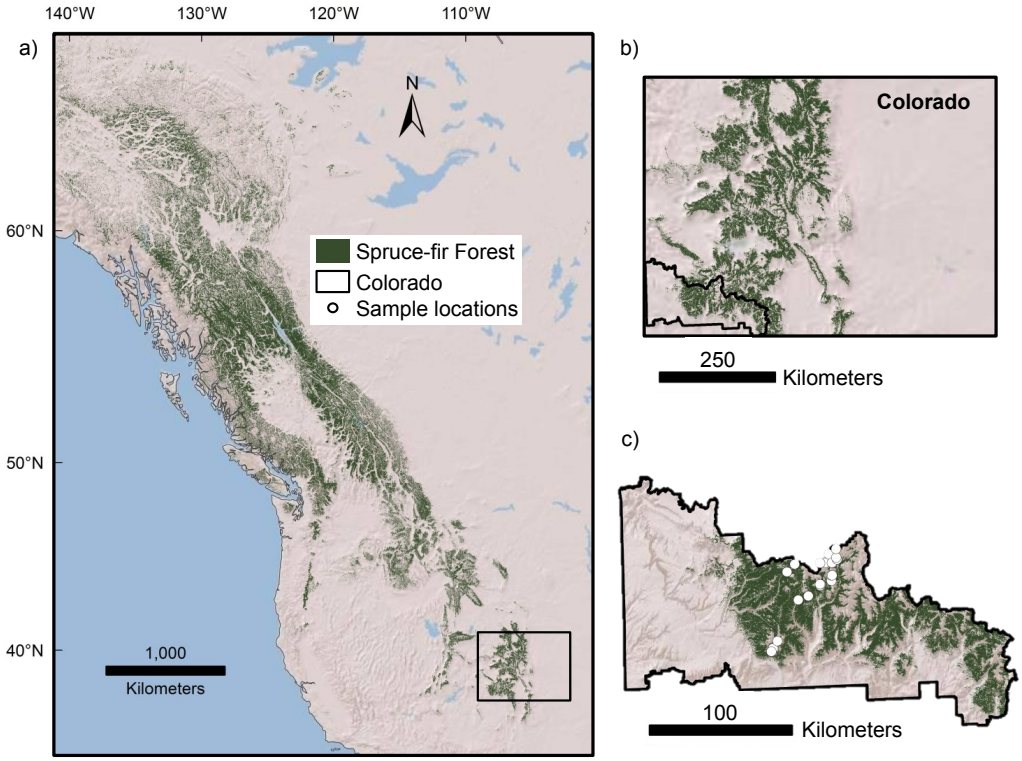

The climate of this region is characterized by low temperatures with high snowfall between November and April, and monsoonal rainfall from July through October [*Blair*, 1996]. This region receives approximately 98 cm of precipitation annually; average maximum temperatures (~19.5°C) occur in late summer, and minimum temperatures (-13.9°C) occur mid-winter (http://www.wcc.nrcs.usda.gov/snow/). Treeline in this region is approximately 3600 meters. The geology of this region consists of interbedded sandstone, limestone and shale of Pennsylvanian and Mississippian age, with some Tertiary volcanics [*Yager and Bove*, 2002]. Soils are predominantly cobbly sand clay loam (NRCS).

4.2.2 Sampling Design and Tree Growth Data. Tree ring data was collected from 23 sites within a subalpine spruce-fir forest (Table 4.1).

Table 4.1 Site characteristics of tree ring sampling sites derived from PRISM data. Abbreviations: AWC- available water capacity; Precip – annual mean precipitation; T max – annual mean monthly maximum temperature; T min – annual mean monthly minimum temperature, N – north, S – south, E – east, W – west, ES – Engelmann Spruce, SF – Subalpine Fir.

Site	Latitude	Longitude	Elevation (m)	Aspect	AWC (cm)	Precip (cm)	T max (°C)	T min (°C)	Species Sampled
1	37.72	-107.71	3366	N	355.0	78.9	9.3	-6.0	ES
2	37.81	-107.70	3011	N	117.0	76.7	8.9	-6.9	ES/SF
3	37.81	-107.70	3019	E	81.8	76.7	8.9	-6.9	ES/SF
4	37.83	-107.67	2940	N	273.5	57.6	9.2	-6.9	ES
5	37.84	-107.68	2997	W	244.7	57.6	9.2	-6.9	ES/SF
6	37.88	-107.68	3365	N	237.3	66.7	8.3	-6.9	ES/SF
7	37.65	-107.85	3114	E	217.6	69.5	10.5	-5.6	ES/SF
8	37.39	-108.06	2979	N	273.1	61.2	9.8	-5.5	ES/SF
9	37.39	-108.07	2793	N	274.3	61.2	9.8	-5.5	ES
10	37.37	-108.08	2710	N	242.9	61.2	9.8	-5.5	ES
11	37.43	-108.04	3041	W	178.9	69.1	8.8	-5.4	ES
12	37.81	-107.74	3001	E	405.0	66.2	8.1	-6.8	ES
13	37.81	-107.74	2998	W	136.7	74.4	8.7	-6.6	ES/SF
14	37.85	-107.72	3254	W	215.3	63.6	8.7	-6.7	ES/SF
15	37.81	-107.78	3095	S	145.0	70.2	7.6	-7.1	ES/SF
16	37.70	-107.78	3235	E	155.2	78.8	9.7	-5.6	ES/SF
17	37.71	-107.77	3320	N	158.7	78.8	9.8	-5.6	ES/SF
18	37.75	-107.71	3379	S	288.0	72.8	9.1	-6.6	ES/SF
19	37.75	-107.70	3388	E	75.6	72.8	9.1	-6.6	ES/SF
20	37.71	-107.78	3380	N	300.9	78.8	9.8	-5.6	ES/SF
21	37.77	-107.98	2874	N	147.1	57.8	9.3	-7.0	ES/SF
22	37.77	-107.98	2924	N	235.7	57.8	9.3	-7.0	ES
23	37.80	-107.93	3125	S	280.3	62.3	8.3	-7.8	ES

Sites were chosen to represent a variety of soil types on north, east, south and west facing aspects across an elevational gradient from 2700m to 3400m. At each site I selected approximately 20 individuals of both subalpine fir (*Abies lasiocarpa* (hook.) Nutt.) and Engelmann spruce (*Picea engelmannii* Parry ex Engelm.). A 50 meter transect was established perpendicular to the slope, and trees were selected as those closest to the transect that were greater than 20cm diameter at

breast height (DBH) with no visible damage to crowns or stems. At sites where subalpine fir was not present, only Engelmann spruce were sampled.

I collected a total of 450 cores from Engelmann spruce and 210 cores from subalpine fir. An increment borer was used to extract one core from each tree at a height of 1.3 meters. The cores were mounted and then sanded with progressively finer grades of sand paper in order to produce a flat surface on which tree rings were easily visible. Cores were measured using the Velmex ring-measurement system (Velmex Inc., Bloomfield, NY), and cross-dated visually and statistically. Cross-dating accuracy was checked using the program COFECHA [*Holmes*, 1983; *Grissino-Mayer*, 2001].

4.2.3 Physiographic Variables. At each site I also obtained measurements of site elevation, aspect, and soil available water capacity (AWC). Elevation and aspect were measured at three points along the 50 meter transect (at 0m, 25m and 50m). AWC was calculated from soil texture information and soil depth [*Saxton and Rawls*, 2006]. To quantify soil texture, I collected 6 soil samples (10 cm in depth) at each site. Soils were then sieved through a 2 mm sieve; the >2mm fraction was weighed as gravel and the <2mm fraction was used to estimate percent sand, silt and clay using the hydrometer method [*Gee and Or*, 2002]. Soil depth at each site was determined at 6 locations along the transect by inserting a 2 meter soil probe into the soil until resistance. Where the probe was fully inserted without meeting bedrock, the soil depth was recorded as greater than 2 meters. I used the estimates of soil depth and percentage sand, silt, clay and gravel from each site to calculate soil available water capacity by subtracting the wilding point (θ_{1500}) from field capacity (θ_{33}), which I calculated following the equations in Table 2 of Saxton & Rawls (2006), and multiplying by the soils depth.

4.2.4 Climate Data and Variable Selection. Long records of measurement of mountain climate are not available in this study area, and therefore I chose to evaluate monthly state climate-division data from the NOAA National Climatic Data Center (Divisional data hereafter), and gridded climate data from the PRISM climate group (PRISM data hereafter). Divisional data consist of regional monthly temperature and precipitation values which are computed from area-weighted observational data [*Karl and Koss*, 1984]. PRISM data is also based on observational data, which is used as input for models that use complex algorithms to anticipate how precipitation and temperature values will vary over regions of complex terrain [*PRISM*, 2004]. For my purposes, Divisional data have the disadvantage of a rather course spatial scale (the area of the climate division containing this study site is 99763 km^2), whereas the PRISM data, which are available at a much higher spatial resolution, are based on algorithms that do not always perform well in this topographically complex region [*Gutmann et al*., 2012]. I used both Divisional data and PRISM data to see which dataset produced the strongest correlations between climate and growth, and as Divisional data consistently produced stronger correlations between climate and growth, Divisional data were used in all subsequent analyses. Divisional data were also used to investigate trends in temperature through this time for the region of this study (Figure 4.2).

Figure 4.2 a) Average annual temperature and b) summer average monthly minimum temperature from NOAA Divisional Data for western Colorado during the period 1895 through 2012. The dashed line shows the temperature trend from 1895-2012 and the solid line shows the temperature trend from 1975-2012. The slopes and correlations for 1985-2012 are 0.014 and 0.61 ($p<0.00$) respectively for a) and 0.016 and 0.71 ($p<0.00$) respectively for b). The slopes and correlations for 1975-2012 are 0.033 and 0.55 ($p<0.00$) respectively for a) and 0.029 and 0.44 ($p=0.004$) for b).

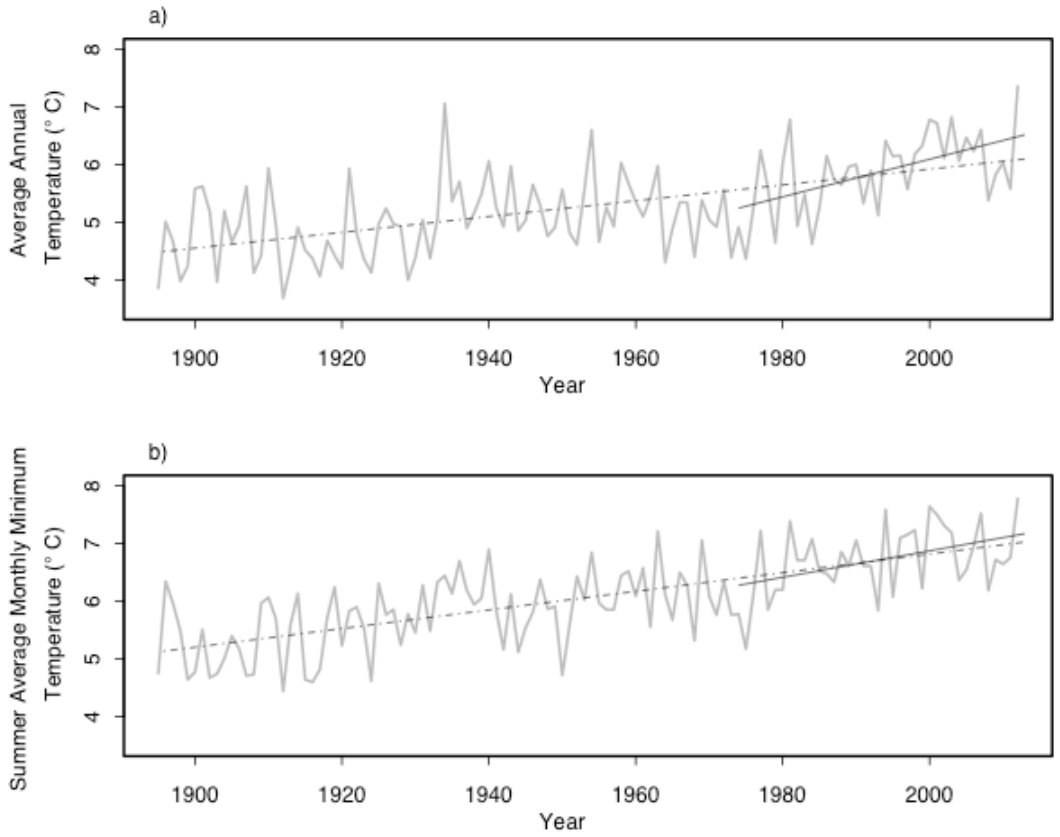

Correlations between climate and growth were calculated from Divisional climate data and detrended ring width index values for the time period 1895 through 2012. Detrended ring width index values were determined by fitting a cubic smoothing spline with a 50% frequency response cutoff of 20 years, followed by an autoregressive model to remove autocorrelation present within each series (dplR package, Bunn, 2008, R Core Development Team). This method produces a unitless ring-width index (RWI) for each tree, consisting of one value for each year of growth. RWI values for a given tree have a mean of one; values less than one indicate a year of

relatively small growth, and values greater than 1 indicate a year of relatively large growth. I chose to use correlations between RWI and climatic variables to identify the most important climate variables affecting growth because this method was developed to identify climate influence on growth, independent of tree age and stand dynamics. I used Pearson product-moment correlations to compare growth in a given year within a given tree to the seasonal climate time series from the Divisional data from 1895 to 2012. I calculated the correlation between growth and aggregated seasonal variables because seasonal variables can be better than monthly climate data at approximating the actual ecophysiological mechanisms leading to annual growth-climate correlations [*Fritts*, 1976; *Watson and Luckman*, 2002; *Littell and Peterson*, 2011], and secondly, seasonal aggregations are less likely to produce spurious significant correlations. Seasonal aggregations for this study were created as follows: Spring was defined as April through June of the year of ring formation, Summer was defined as May through September of the year of ring formation, and winter was defined as October through February starting in the year preceding ring formation. All variables (monthly maximum temperature, monthly minimum temperature, monthly precipitation and monthly growing degree days) were averaged over these time periods to produce seasonal aggregations with the exception of precipitation, which was summed. Growing degree days (GDD) represent the number of days each month that temperatures were above freezing. The most important climatic variables were identified as those that yielded the highest mean correlation between climate and growth. Mean correlations were calculated from all trees, rather than chronologies, according to the suggestion of Galván *et al*., (2014) who show that an individual tree-scale approach to quantifying climate-growth relationships is necessary to investigate the climate sensitivity of trees.

4.2.5 Modeling the Effects of Climate and Physiography on Tree Growth. I examined the relationship between tree growth and climate, including the interaction of climate and site-level physiographic variables, by the means of linear-mixed effects models. For this modeling approach, detrended RWI data are an inappropriate choice as a tree growth metric because, due to the detrending, the mean growth of each tree is the same making it impossible to evaluate the effect of site level physiographic variables (elevation, aspect, soil type) on growth. Instead, I use a measure of standardized basal area increment (BAI). BAI is the cross-sectional area of new growth that a tree produces each year according to the following formula:

$$BAI = \pi(R_n^2 - R_{n-1}^2)$$

where R is the radius of the tree and n is the year of ring formation. Because BAI will increase through a tree's life, particularly in younger trees, I chose to standardize BAI by the basal area (BA) of the tree in the year of ring formation, (BAI/BA), as used in McDowell et al. (2009). This standardized BAI, BAI/BA, was used as the response variable in the generalized linear-mixed models with seasonal climatic variables and site level physiographic variables as predictor variables. The models were constructed as follows:

$$y_i = \alpha + X_i\beta + b_i + \varepsilon_i$$

where y_i represents the growth index value for each year from tree i, α is the intercept, X_i is the fixed effects (climatic variables) and β is the vector of parameters associated to the fixed effects, b_i is the matrix including the vectors of random effects, and ε_i is the within group error vector. I used a random slopes model to estimate the effect of the predictor variables on tree growth. The intercept for tree and site were included as random effects (*lmer* function in th R package lme4; Bates D., Bolker B., and Walker S., 2014, R Core Development Team).

I adjusted 24 candidate models using different combinations of climatic and site level physiographic variables and their interactions, with the 25th model as a null model that did not include any climatic or physiographic variables. The specific climatic variables used in the models were: summer average monthly maximum temperature, summer average monthly minimum temperature, summer total monthly precipitation, summer average monthly GDD. The specific physiographic variables included in the models were elevation, aspect, and AWC. The seasonal variables were chosen according to the results of the climate-growth correlation analyses. The candidate models included all possible combinations of one climate variable and one physiographic variable, with and without interactions. The response variable, BAI/BA was transformed using a logarithm transformation to produce a normal distribution prior to analyses. All climate and physiographic variables were centered and scaled such that the mean value is equal to zero and the standard deviation is equal to 1.

For each model I determined the Akaike Information Criteria (AIC) and Bayes Information Criteria (BIC; MuMIn package, Bartón, K., 2014, R Core Development Team). AIC and BIC are model evaluation metrics that reward parsimonious models and penalize complex models. I based the model selection on BIC because the sample size I use here greatly exceeds the parameter space of the model [*Aho et al*., 2014]. In order to determine the goodness-of-fit I use pseudo r^2 calculated according to the recommendation of Nakagawa and Schielzeth (2012), which provides a 'variance explained' term for generalized linear mixed effects models. The climatic and physiographic variables and interactions present in the best fitting model were taken as the variables most important for determining growth.

4.2.6 Analysis of Long Term Growth Trends. To assess long-term trends in tree growth, I examined the trend in BAI over time. I used the time period 1974-2012 because this is the time for which there is a complete record for each tree. I chose to use the trend of BAI over time for this analysis because the other methods of quantifying tree growth through time, the detrended RWI and standardized BAI/BA, remove trends of growth with time through their standardization procedures. BAI preserves the growth trend of a tree through time, and provides a conservative way to detect growth declines [*Duchesne et al*., 2003]. In a mature tree BAI will typically increase through time or stabilize [*Phipps and Whiton*, 1988; *Duchesne et al*., 2002; *Biondi and Qeadan*, 2008], but BAI will not decline over time until the tree begins to senesce [*Pedersen*, 1998; *Duchesne et al*., 2003; *Elvir et al*., 2003]. Therefore, trends of decreasing BAI are indicative of tree decline.

To evaluate trends of BAI over time, I calculated annual BAI for each tree, and then used Pearson product-moment correlations to determine the correlation of BAI and year, which is equal to the trend of growth over time. The result is one value for each tree indicating the magnitude and sign of its growth trend over time. A decrease in BAI at the tree level could occur as a result of competition for space and resources, and therefore to account for the variation in BAI trend among trees, and to determine if specific physiographic variables were important in determining the sign and magnitude of the growth trends from 1974 to the present, I used these trends as the response variable in a generalized linear-mixed effects modeling framework. Nine models were constructed including a null model and the best model was selected using BIC. The physiographic variables included in the mixed models were determined as those variables found to be most important in predicting growth in the analyses above: aspect, elevation, and average temperature at each site from 1974 to the present from the Divisional

climate dataset. Site temperature was included because temperature was the most important climate variable identified in the climate-growth relationships. The diameter of each tree was also included as a fixed effect to account for variable sized trees.

4.3 Results

Within this study site of San Juan National Forest, I found that Engelmann spruce were on average slightly older than subalpine fir. The mean series length was 126 (± 58 [standard deviation]) years for Engelmann spruce and 103 (± 31 [standard deviation]) for subalpine fir. These analyses included approximately 78,330 ring widths in all. The longest series was that of an Engelmann spruce, at 433 years, with the longest subalpine fir series at 207 years.

4.3.1 Climate Growth Relations. Subalpine fir growth was the lowest in years with warm temperatures, and was slightly greater in years with more precipitation. Subalpine fir grew less in years with more monthly GDDs in summer months ($r = -0.24$, $p<0.05$), and warmer summer average monthly maximum and minimum temperatures ($r = -0.21$, $p<0.05$ and $r=-0.23$, $p<0.05$ respectively). Subalpine fir growth was less responsive to spring and winter temperatures than summer temperatures (Figure 4.3).

Figure 4.3 Boxplot of Pearson product moment correlation between ring width index and seasonal climate variables calculated from National Ocean and Atmospheric Administration Divisional climate data for a) subalpine fir and b) Engelmann spruce. Spring was defined as April-June of the year of ring formation, Summer was defined as May-September of the year of ring formation, and winter was defined as October-February starting in the year preceding ring formation. Lines represent the median, bars represent the interquartile range, whiskers represent the range and open circles are outliers. The gray horizontal lines show the 0.05 significance thresholds given the sample size.

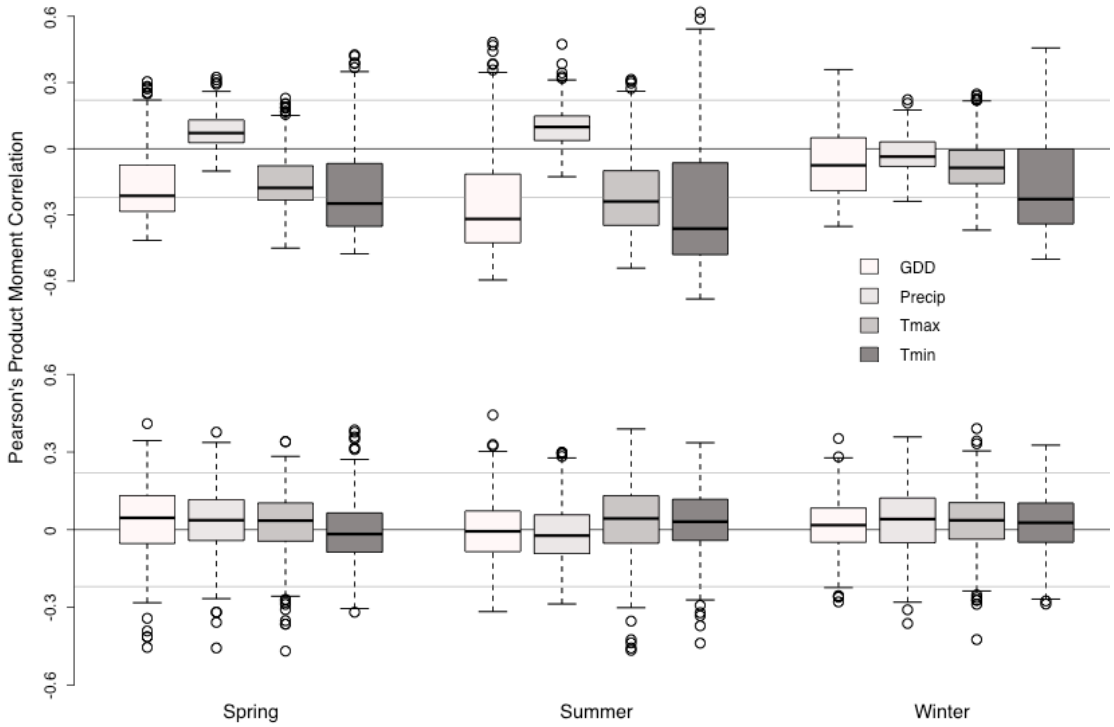

Abbreviations: *Precip* – seasonal total precipitation, *GDD* – seasonal average monthly growing degree days, *Tmax* – seasonal average monthly maximum temperature, *Tmin* – seasonal average monthly minimum temperature.

In terms of precipitation, subalpine fir had slightly greater growth in years with more spring and summer precipitation, but the correlation between growth and precipitation was weak (Figure 4.3). Engelmann spruce generally grew more in warmer years, but overall Engelmann spruce growth was largely unresponsive to climatic variables (Figure 4.3).

4.3.2 Interactions of Climate and Physiography. Climate and physiography were both important drivers of growth in subalpine fir and had interacting effects on growth. Summer average monthly minimum temperature, elevation and the interaction between temperature and elevation were all included in the best performing mixed models of subalpine fir growth, determined by BIC (Table 4.2).

Table 4.2 Statistical parameters (± 1 standard error) of the top three performing linear mixed effects models evaluated by BIC for growth of Subalpine Fir (top) and Engelmann Spruce (bottom). Growth is equal to basal area increment standardized by tree size. All parameters were centered and scaled such that the mean is equal to zero, and the standard deviation equal to 1.

Subalpine Fir:

Model	Tmin	Tmax	Precip	GDD	Elevation	Aspect[1]	AWC	Interaction	Δ BIC	Δ AIC	R^2
m2	-0.39 (±0.01)	--	--	--	-0.06 (±0.08)	--	--	Elev*Tmin; 0.07 (±0.01)	0	0	0.55
m10	-0.39 (±0.01)	--	--	--	--	x	--	Aspect*Tmin	149	118	0.54
m18	-0.39 (±0.01)	--	--	--	--	--	-0.158 (±0.07)	AWC*Tmin; 0.02 (±0.01)	228	229	0.54

Engelmann Spruce:

Model	Tmin	Tmax	Precip	GDD	Elevation	Aspect[1]	AWC	Interaction	Δ BIC	Δ AIC	R^2
m10	-0.44 (±0.01)	--	--	--	--	x	--	Aspect*Tmin	0	0	0.23
m2	-0.39 (±0.06)	--	--	--	0.05 (±0.06)	--	--	Elev*Tmin; -0.03 (±0.01)	10	63	0.23
m6	-0.39 (±0.01)	--	--	--	0.05 (±0.06)	--	--	--	19	80	0.23

[1] Statistical parameters for 'Aspect' are denoted as "x" because aspect is a categorical variable and therefore has more than one statistical parameter for each model.
Abbreviations: *Tmin* - growing season average monthly minimum temperature, *Tmax* - growing season average monthly maximum temperature, *Precip*-growing season total precipitation, *GDD* - Growing Degree Days, *AWC* - Available Water Capacity, *AIC* - Akaike's Information Criteria, *BIC* - Bayes Information Criteria.

The interaction between temperature and elevation indicates that in warm years, growth was greater at high elevations (above ~ 3100m) and lower at low elevations, and in cool years growth was lower at high elevations and greater at low elevations (Figure 4.4).

Figure 4.4 Interaction effect of summer average monthly minimum temperature by elevation on tree growth (expressed as basal area increment standardized by basal area; BAI/BA) for Subalpine Fir. Growth versus elevation is shown for five progressive temperature intervals: a) lowest 0-19%, b) 20-39%, c) 40-59%, d) 60-79% and e) 80-100%. This interaction was identified in the top-performing model (evaluated by BIC) generated in a generalized linear-mixed modeling framework. Dashed lines denote the 95% confidence intervals.

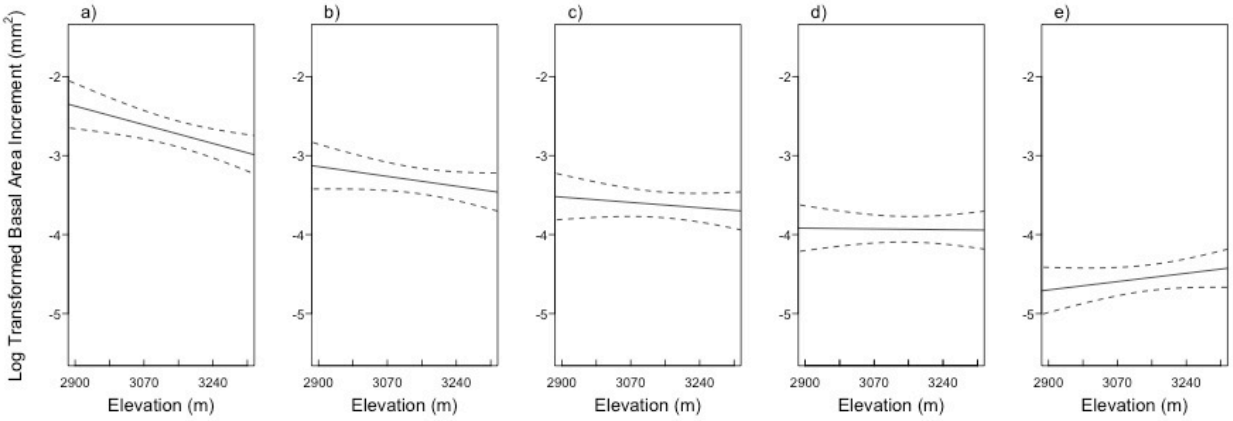

These results are consistent with the results from the correlation analysis above that indicate summer temperature the most important climatic variable in determining growth of subalpine fir. Elevation was the most influential physiographic variable and was more important than aspect or soil AWC in determining growth of subalpine fir.

Climate and physiography also had interacting effects on Engelmann spruce growth (Table 4.2), but mixed models of Engelmann spruce growth explained only a small proportion of the inter-annual variation in growth. Average summer minimum temperature, aspect and the interaction between aspect and temperature were all included in the best performing mixed models of Engelmann spruce growth (Table 4.2; Figure 4.4).

4.3.3 Trends in Growth. Subalpine fir growth is declining through time. I used the correlation between BAI and year for the time period 1975 through 2012 to determine the growth trend, and I modeled the trend for each tree using site and tree level variables to determine which trees are declining the most. Tree diameter and aspect were the two most important variables in

determining the growth trend of subalpine fir (pseudo r^2 = 0.36, Table 4.3). Trees growing on east facing aspects have the largest declines (negative trends) in growth (Figure 4.5) followed by those trees growing on south and west facing aspects, respectively. Only subalpine fir growing on north facing aspects had positive trends of growth through time. Engelmann spruce growth is increasing through time on all landscape positions (Table 4.3).

Figure 4.5 Top: Mean basal area increment (BAI) through time for trees located on different aspects, north (N), south (S), east (E), west (W), for a) Subalpine Fir and b) Engelmann Spruce. Bottom: Box plot of BAI trend (correlation of BAI and year) from 1975-2012 by aspect for c) subalpine fir and d) Engelmann spruce; bars represent median trend, boxes represent 25-75 quartiles, whiskers represent range and open circles are outliers.

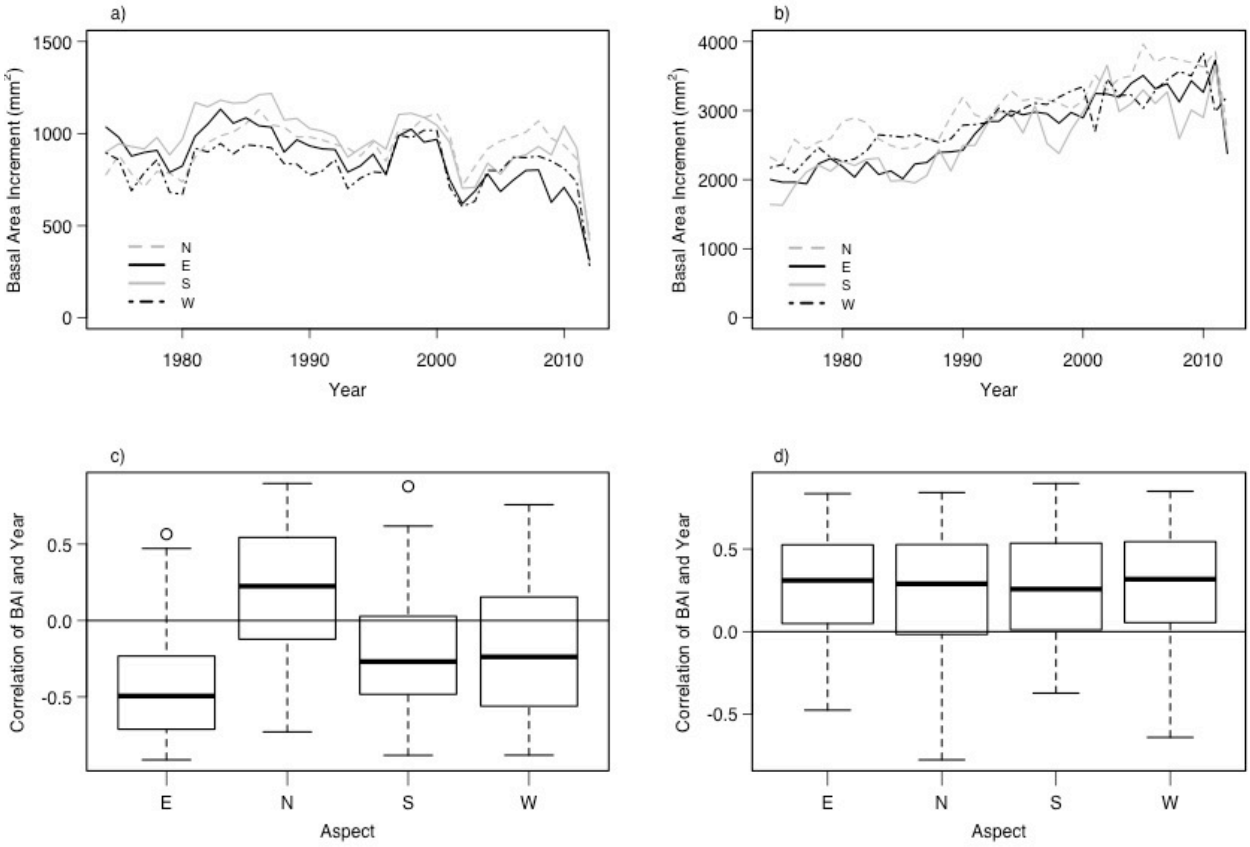

Table 4.3 Statistical parameters of the top five performing linear mixed effects models for basal area increment trend for Subalpine Fir (top) and Engelmann Spruce (bottom). Site temperature refers to the average monthly minimum temperature for the growing season from 1975 through 2012.

Engelmann spruce

Model	Diameter	Elevation	Aspect[1]	Site Temperature[2]	Δ BIC	Δ AIC	R^2
baim2	-0.128	--	x	--	0	0	0.36
baim5	-0.121	--	x	-0.005	4	1	0.36
baim0	-0.120	--	--	--	5	15	0.37

Subalpine fir

Model	Diameter	Elevation	Aspect[1]	Site Temperature[2]	Δ BIC	Δ AIC	R^2
baim0	-0.019	--	--	--	0	0	0.08
baim1	-0.019	-0.107	--	--	5	2	0.08
baim2	0.039	--	x	--	17	5	0.08

[1] Statistical parameters for 'Aspect' are denoted as "x" because aspect is a categorical variable and therefore has more than one statistical parameter for each model.
[2]Average growing season monthly minimum temperature from 1975 – 2012

4.4 Discussion

Interacting effects of regional climate and local physiography dictate the response of forests to climate change. This interaction is particularly important in subalpine forests of the western US that are characterized by complex topography and have experienced greater warming than lower elevation regions over the past several decades [*Diaz and Eischeid*, 2007]. My results indicate that increasing temperatures may be reducing rates of forest growth in subalpine regions in the Southwest. I find that warm summer minimum temperatures reduce growth in subalpine fir, and this effect is greatest in the lower elevation portion of its range. This species has also experienced growth declines over the past 40 years and declines are most pronounced on specific landscape positions. Climate projections indicate that the subalpine regions explored in this study will likely experience continued warming in the future, with temperature increases

potentially as great as 4ºC by 2070 [*Rangwala et al*., 2012]. My results indicate that subalpine fir is already responding to changes in climate, and that this species is particularly vulnerable to temperature trends that are expected to intensify in the future. Engelmann spruce growth, in contrast, is not experiencing declines under current climate conditions.

4.4.1 Climate Growth Relations. Within the subalpine regions of San Juan National Forest, growth of subalpine fir is reduced in years with warm summer temperatures. Specifically, subalpine fir growth is lowest in years with high summer minimum temperatures. Subalpine fir growth is affected more by summer minimum temperatures than by summer maximum temperatures, potentially because while high maximum temperatures may be the result of one or two warm days, high minimum temperatures indicate that temperatures never become cool. Subalpine fir also shows some climate sensitivity to precipitation. Although the correlations between growth and precipitation are much weaker, the correlations between subalpine fir growth and precipitation are consistent with a signal of drought stress as they show a weak positive correlation with precipitation in the same months that tree growth is negatively correlated to warm temperatures. Previous research in other parts of North America indicates that in locally dry and warm locations, low soil water availability reduced growth of subalpine fir in the summer months [*Splechtna et al*., 2000; *Peterson et al*., 2002]. This observation is consistent with the results observed here where subalpine fir growth is negatively associated with summer temperature, and weakly positively associated with summer precipitation.

Engelmann spruce of this region have a low sensitivity to climate, but do grow slightly more in years with warmer temperatures (Figure 4.3). My observations of the climate-growth relationships of Engelmann spruce are consistent with those from other regions of North

America such as the Northern Cascade and Rocky Mountains where Engelmann spruce grew more in response to warm summer temperatures [*Peterson and Peterson*, 1994; *Villalba and Veblen*, 1994]. Engelmann spruce may respond positively to warm summer temperatures because warm summers are indicative of a below-average snowpack which means earlier snow melt and longer growing seasons [*Peterson and Peterson*, 1994]. Additionally, if warm summer temperatures are associated with less cloud cover, then temperature may also act as a surrogate measure of light intensity and thus increase stomatal conductance [*Kaufmann*, 1982]. In either case, the warm summer temperatures have a slightly positive effect on growth of Engelmann spruce.

The greater climate sensitivity of subalpine fir relative to Engelmann spruce may be due in part to physiological differences. Subalpine fir has greater transpiration flux density and greater leaf conductance than Engelmann spruce [*Knapp and Smith*, 1981], and subalpine fir exhibit generally higher isotopic discrimination against $^{13}CO_2$ relative to $^{12}CO_2$ across their elevational range, suggesting that subalpine fir has lower water-use efficiency than Engelmann spruce [*Marshall and Zhang*, 1994]. These physiological differences may account for some of the divergence in how these two species respond to regional climate.

The negative effect of high summer temperatures on subalpine fir growth is a particularly noteworthy result in light of the projected temperature increases for the southwestern US in upcoming decades. Downscaled regional climate models predict an increase of 2ºC of both minimum and maximum temperatures in all seasons for this region [*Rangwala et al.*, 2012]. For the elevation band stretching from 2450m to 3350m, the increase in summer maximum temperatures is expected to be even greater, at 3 to 4ºC. In other words, the warm temperatures that reduce subalpine fir growth are expected to increase the most in the exact season, and the

exact location, where they will have the greatest negative effect on subalpine fir. This temperature increase, and the stress associated with high temperatures, may leave subalpine fir more vulnerable to other short-term stresses [*Pedersen*, 1998].

4.4.2 Interactions of Climate and Physiography. Subalpine fir growth is governed not only by climate, but also by physiography, and the interaction between the two. Specifically, summer minimum temperature, elevation and their interaction were the most important variables determining subalpine fir growth (Table 4.2). The nature of this interaction indicates that in the coolest years, subalpine fir growth was greater in lower elevations, and lower in higher elevations. However, this relationship reversed during warm years. In warmer conditions, subalpine fir at high elevations grew the most while growth at low elevations was reduced (Figure 4.4). Similar variations in the climate-growth relationship of subalpine fir across an elevational gradient have been observed in other regions including the Pacific Northwest and British Columbia. In Southern British Columbia, subalpine fir growth was controlled by interacting effects of elevation and temperature such that low summer temperatures limited wood formation in high elevation trees, but warm spring temperatures limited growth in low elevation trees [*Splechtna et al*., 2000]. This switch in limiting climatic factors between lower and higher elevations may represent a transition from a large snowpack limiting growth by shortening the growing season in the case of high elevation trees in cold years, to growth being limited by potential moisture stress in the low elevation sites in warm years [*Splechtna et al*., 2000]. In addition to subalpine fir, these results also indicate that Engelmann spruce growth is also governed by interactions between climate and physiography, but the interactions are not nearly as strong (Table 4.2).

4.4.3 Trends in Growth. Subalpine fir growth is declining through time among trees in specific physiographic positions. Subalpine fir present on east facing aspects are experiencing the most precipitous declines in BAI, followed by trees on south and west facing aspects (Figure 4.5). Only trees present on north facing aspects do not show a pattern of mean declines in BAI through time from 1975 to the present. I recognize this pattern of BAI through time as a decline because in a mature healthy tree, BAI should either increase over time or remain static [*Biondi and Qeadan*, 2008]. Sustained decreases in BAI in a mature tree are associated with tree decline [*Phipps and Whiton*, 1988; *Duchesne et al*., 2002] and eventual senescence [*LeBlanc*, 1990a, 1990b; *Pedersen*, 1998]. Causes of BAI decline in a mature tree can be related to an external stressor such as atmospheric pollutants [*LeBlanc*, 1990b; *Duchesne et al*., 2002] drought and insect outbreaks [*Pedersen*, 1998; *Hogg et al*., 2002] or unfavorable changes in climate such as drought stress related to climate warming [*Jump et al*., 2006]. Drought stress of high elevation trees in response to warmer temperatures has resulted in growth declines of tree species in other alpine environments [*Jump et al*., 2006; *Linares and Camarero*, 2011]. In the case of subalpine fir present within San Juan National Forest, the trends in decreasing BAI may be a response to warm summer temperatures. Both mean annual temperature and summer average monthly minimum temperature, the variable that has the strongest negative effect on growth, have been increasing during the time period where I see evidence of decline (Figure 4.2), and therefore the decline may be due to increasing temperatures and associated drought stress in subalpine regions. In contrast to subalpine fir, Engelmann spruce in this region show trends of increasing BAI through time for most trees, regardless of elevation, aspect or site temperature (Figure 4.5, Table 4.3).

4.5 Conclusions

Forests of the Rocky Mountains are already responding to climate change through increasing rates of background tree mortality [*van Mantgem et al*., 2009], greater instances of insect outbreaks occurring at unusually high elevations and latitudes [*Hicke et al*., 2006; *Raffa et al*., 2008], and wide-spread mortality due to drought [*Breshears et al*., 2005]. In this study I show that forest growth rates are also changing, potentially as a result of climate change. Subalpine fir, which exists within 17,000 km^2 of subalpine forests of the southern and central Rocky Mountains, show trends of decreasing growth over the past several decades, and declines are most evident on specific landscape positions. Subalpine fir trees with depressed growth rates prior to drought are more likely to be killed by short duration severe drought conditions [*Bigler et al*., 2007], and therefore subalpine fir within southwest Colorado may be particularly vulnerable to future drought conditions. Furthermore, as declines are more evident in specific landscape positions, the vulnerability of these trees may also be dependent on local physiography. These declines could have substantial effects on subalpine forests. Prolonged drought stress can leave forests more vulnerable to disturbance such as beetle outbreaks [*Breshears et al*., 2005; *Raffa et al*., 2008]. Selective mortality from drought or insect outbreaks may result in changes in forest species composition, and in more extreme cases, widespread mortality from severe disturbance could ultimately result in shifts of vegetation boundaries [*Allen and Breshears*, 1998]. Such large-scale changes in forest condition at regional and global scales could ultimately impact how forests contribute to the interaction between the terrestrial biosphere and the atmosphere to control global climate.

CHAPTER V

CONCLUSIONS

Forests globally are in a rapid period of change in response to changing climate and mounting pressures from human populations. In many regions forests are experiencing declines due largely to trends of increasing temperatures [*Allen et al*., 2010; *Williams et al*., 2010; *Choat et al*., 2012]. Particularly dramatic changes in forest condition have been observed in the semi-arid regions of the western US where forests are responding to large wildfires, increased instances of insect outbreaks and drought, and intense management in regions where urban centers abut forested land [*Breshears et al*., 2005; *Westerling et al*., 2006; *Theobald and Romme*, 2007; *Raffa et al*., 2008]. These trends of forest decline and mortality in response to climate change create the potential for a feedback within the global climate system, and therefore it is important quantify changes in forest carbon in response to these trends.

Climate-driven changes in forest carbon dynamics vary between individual forests, making carbon exchange at the forest-scale an important component of terrestrial carbon fluxes. Further, changes in forest carbon balance occurring over decadal timescales are particularly important because these changes affect forest carbon storage over the timeframe relevant for carbon and climate policy. Therefore, forest changes taking place on the scale of an individual forest over a period of decades - specifically the processes of forest disturbance, recovery, and growth - are highly important for determining carbon exchange between forests and the atmosphere. In this dissertation I further efforts to quantify these processes within the region of San Juan National Forest in southwest Colorado, USA by developing a method to improve

estimates of forest carbon stocks in regions of forest disturbance (*Chapter 2*), projecting climate and management impacts on forest recovery following disturbance (*Chapter 3*), and investigating climate-induced patterns of forest growth and decline (*Chapter 4*).

Spatial representations of forest carbon storage, or carbon maps, are frequently used to inventory carbon stocks from the forest scale to the continental scale, and can inform estimates of changes in forest carbon stocks from disturbance events. Despite their importance, maps of forest carbon stocks are frequently only available at limited spatial resolution and include large uncertainties. In Chapter 2 of this dissertation I presented a method of mapping forest carbon stocks present in forest biomass using a combination of physical variables and texture analysis performed on remotely sensed images, and I used this method to create a map of carbon stocks in forest biomass within San Juan National Forest. I found that spatial forest carbon models created from image texture metrics were more strongly correlated with ground-based measurements of forest carbon, and therefore had smaller errors, than models created using only spectral information from remotely sensed imagery. Furthermore, the texture-based model was sensitive to changes in forest carbon following disturbance such as wildfire or logging, and was a better predictor of forest carbon stocks following disturbance than maps created from spectral information alone.

In the future, the texture-based forest carbon model I presented in this dissertation could be used for creating and updating maps of carbon storage in forest biomass throughout the forested regions of the United States. The LandsatTM imagery I used to create this model is available at sub-annual time scales and therefore current LandsatTM images can be obtained to update maps of forest carbon storage following a disturbance. In addition, the methods I used in the creation of this carbon model are based on entirely publically available data: the image

texture analysis was performed on publically available LandsatTM imagery and the forest inventory information obtained to train and validate the model was from the national Forest Inventory and Analysis program. This texture-based method of mapping carbon storage in forest biomass could be particularly important in the future if climate trends continue to influence forest disturbance regimes, and ultimately lead to forest or regional scale changes in forest carbon stocks.

Forest recovery following disturbance and management is another important factor in determining forest-scale carbon stocks in the western US over the coming decades. In many regions of the western US, forest fuel-reduction treatments are used to reduce the risk of high severity wildfire [*Agee and Skinner*, 2005]. These treatments can provide a carbon mitigation benefit if they reduce pyrogenic emissions from a future wildfire, but that benefit is contingent on forest recovery to re-sequester the carbon removed during treatment [*Hurteau and North*, 2010]. In Chapter 3 of my dissertation I investigated the carbon balance of a forest fuel reduction treatment considering variable scenarios of forest recovery, and also varying scenarios of the fate of forest biomass removed during treatment. My results indicate that carbon emissions to the atmosphere are lowest when the biomass removed from the forest is used for bioenergy electricity generation, because of the carbon offset from avoided fossil fuel electricity production emissions. Furthermore, my results indicated that the carbon benefit achieved through bioenergy electricity production will increase through time as offset emissions accumulate. In contrast, projections of climate-induced changes in forest disturbance regimes and regeneration had the potential to decrease future forest carbon storage, and the effect of climate was as great, or greater, than the benefit obtained from bioenergy electricity production. In summary, forest-scale carbon balance following management is dependent both on the fate of

the biomass removed from the forest and future climate trends, and bioenergy electricity production may not provide the same carbon benefit under future climate conditions.

Forest-scale changes in carbon storage can also be affected by trends in forest demographic processes such as growth. Trends of this nature have received little attention compared to climate-related disturbance events and forest die-offs globally, but may have widespread implications [*Jump et al*., 2006; *van Mantgem et al*., 2009; *Beck et al*., 2011]. In Chapter 4 of my dissertation I investigated the effects of climate warming on forest growth at the forest scale. I used correlations between historical climate and tree ring widths through time to determine the most important climate variables driving growth in subalpine conifer species and to detect trends in tree growth through time. My results indicated that subalpine fir, a species found in subalpine regions throughout the Rocky Mountains, grew less in years with warm summer temperatures and that subalpine fir growth has been declining over the past several decades. The observed trends of subalpine fir decline are most pronounced on specific landscape positions, and occurred concurrent with increasing temperatures in this region. These results indicate that subalpine fir growth declines may be in response to drought stress induced by increasing summer temperatures, particularly in the warmest landscape positions.

Summer temperatures within San Juan National Forest are expected to increase over the coming decades. Projections of future climate in this region indicate an increase of 2ºC by 2070 under a relatively high emissions scenario, with increases up to 4ºC at elevations above 2500 meters [*Rangwala et al*., 2012]. Increasing temperatures will likely further stress the subalpine forests of this region and could leave these forests more susceptible to other types of disturbance such as insect outbreaks or severe, short-duration drought [*Bigler et al*., 2007; *Bentz et al*., 2010]. Previous studies have suggested that future temperature increases could dramatically decrease

growth in many low-elevation tree species of this region in coming decades [*Williams et al.*, 2010]. My results suggest that subalpine species of the southwest may also be vulnerable to climate change, specifically increasing temperatures. This work contributes to a growing body of literature demonstrating the changes taking place in forests globally in response to climate change, and in particular emphasizes the importance of studying decadal trends of forest response to climate change in addition to the effects of climate-driven forest disturbance events.

REFERENCES

Adams, H. D., and T. E. Kolb (2005), Tree growth response to drought and temperature in a mountain landscape in northern Arizona, USA, *J. Biogeogr.*, *32*(9), 1629–1640, doi:10.1111/j.1365-2699.2005.01292.x.

Agee, J. K., and C. N. Skinner (2005), Basic principles of forest fuel reduction treatments, *For. Ecol. Manage.*, *211*(1-2), 83–96, doi:10.1016/j.foreco.2005.01.034.

Aho, K., D. Derryberry, and T. Peterson (2014), Model selection for ecologists: the worldviews of AIC and BIC, *Ecology*, *95*(3), 631–636.

Allen, C. D., and D. D. Breshears (1998), Drought-induced shift of a forest-woodland ecotone: Rapid landscape response to climate variation, *Proc. Natl. Acad. Sci.*, *95*(December), 14839–14842.

Allen, C. D. et al. (2010), A global overview of drought and heat-induced tree mortality reveals emerging climate change risks for forests, *For. Ecol. Manage.*, *259*(4), 660–684, doi:10.1016/j.foreco.2009.09.001.

ArcGIS Services Directory (2013), ArcGIS Services Directory, *http://server.arcgisonline.com*.

Arora, V. K. et al. (2013), Carbon-concentration and carbon-climate feedbacks in CMIP5 earth system models, *J. Clim.*, *26*, 5289–5314, doi:10.1175/JCLI-D-12-00494.1.

Azpeleta, A., P. Fule, K. Shive, C. Sieg, and A. Sanchez-Meador (2014), Simulating post-wildfire forest trajectories under alternative climate and management scenarios, *Ecol. Appl.*, *24*(7), 1626–1637.

Basu, P. (2010), *Biomass Gasification and Pyrolysis: Practical Design and Theory*, Elsevier Inc., Oxford, UK.

Beck, P. S. A., G. P. Juday, C. Alix, V. A. Barber, S. E. Winslow, E. E. Sousa, P. Heiser, J. D. Herriges, and S. J. Goetz (2011), Changes in forest productivity across Alaska consistent with biome shift., *Ecol. Lett.*, *14*(4), 373–9, doi:10.1111/j.1461-0248.2011.01598.x.

Bentz, B. J., J. A. Logan, and G. D. Amman (1991), Temperature-Dependent Development of the Mountain Pine Beetle (Coleoptera: Scolytidae) and Simulation of Its Phenology, *Can. Entomol.*, *123*(5), 1083–1094, doi:10.4039/Ent1231083-5.

Bentz, B. J., J. Régnière, C. J. Fettig, E. M. Hansen, J. L. Hayes, J. A. Hicke, R. G. Kelsey, J. F. Negrón, and S. J. Seybold (2010), Climate Change and Bark Beetles of the Western United States and Canada: Direct and Indirect Effects, *Bioscience*, *60*(8), 602–613, doi:10.1525/bio.2010.60.8.6.

Bigler, C., D. G. Gavin, C. Gunning, and T. T. Veblen (2007), Drought induces lagged tree mortality in a subalpine forest in the Rocky Mountains, *Oikos*, *166*, 1983–1994, doi:10.1111/j.2007.0030-1299.16034.x.

Biondi, F., and F. Qeadan (2008), A Theory-Driven Approach to Tree-Ring Standardization: Defining the Biological Trend from Expected Basal Area Increment, *Tree-Ring Res.*, *64*(2), 81–96, doi:10.3959/2008-6.1.

Blackard, J., M. Finco, E. Helmer, G. Holden, M. Hoppus, D. Jacobs, A. Lister, G. Moisen, M. Nelson, and R. Reimann (2008), Mapping U.S. forest biomass using nationwide forest inventory data and moderate resolution information, *Remote Sens. Environ.*, *112*(4), 1658–1677, doi:10.1016/j.rse.2007.08.021.

Blair, R. (1996), *The Western San Juan Mountains; Their Geology, Ecology and Human History*, edited by T. A. Casey, W. H. Romme, and R. N. Ellis, University Press of Colorado, Niwot, Colorado.

Breshears, D. D. et al. (2005), Regional vegetation die-off in response to global-change-type drought., *Proc. Natl. Acad. Sci. U. S. A.*, *102*(42), 15144–8, doi:10.1073/pnas.0505734102.

Bunn, A. G. (2008), A dendrochronology program library in R (dplR), *Dendrochronologia*, *26*(2), 115–124, doi:10.1016/j.dendro.2008.01.002.

Bunn, A. G., L. a Waggoner, and L. J. Graumlich (2005), Topographic mediation of growth in high elevation foxtail pine, *Glob. Ecol. Biogeogr.*, 103–114.

Campbell, J. L., M. E. Harmon, and S. R. Mitchell (2012), Can fuel-reduction treatments really increase forest carbon storage in the western US by reducing future fire emissions?, *Front. Ecol. Environ.*, *10*(2), 83–90, doi:10.1890/110057.

Cansler, C. A., and D. Mckenzie (2014), Climate, fire size, and biophysical setting control fire severity and spatial pattern in the northern Cascade Range, USA, *Ecol. Appl.*, *24*(5), 1037–1056, doi:10.1890/13-1077.1.

Carlson, C. H., S. Z. Dobrowski, and H. D. Safford (2012), Variation in tree mortality and regeneration affect forest carbon recovery following fuel treatments and wildfire in the Lake Tahoe Basin, California, USA., *Carbon Balance Manag.*, *7*(1), 7, doi:10.1186/1750-0680-7-7.

Carnicer, J., M. Coll, M. Ninyerola, X. Pons, G. Sánchez, and J. Peñuelas (2011), Widespread crown condition decline, food web disruption, and amplified tree mortality with increased climate change-type drought., *Proc. Natl. Acad. Sci. U. S. A.*, *108*(4), 1474–1478, doi:10.1073/pnas.1010070108.

CGEO (2010), 2010 Colorado Utilities Report, *Color. Governor's Energy Off.*

Chander, G., B. L. Markham, and D. L. Helder (2009), Summary of current radiometric calibration coefficients for Landsat MSS, TM, ETM+, and EO-1 ALI sensors, *Remote Sens. Environ.*, *113*(5), 893–903, doi:10.1016/j.rse.2009.01.007.

Chavez, P. S. (1988), An improved dark-object subtraction technique for atmospheric scattering correction of multispectral data, *Remote Sens. Environ.*, *24*(3), 459–479.

Choat, B. et al. (2012), Global convergence in the vulnerability of forests to drought., *Nature*, *491*(V), 752–5, doi:10.1038/nature11688.

Clausi, D. A. (2002), An analysis of co-occurrence texture statistics as a function of grey level quantization, *Can. J. For. Res.*, *28*(1), 45–62.

Cram, D. S., T. T. Baker, and J. C. Boren (2006), Wildland Fire Effects in Silviculturally Treated vs . Untreated Stands of New Mexico and Arizona, *USDA For. Serv. Res. Pap.*, *RMRS-RP-55*(February), 1–23.

Cutler, M. E. J., D. S. Boyd, G. M. Foody, and A. Vetrivel (2012), Estimating tropical forest biomass with a combination of SAR image texture and Landsat TM data: An assessment of predictions between regions, *ISPRS J. Photogramm. Remote Sens.*, *70*, 66–77, doi:10.1016/j.isprsjprs.2012.03.011.

Diaz, H. F., and J. K. Eischeid (2007), Disappearing "alpine tundra" Koppen climatic type in the western United States, *Geophys. Res. Lett.*, *34*, 1–4, doi:10.1029/2007GL031253.

Dixon, G. E. (2008), Essential FVS: A User's Guide to the Forest Vegetation Simulator, *For. Manag. Serv. Center, Fort Collins, CO*.

Dolman, A. J., G. R. van der Werf, J. K. van der Molen, G. Ganssen, J.-W. Erisman, and B. Strenger (2010), A Carbon Cycle Science Update Since IPCC AR-4, *Ambio*, *39*(5/6), 402–412.

Donato, D. C., J. B. Fontaine, J. L. Campbell, W. D. Robinson, J. B. Kauffman, and B. E. Law (2009), Conifer regeneration in stand-replacement portions of a large mixed-severity wildfire in the Klamath–Siskiyou Mountains, *Can. J. For. Res.*, *39*, 823–838, doi:10.1139/X09-016.

Dore, S., T. E. Kolb, M. Montes-Helu, S. E. Eckert, B. W. Sullivan, B. A. Hungate, J. P. Kaye, S. C. Hart, G. W. Koch, and A. Finkral (2010), Carbon and water fluxes from ponderosa pine forests disturbed by wildfire and thinning, *Ecol. Appl.*, *20*(3), 663–683, doi:10.1890/09-0934.1.

Dubayah, R. O., and J. B. Drake (2000), Lidar Remote Sensing for Forestry, *J. For.*, *98*(6), 44–46.

Duchesne, L., R. Ouimet, and D. Houle (2002), Basal Area Growth of Sugar Maple in Relation to Acid Deposition, Stand Health, and Soil Nutrients, *J. Environ. Qual.*, *31*(5), 1676–83.

Duchesne, L., R. Ouimet, and C. Morneau (2003), Assessment of sugar maple health based on basal area growth pattern, *Can. J. For. Res.*, *33*(11), 2074–2080, doi:10.1139/x03-141.

Eckert, S. (2012), Improved Forest Biomass and Carbon Estimations Using Texture Measures from WorldView-2 Satellite Data, *Remote Sens.*, *4*(12), 810–829, doi:10.3390/rs4040810.

Elvir, J. A., G. B. Wiersma, A. S. White, and I. J. Fernandez (2003), Effects of chronic ammonium sulfate treatment on basal area increment in red spruce and sugar maple at the Bear Brook Watershed in Maine, *Can. J. For. Res.*, *33*(5), 862–869, doi:10.1139/x03-016.

EPA (2010), Environmental Protection Agency Department of Emission Standards, *Fed. Regist.*, *75*(88), 25324–25728.

EPA (2011), *Inventory of U.S. Greenhouse Gas Emissions and Sinks: 1990 - 2009*.

FIA (2013), Forest Inventory and Analysis National Program, Data-Mart, *http://www.fia.fs.fed.us/tools-data/*.

Finkral, A. J., and A. M. Evans (2008), The effects of a thinning treatment on carbon stocks in a northern Arizona ponderosa pine forest, *For. Ecol. Manage.*, *255*(7), 2743–2750, doi:10.1016/j.foreco.2008.01.041.

Finney, M. A., C. W. Mchugh, and I. C. Grenfell (2005), Stand- and landscape-level effects of prescribed burning on two Arizona wildfires, *Can. J. For. Res.*, *1722*, 1714–1722, doi:10.1139/X05-090.

Friedlingstein, P. et al. (2006), Climate–Carbon Cycle Feedback Analysis: Results from the C 4 MIP Model Intercomparison, *J. Clim.*, *19*, 3337–3353, doi:10.1175/JCLI3800.1.

Fritts, H. C. (1976), *Tree Rings and Climate*, Academic Press, San Francisco.

Fulé, P. Z., J. E. Crouse, J. P. Roccaforte, and E. L. Kalies (2012), Do thinning and/or burning treatments in western USA ponderosa or Jeffrey pine-dominated forests help restore natural fire behavior?, *For. Ecol. Manage.*, *269*, 68–81, doi:10.1016/j.foreco.2011.12.025.

Galván, J. D., J. J. Camarero, and E. Gutiérrez (2014), Seeing the trees for the forest: drivers of individual growth responses to climate in Pinus uncinata mountain forests, edited by P. Zuidema, *J. Ecol.*, *102*(5), 1244–1257, doi:10.1111/1365-2745.12268.

Gee, G. W., and D. Or (2002), *Particle-size analysis*, Part 4., edited by J. H. Dane and G. C. Topp, SSSA, Madison, WI.

Goetz, S. J., A. Baccini, N. T. Laporte, T. Johns, W. Walker, J. Kellndorfer, R. A. Houghton, and M. Sun (2009), Mapping and monitoring carbon stocks with satellite observations: a comparison of methods., *Carbon Balance Manag.*, *4*(1), 2, doi:10.1186/1750-0680-4-2.

Greene, D. F., and E. A. Johnson (2011), Tree recruitment from burn edges, *Can. J. For. Res.*, *30*(8), 1264–74, doi:10.1139/x00-040.

Grissino-Mayer, H. D. (2001), Evaluating Crossdating Accuracy: A Manual and Tutorial for the Computer Program COFECHA, *Tree-Ring Res.*, *57*(2), 205–221.

Gutmann, E. D., R. M. Rasmussen, C. Liu, K. Ikeda, D. J. Gochis, M. P. Clark, J. Dudhia, and G. Thompson (2012), A comparison of statistical and dynamical downscaling of winter precipitation over complex terrain, *J. Clim.*, *25*, 262–281, doi:10.1175/2011JCLI4109.1.

Haralick, R. M., K. Shanmugam, and I. Dinstein (1973), Textural Features for Image Classification, *IEEE Trans. Syst. Man. Cybern.*, *3*(6), 610–621, doi:10.1109/TSMC.1973.4309314.

Hicke, J. A., J. A. Logan, J. Powell, and D. S. Ojima (2006), Changing temperatures influence suitability for modeled mountain pine beetle (Dendroctonus ponderosae) outbreaks in the western United States, *J. Geophys. Res. Biogeosciences*, *111*, 1–12, doi:10.1029/2005JG000101.

Hogg, E. H., J. P. Brandt, and B. Kochtubajda (2002), Growth and dieback of aspen forests in northwestern Alberta, Canada, in relation to climate and insects, *Can. J. For. Res.*, *32*(5), 823–832, doi:10.1139/x01-152.

Holmes, R. L. (1983), Computer-Assisted Quality Control in Tree-Ring Dating and Measurement, *Tree-Ring Bull.*, *43*, 69–78.

Hoppus, M., and A. Lister (2005), The Status of Accurately Locating Forest Inventory and Analysis Plots Using the Global Positioning System, *Proc. Seventh Annu. For. Invent. Anal. Symp.*, 179–184.

Huete, A. R., and W. J. D. van Leeuwen (1997), The use of vegetation indices in forested regions: issues of linearity and saturation, in *IGARSS'97. 1997 IEEE International Geoscience and Remote Sensing Symposium Proceedings. Remote Sensing - A Scientific Vision for Sustainable Development*, vol. 4, pp. 1966–1968, IEEE.

Hurteau, M., and M. North (2009), Fuel treatment effects on tree-based forest carbon storage and emissions under modeled wildfire scenarios, *Front. Ecol. Environ.*, *7*(8), 409–414, doi:10.1890/080049.

Hurteau, M. D., and M. L. Brooks (2011), Short- and Long-term Effects of Fire on Carbon in US Dry Temperate Forest Systems, *Bioscience*, *61*(2), 139–146, doi:10.1525/bio.2011.61.2.9.

Hurteau, M. D., and M. North (2010), Carbon recovery rates following different wildfire risk mitigation treatments, *For. Ecol. Manage.*, *260*(5), 930–937, doi:10.1016/j.foreco.2010.06.015.

Hurteau, M. D., G. W. Koch, and B. A. Hungate (2008), Carbon protection and fire risk reduction: toward a full accounting of forest carbon offsets, *Front. Ecol. Environ.*, *6*(9), 493–498, doi:10.1890/070187.

Hurteau, M. D., M. T. Stoddard, and P. Z. Fulé (2011), The carbon costs of mitigating high-severity wildfire in southwestern ponderosa pine, *Glob. Chang. Biol.*, *17*(4), 1516–1521, doi:10.1111/j.1365-2486.2010.02295.x.

Jenkins, J. C., D. C. Chojnacky, L. S. Heath, and R. A. Birdsey (2004), Comprehensive Database of Diameter-based Biomass Regressions for North American Tree Species, *USDA For. Serv. Gen. Tech. Rep.*, (NE-319).

Jump, A. S., J. M. Hunt, and J. Penuelas (2006), Rapid climate change-related growth decline at the southern range edge of Fagus sylvatica, *Glob. Chang. Biol.*, *12*(11), 2163–2174, doi:10.1111/j.1365-2486.2006.01250.x.

Karl, T. R., and W. J. Koss (1984), Regional and National Monthly, Seasonal and annual Temperature Weighted by Area, 1895-1983, in *Historical Climatology Series 4-3*.

Kasischke, E. S., J. M. Melack, and M. Craig Dobson (1997), The use of imaging radars for ecological applications—A review, *Remote Sens. Environ.*, *59*(2), 141–156.

Kaufmann, M. R. (1982), Leaf Conductance as a Function of Photosynthetic Photon Flux Density and Absolute Humidity Difference from Leaf to Air, *Plant Physiol.*, *69*(5), 1018–1022, doi:10.1104/pp.69.5.1018.

Kaye, J. P., S. C. Hart, P. Z. Fulé, W. W. Covington, M. M. Moore, and M. W. Kaye (2005), Initial Carbon, Nitrogen, and Phosphorus Fluxes Following Ponderosa Pine Restoration Treatments, *Ecol. Appl.*, *15*(5), 1581–1593, doi:10.1890/04-0868.

Kellndorfer, J., W. Walker, E. LaPoint, J. Bishop, T. Cormier, G. Fiske, M. Hoppus, K. Kirsh, and J. Westfall (2000), NACP Aboveground Biomass and Carbon Baseline Data, , (http://daac.ornl.gov).

Knapp, A. K., and W. K. Smith (1981), Water Relations and Succession in Subalpine Conifers in Southeastern Wyoming, *Bot. Gaz.*, *142*(4), 502–511.

Kurz, W. A., C. C. Dymond, G. Stinson, G. J. Rampley, E. T. Neilson, A. L. Carroll, T. Ebata, and L. Safranyik (2008), Mountain pine beetle and forest carbon feedback to climate change, *Nature*, *452*(April), 987–990, doi:10.1038/nature06777.

LeBlanc, D. C. (1990a), Red Spruce Decline on Whiteface Mountain, New York. 1. Relationships with Elevation, Tree Age, and Competition, *Can. J. For. Res.*, *20*(9), 1408–1414.

LeBlanc, D. C. (1990b), Red Spruce Decline on Whiteface Mountain, New York. 2. Relationships between Apical and Radial Growth, *Can. J. For. Res.*, *20*(9), 1415–1421.

Lim, K., P. Treitz, M. Wulder, B. St-Onge, and M. Flood (2003), LiDAR remote sensing of forest structure, *Prog. Phys. Geogr.*, *27*(1), 88–106, doi:10.1191/0309133303pp360ra.

Linares, J. C., and J. J. Camarero (2011), Growth patterns and sensitivity to climate predict silver fir decline in the Spanish Pyrenees, *Eur. J. For. Res.*, *131*(4), 1001–1012, doi:10.1007/s10342-011-0572-7.

Littell, J., and D. Peterson (2011), A method for estimating vulnerability of Douglas-fir growth to climate change in the northwestern U.S.,

Littell, J. S., D. L. Peterson, and M. Tjoelker (2008), Douglas-fir growth in mountain ecosystems: Water limits tree growth from stand to region, *Ecol. Monogr.*, *78*(3), 349–368, doi:10.1890/07-0712.1.

Littell, J. S., D. McKenzie, D. L. Peterson, and A. L. Westerling (2009), Climate and wildfire area burned in western U.S. ecoprovinces, 1916–2003, *Ecol. Appl.*, *19*(4), 1003–1021, doi:10.1890/07-1183.1.

Lo, Y.-H., J. A. Blanco, B. Seely, C. Welham, and J. P. (Hamish) Kimmins (2010), Relationships between climate and tree radial growth in interior British Columbia, Canada, *For. Ecol. Manage.*, *259*(5), 932–942, doi:10.1016/j.foreco.2009.11.033.

Logan, J. A., J. Régnière, and J. A. Powell (2003), Assessing the impacts of global warming on forest pest dynamics, *Front. Ecol.*, *1*(3), 130–137.

Lu, D. (2005), Aboveground biomass estimation using Landsat TM data in the Brazilian Amazon, *Int. J. Remote Sens.*, *26*(12), 2509–2525, doi:10.1080/01431160500142145.

Lu, D., and M. Batistella (2005), Exploring TM image texture and its relationships with biomass estimation in Rondônia, Brazilian Amazon, *Acta Amaz.*, *35*(2), 249–257, doi:10.1590/S0044-59672005000200015.

Van Mantgem, P. J. et al. (2009), Widespread increase of tree mortality rates in the western United States., *Science*, *323*(5913), 521–4, doi:10.1126/science.1165000.

Marshall, J. D., and J. Zhang (1994), Carbon Isotope Discrimination and Water-Use Efficiency in Native Plants of the North- Central Rockies Author, *Ecology*, *75*(7), 1887–1895.

Martín-Benito, D., P. Cherubini, M. del Río, and I. Cañellas (2007), Growth response to climate and drought in Pinus nigra Arn. trees of different crown classes, *Trees*, *22*(3), 363–373, doi:10.1007/s00468-007-0191-6.

McDowell, N. G., D. J. Beerling, D. D. Breshears, R. A. Fisher, K. F. Raffa, and M. Stitt (2011), The interdependence of mechanisms underlying climate-driven vegetation mortality, *Trends Ecol. Evol.*, *26*, 523–532, doi:10.1016/j.tree.2011.06.003.

McKenzie, D., Z. Gedalof, D. L. Peterson, and P. Mote (2004), Climatic Change, Wildfire, and Conservation, *Conserv. Biol.*, *18*(4), 890–902.

Meigs, G. W., D. C. Donato, J. L. Campbell, J. G. Martin, and B. E. Law (2009), Forest Fire Impacts on Carbon Uptake, Storage, and Emission: The Role of Burn Severity in the Eastern Cascades, Oregon, *Ecosystems*, *12*(8), 1246–1267, doi:10.1007/s10021-009-9285-x.

Mitchell, S. R., M. E. Harmon, and K. E. B. O'Connell (2009), Forest fuel reduction alters fire severity and long-term carbon storage in three Pacific Northwest ecosystems, *Ecol. Appl.*, *19*(3), 643–655, doi:10.1890/08-0501.1.

Miyamoto, Y., H. P. Griesbauer, and D. S. Green (2010), Growth responses of three coexisting conifer species to climate across wide geographic and climate ranges in Yukon and British Columbia, *For. Ecol. Manage.*, *259*(3), 514–523, doi:10.1016/j.foreco.2009.11.008.

Moorcroft, P. R. (2006), How close are we to a predictive science of the biosphere?, *Trends Ecol. Evol.*, *21*(7), 400–407, doi:10.1016/j.tree.2006.04.009.

NED (2014), National Elevation Dataset, *http://ned.usgs.gov*.

North, M., M. Hurteau, and J. Innes (2009), Fire suppression and fuels treatment effects on mixed-conifer carbon stocks and emissions, *Ecol. Appl.*, *19*(6), 1385–1396.

North, M. P., and M. D. Hurteau (2011), High-severity wildfire effects on carbon stocks and emissions in fuels treated and untreated forest, *For. Ecol. Manage.*, *261*(6), 1115–1120, doi:10.1016/j.foreco.2010.12.039.

NRCS (n.d.), National Resource Conservation Service, *http://www.nrcs.usda.gov/wps/portal/nrcs/site/soils/home/*.

Ouchi, K. (2013), Recent Trend and Advance of Synthetic Aperture Radar with Selected Topics, *Remote Sens.*, *5*(2), 716–807, doi:10.3390/rs5020716.

Pachauri, R. K. et al. (2014), *CLIMATE CHANGE 2014 Synthesis Report Summary for Policymakers*.

Pedersen, B. S. (1998), The Role of Stress in the Mortality of Midwestern Oaks as Indicated by Growth Prior to Death, *Ecology*, *79*(1), 79–93, doi:10.1890/0012-9658(1998)079[0079:TROSIT]2.0.CO;2.

Penman, J., M. Gytarsky, T. Hiraishi, T. Krug, D. Kruger, R. Pipatti, L. Buendia, K. Miwa, and T. Ngara (2003), *Intergovernmental Panel on Climate Change Good Practice Guidance for Land Use , Land-Use Change and Forestry*.

Pereira, E. G., J. N. da Silva, J. L. de Oliveira, and C. S. Machado (2012), Sustainable energy: A review of gasification technologies, *Renew. Sustain. Energy Rev.*, *16*(7), 4753–4762, doi:10.1016/j.rser.2012.04.023.

Peterson, D. W., and D. L. Peterson (1994), Effects of climate on radial growth of subalpine conifers in the North Cascade Mountains, *Can. J. For. Res.*, *24*(9), 1921–1932, doi:10.1139/x94-247.

Peterson, D. W., D. L. Peterson, and G. J. Ettl (2002), Growth responses of subalpine fir to climatic variability in the Pacific Northwest, *Can. J. For. Res.*, *32*(9), 1503–1517, doi:10.1139/x02-072.

Phipps, R. L., and J. C. Whiton (1988), Decline in long-term growth trends of white oak, *Can. J. For. Res.*, *18*, 24–32.

Pollet, J., and P. N. Omi (2002), Effect of thinning and prescribed burning on crown fire severity in ponderosa pine forests, *Int. J. Wildl. Fire*, *11*(1), 1–10, doi:10.1071/WF01045.

PRISM (2004), PRISM Climate Group, Oregon State University, *http://prism.oregonstate.edu*.

PRISM (2013), PRISM Climate Group, Oregon State University, *http://www.prism.oregonstate.edu*.

Purves, D., and S. Pacala (2008), Predictive Models of Forest Dynamics, *Science*, *320*, 1452–1453, doi:10.1126/science.1155359.

Radeloff, V. C., R. B. Hanner, S. I. Stewart, J. S. Fried, S. S. Holcomb, and J. F. McKeefry (2005), The Wildland – Urban Interface in the United States, *Ecol. Appl.*, *15*(3), 799–805.

Raffa, K. F., B. H. Aukema, B. J. Bentz, A. L. Carroll, J. A. Hicke, M. G. Turner, and W. H. Romme (2008), Cross-scale Drivers of Natural Disturbances Prone to Anthropogenic Amplification: The Dynamics of Bark Beetle Eruptions, *Bioscience*, *58*(6), 501, doi:10.1641/B580607.

Rangwala, I., J. Barsugli, K. Cozzetto, J. Neff, and J. Prairie (2012), Mid-21st century projections in temperature extremes in the southern Colorado Rocky Mountains from regional climate models, *Clim. Dyn.*, *39*(7-8), 1823–1840, doi:10.1007/s00382-011-1282-z.

Reichstein, M. et al. (2013), Climate extremes and the carbon cycle., *Nature*, *500*(7462), 287–95, doi:10.1038/nature12350.

Reinhardt, E., and L. Holsinger (2010), Effects of fuel treatments on carbon-disturbance relationships in forests of the northern Rocky Mountains, *For. Ecol. Manage.*, *259*(8), 1427–1435, doi:10.1016/j.foreco.2010.01.015.

Ribert, G., P. Thakre, Z. Wang, R. A. Yetter, and V. Yang (2010), *Synthesis Gas Combustion: Fundamentals and Applications*, edited by T. C. Lieuwen, V. Yang, and R. A. Yetter, Taylor & Francis Group, Boca Raton, USA.

Richards, J. A. (2013), *Remote Sensing Digital Image Analysis; CH 5, Geometric Processing and Enhancement: Image Domain Techniques*, 5th ed., Springer, London.

Ritchie, M. W., C. N. Skinner, and T. Hamilton (2007), Probability of tree survival after wildfire in an interior pine forest of northern California: Effects of thinning and prescribed fire, *For. Ecol. Manage.*, *247*(1-3), 200–208, doi:10.1016/j.foreco.2007.04.044.

Roccaforte, J. P., P. Z. Fulé, W. W. Chancellor, and D. C. Laughlin (2012), Woody debris and tree regeneration dynamics following severe wildfires in Arizona ponderosa pine forests, *Can. J. For. Res.*, *42*, 593–604, doi:10.1139/x2012-010.

Ruiz, J. A., M. C. Juárez, M. P. Morales, P. Muñoz, and M. A. Mendívil (2013), Biomass gasification for electricity generation: Review of current technology barriers, *Renew. Sustain. Energy Rev.*, *18*, 174–183, doi:10.1016/j.rser.2012.10.021.

Ryan, M. G. et al. (2010), A Synthesis of the Science on for U . S . Forests, *Issues Ecol.*, (13), 1–16.

Sabine, C. et al. (2004), Current Status and Past Trends of the Global Carbon Cycle, in *The Global Carbon Cycle; Integrating Humans, Climate and the Natural World*, edited by C. B. Field and M. R. Raupach, pp. 17–44, Island Press, Washington, D.C.

Safford, H. D., J. T. Stevens, K. Merriam, M. D. Meyer, and a. M. Latimer (2012), Fuel treatment effectiveness in California yellow pine and mixed conifer forests, *For. Ecol. Manage.*, *274*, 17–28, doi:10.1016/j.foreco.2012.02.013.

Savage, M., and J. N. Mast (2005), How resilient are southwestern ponderosa pine forests after crown fires?, *Can. J. For. Res.*, *35*(4), 967–977, doi:10.1139/x05-028.

Saxton, K. E., and W. J. Rawls (2006), Soil Water Characteristic Estimates by Texture and Organic Matter for Hydrologic Solutions, *Soil Sci. Soc. Am. J.*, *70*(5), 1569–1578, doi:10.2136/sssaj2005.0117.

Seager, R. et al. (2007), Model projections of an imminent transition to a more arid climate in southwestern North America., *Science*, *316*(5828), 1181–4, doi:10.1126/science.1139601.

SJNF (2013), San Juan National Forest, Geospatial Data, *http://www.fs.usda.gov/main/sanjuan/landmanagement/gis*.

Skog, K. E., and G. A. Nicholson (2000), Carbon Sequestration in Wood and Paper Products, *USDA For. Serv. Gen. Tech. Rep.*, *RMRS-GTR-5*.

Soja, A. J., N. M. Tchebakova, N. H. F. French, M. D. Flannigan, H. H. Shugart, B. J. Stocks, A. I. Sukhinin, E. I. Parfenova, F. S. Chapin, and P. W. Stackhouse (2007), Climate-induced boreal forest change: Predictions versus current observations, *Glob. Planet. Change*, *56*, 274–296, doi:10.1016/j.gloplacha.2006.07.028.

Spath, P. L., M. K. Mann, and D. R. Kerr (1999), Life Cycle Assessment of Coal-fired Power Production, *NREL Live Cycle Assess.*, *NREL/TP-57*, 1–92, doi:10.2172/12100.

Spendelow, J. A., J. D. Nichols, I. C. T. Nisbet, H. Hays, and G. D. Cormons (1995), Estimating Annual Survival and Movement Rates of Adults within a Metapopulation of Roseate Terns, *Ecology*, *76*(8), 2415–2428.

Splechtna, B. E., J. Dobry, and K. Klinka (2000), Tree-ring characteristics of subalpine fir (Abies lasiocarpa (Hook .) Nutt .) in relation to elevation and climatic fluctuations, *Ann. For. Sci.*, *57*, 89–100.

Stephens, S. L. et al. (2009), Fire treatment effects on vegetation structure, fuels, and potential fire severity in western U.S. forests, *Ecol. Appl.*, *19*(2), 305–320, doi:10.1890/07-1755.1.

Teck, R., M. Moerur, and B. Eav (1996), Forecasting ecosystems with the forest vegetation simulator, *J. For.*, *94*, 7–10.

Teillet, P. M., B. Guindon, and D. G. Goodenough (1982), On the slope-aspect correction of multispectral scanner data, *Can. J. Remote Sens.*, *8*(2), 84–106.

Theobald, D. M., and W. H. Romme (2007), Expansion of the US wildland–urban interface, *Landsc. Urban Plan.*, *83*(4), 340–354, doi:10.1016/j.landurbplan.2007.06.002.

Le Toan, T., A. Beaudoin, J. Riom, and D. Guyon (1992), Relating forest biomass to SAR data, *IEEE Trans. Geosci. Remote Sens.*, *30*(2), 403–411, doi:10.1109/36.134089.

Turner, M. G., and W. H. Romme (1994), Landscape dynamics in crown fire ecosystems, *Landsc. Ecol.*, *9*(1), 59–77, doi:10.1007/BF00135079.

USDA (2011), *Navigating the Climate Change Performance Scorecard; Dimension 4: Mitagation and Sustainable Consumption*.

USDA-USDI (2000), Managing the Impact of Wildfires on Communities and the Environment: A Report to the President in Response to the Wildfires of 2000, *www.fireplan.gov\president.cfm*, 1–35.

Villalba, R., and T. T. Veblen (1994), Climate Influences on the Growth of Sub-Alpine Trees in the Colorado Front Range, *Ecology*, 1450–1462.

Waring, R. H., and S. W. Running (2007), *Forest Ecosystems; Analysis at Multiple Scales*, 3rd Editio., Elsevier Academic Press, Burlington MA.

Watson, E., and B. H. Luckman (2002), The dendroclimatic signal in Douglas-fir and ponderosa pine tree-ring chronologies from the southern Canadian Cordillera, *Can. J. For. Res.*, *32*(10), 1858–1874, doi:10.1139/x02-096.

Weatherspoon, C. P., and C. N. Skinner (1995), An Assessment of Factors Associated with Damage to Tree Crowns from the 1987 Wildfires in Northern California, *For. Sci.*, *41*(3), 430–451.

Westerling, A. L., H. G. Hidalgo, D. R. Cayan, and T. W. Swetnam (2006), Warming and earlier spring increase western U.S. forest wildfire activity., *Science*, *313*(5789), 940–3, doi:10.1126/science.1128834.

Westerling, A. L., M. G. Turner, E. A. H. Smithwick, W. H. Romme, and M. G. Ryan (2011), Continued warming could transform Greater Yellowstone fire regimes by mid-21st century., *Proc. Natl. Acad. Sci. U. S. A.*, *108*(32), 13165–70, doi:10.1073/pnas.1110199108.

Williams, A. P., C. D. Allen, C. I. Millar, T. W. Swetnam, J. Michaelsen, C. J. Still, and S. W. Leavitt (2010), Forest responses to increasing aridity and warmth in the southwestern United States., *Proc. Natl. Acad. Sci. U. S. A.*, *107*(50), 21289–94, doi:10.1073/pnas.0914211107.

Williams, P. A. et al. (2012), Temperature as a potent driver of regional forest drought stress and tree mortality, *Nat. Clim. Chang.*, *3*(3), 292–297, doi:10.1038/nclimate1693.

Yager, D., and D. Bove (2002), Generalized Geologic Map of Part of the Upper Animas River Watershed and Vicinity, Silverton, Colorado., *Geol. Surv. Inf. Serv. Misc. F. Stud. Map MF-2377*.